

2013

Photochemical Reactions of Naproxen, Ibuprofen and Tylosin

Yang He

Purdue University, heyang1024@gmail.com

Follow this and additional works at: https://docs.lib.purdue.edu/open_access_theses

 Part of the [Environmental Engineering Commons](#)

Recommended Citation

He, Yang, "Photochemical Reactions of Naproxen, Ibuprofen and Tylosin" (2013). *Open Access Theses*. 32.
https://docs.lib.purdue.edu/open_access_theses/32

This document has been made available through Purdue e-Pubs, a service of the Purdue University Libraries. Please contact epubs@purdue.edu for additional information.

PURDUE UNIVERSITY
GRADUATE SCHOOL
Thesis/Dissertation Acceptance

This is to certify that the thesis/dissertation prepared

By Yang He

Entitled
Photochemical Reactions of Naproxen, Ibuprofen and Tylosin.

For the degree of Master of Science in Engineering

Is approved by the final examining committee:

Inez Hua
Chair

Chad Jafvert

Ronald Turco

To the best of my knowledge and as understood by the student in the *Research Integrity and Copyright Disclaimer (Graduate School Form 20)*, this thesis/dissertation adheres to the provisions of Purdue University's "Policy on Integrity in Research" and the use of copyrighted material.

Approved by Major Professor(s): Inez Hua

Approved by: Garrett Jeong 7/24/2013
Head of the Graduate Program Date

PHOTOCHEMICAL REACTIONS OF NAPROXEN, IBUPROFEN AND TYLOSIN

A Thesis

Submitted to the Faculty

of

Purdue University

by

Yang He

In Partial Fulfillment of the

Requirements for the Degree

of

Master of Science in Engineering

December 2013

Purdue University

West Lafayette, Indiana

ACKNOWLEDGEMENTS

I would like to express my sincere gratitude to my parents and my family for all the sacrifices they have made to support me to continue my education.

I would like to thank Professor Inez Hua, who guided me through my Master's study and for her help in making me a better person and researcher. I am really fascinated about her teaching style and research attitude. I would also like to show my appreciation to Professor Chad Jafvert. I really appreciate his guidance and suggestions on my research and thesis. Finally, I appreciate the comments and input on my thesis from Professor Ronald Turco in the Agronomy Department.

I would also like to thank those who helped me completed my degree and research, and to those that have supported me throughout this process. Thank you to Dr. Changhe Xiao, Zhe Sun, Somayeh Beigzadehmilani, Dan Su and Hsinse Hsieh, for your help in my research. Special thanks to Dr. Karl Wood for your help in understanding mass spectrum. Thank you all other old and new friends for giving me the opportunity to meet you and learn all that I have.

TABLE OF CONTENTS

	Page
LIST OF TABLES	vi
LIST OF FIGURES	vii
ABSTRACT	ix
CHAPTER 1. INTRODUCTION	1
1.1 Background	1
1.2 Pharmaceuticals and Personal Care Products (PPCPs).....	5
1.2.1 Naproxen (NXP).....	5
1.2.2 Ibuprofen (IBP)	6
1.2.3 Tylsoin (TYL)	7
1.3 Photochemistry.....	9
1.3.1 Direct photolysis.....	10
1.3.2 Indirect photolysis	11
1.3.3 Advanced Oxidation Processes (AOPs).....	11
1.3.4 Kinetics.....	12
1.4 Objectives.....	12
List of References.....	15
CHAPTER 2. UV/H ₂ O ₂ ENHANCED PHOTOCHEMICAL REACTION OF SELECTED PPCPs: KINETICS, MOLAR ABSORPTIVITY AND QUANTUM YIELD	21
2.1 Introduction	21
2.2 Materials and Methods	23
2.2.1 Rayonet 100 UV Reactor.....	23
2.2.2 Chemicals	24
2.2.3 Preparation of aqueous PPCPs solution and standards.....	24
2.2.4 Experimental Procedures	25
2.2.5 Analytical Methods	26
2.2.5.1 High Performance Liquid Chromatography (HPLC)	26
2.2.5.2 UV-vis spectrometer	27
2.3 Kinetics.....	27
2.3.1 Results and Discussion.....	27
2.3.2 Effects of pH.....	30
2.3.2.1 Naproxen and ibuprofen degradation at different pH values.....	31

	Page
2.3.2.2 Tylosin degradation at different pH values	34
2.3.3 Effects of Hydrogen Peroxide (H ₂ O ₂)	40
2.3.3.1 Naproxen and ibuprofen degradation with hydrogen Peroxide (H ₂ O ₂)	40
2.3.3.2 Hydrogen Peroxide (H ₂ O ₂) effect on Tylosin	43
2.4 Direct photolysis Molar Absorptivity (ε) and Quantum Yield (φ)	45
2.4.1 Molar absorptivity (ε).....	45
2.4.2 Quantum Yield φ	48
List of References.....	51
 CHAPTER 3 THE ROLES OF NITRATE AND NOM ON PHOTODEGRADATION AND MODELING THE PHOTOCHEMICAL FATE OF NAPROXEN, IBUPROFEN AND TYLOSIN	57
3.1 Introduction	57
3.2 Materials and Methods	58
3.2.1 Chemicals and Preparation of Aqueous PPCPs Solution	59
3.2.2 Experimental Procedures	59
3.2.3 Analytical Methods	60
3.2.3.1 High Performance Liquid Chromatography (HPLC)	60
3.2.3.2 Carbon Dioxide Ion Selective Electrode (ISE).....	60
3.3 Results and Discussion.....	61
3.3.1 Effect of nitrate (NO ₃ ⁻) on photolysis kinetics	64
3.3.1.1 Effect of nitrate (NO ₃ ⁻) on photolysis kinetics of naproxen and ibuprofen.....	64
3.3.1.2 Effect of nitrate (NO ₃ ⁻) on photolysis kinetics of tylosin	67
3.3.2 Effect of Natural organic matter (NOM) on photolysis kinetics	68
3.3.2.1 Effect of NOM on photolysis of NXP and IBP.....	70
3.3.2.2 Effect of NOM on photolysis of TYL.....	75
3.3.3 Model predictions of UV/H ₂ O ₂ process	79
3.3.3.1 NXP and IBP degradation model.....	79
3.3.3.2 The extent of NXP, IBP and TYL mineralization	89
List of Reference	92
 CHAPTER 4. DIRECT AND INDIRECT PHOTOTRANSFORMATION OF PPCPs: PRODUCTS AND PROPOSED REACTION PATHWAYS	96
4.1 Introduction	96
4.2 Materials and Methods	97
4.2.1 Preparation of aqueous PPCPs solution	98
4.2.2 Experimental Procedures	98
4.2.3 Analytical Methods	99
4.2.3.1 Gas Chromatography/ Mass Spectrometry (GC/MS).....	99
4.2.3.2 Liquid Chromatography/ Mass Spectrometry (LC/MS).....	100
4.3 By-Product Study Results and Discussion	100

	Page
4.3.1 NXP degradation mechanism.....	106
4.3.2 IBP degradation mechanism	110
4.3.3 TYL degradation mechanism.....	113
List of References.....	120
CHAPTER 5. OVERALL CONCLUSIONS.....	122
APPENDICES	
Appendix A. Chemical Actinometry	124
Appendix B. Measurement of Residual Concentration of H ₂ O ₂	128
Appendix C. Ion Selective Electrode (ISE)	131

LIST OF TABLES

Table	Page
1.1 Standard One-Electron Reaction Potentials, E_H^1 in water at 25 °C of some common oxidants	11
2.1 Summary of occurrence of PPCPs.....	22
2.2 NXP, IBP and TYL degradation rate constants.....	29
2.3 pH values of unbuffered NXP and IBP solution.....	32
2.4 Quantum Yield at 254 nm	49
3.1 Summary of experiments	62
3.2 Elemental analysis data for different FA and HA	69
3.3 Experimental and light screening corrected rate constants for photodegradation of selected PPCPs at 254 nm	75
3.4 Light screening factors.....	76
3.5 Second-order-rate constant of $\cdot\text{OH}$ with the selected PPCPs.....	81
3.6 Most significant $\cdot\text{OH}$ scavengers and rate constants	82
3.7 Extent of mineralization of NXP, IBP and TYL	90
4.1 Photoproducts of NXP, IBP and TYL	101

LIST OF FIGURES

Figure	Page
1.1: Chemical structure of NXP	6
1.2: Chemical structure of ibuprofen	7
1.3: Chemical structures of TYL A and TYLB	8
1.4: Research Framework	14
2.1: Degradation of Naproxen (NXP Exp.1) at pH = 7 within 9 minutes.....	28
2.2: Direct photo-degradation of naproxen (NXP Exp.1, 2, 3) in buffer solutions ((pH = 2.98, 6.97 and 9.01) and deionized water (DI water, pH = 5.86).....	31
2.3: Direct photo-degradation of ibuprofen (IBP Exp.1, 2, 3) in buffer solutions ((pH = 2.94, 6.97 and 9.07) and deionized water (DI water, pH = 5.59).....	33
2.4: a) Protonated (neutral) and deprotonated (negative charged) speciation of NXP with pKa= 4.15; b) protonated (neutral) and deprotonated (negative charged) speciation of IBP with pKa = 4.9	34
2.5: TYLA and TYLB undergo photoisomerization and photodecomposition.....	35
2.6: Direct photolysis of a) TYLA at pH = 5.06; b) TYLA at pH = 6.98; c) TYLA at pH = 9.05; d) TYLB at pH = 5.06; e) TYLB at pH = 6.98; f) TYLB at pH = 9.05	38
2.7: Comparison of photolysis at different pH a) TYLA; b) TYLB	39
2.8: NXP degradation with increasing oxidant [H ₂ O ₂ =0, 1,3 mM] at pH = 7	41
2.9: IBP degradation with increasing oxidant [H ₂ O ₂ =0, 1,3 mM] at pH = 7.....	43
2.10: Indirect photolysis of a) TYLA with 1mM H ₂ O ₂ ; b) TYLB with 1mM H ₂ O ₂ ; C) TYLA with 3mM H ₂ O ₂ ; d) TYLB with 3mM H ₂ O ₂	44
2.11 Comparison of indirect photolysis of a) TYLA; b) TYLB	45
2.12: UV-vis spectrum of Naproxen, Ibuprofen and tylosin in buffered solution (100 μM, pH = 7)	46
2.13: Linear regression analysis of a) NXP; (b) IBP; c) TYL	47
2.14: a) comparison of the calculated data vs. the experimental data for NXP; b) comparison of the calculated data vs. the experimental data for IBP.....	50
3.1: NXP photodegradation with NO ₃ ⁻ (332 μM) at pH = 7.....	64
3.2: IBP photodegradation with NO ₃ ⁻ (312 μM) at pH 7.....	65
3.3: Photodegradation with NO ₃ ⁻ (320 μM) at pH = 7 of a) TYLA; b) TYLB	67
3.4: Phototransformation with the presence of nitrate of a) TYLA and TYLAiso; b) TYLB and TYLBiso.	68

Figure	Page
3.5: NXP photodegradation with FA (~10 mg/L) and HA (~10 mg/L) (NXP Exp.7 and 8, pH = 7).....	70
3.6: IBP photodegradation with FA (~10 mg/L) and HA (~10 mg/L) (NXP Exp. 7 and 8, pH = 7).....	70
3.7: UV-vis spectra of a) 10 mg/L HA (—) and 10 mg/L FA (---); b) 100 μM NXP solution (—), 100 μM NXP solution with 10 mg/L HA (---) and 100 μM NXP solution with 10 mg/L FA (···); c) 100 μM IBP solution (—), 100 μM IBP solution with 10 mg/L HA (---) and 100 μM IBP solution with 10 mg/L FA (···).....	73
3.8: UV-vis spectra of 100 μM TYL solution (—), 100 μM TYL solution with 10 mg/L FA (---) and 100 μM TYL solution with 10 mg/L HA (···).....	75
3.9: Photodegradation a) TYLA with the presence of HA; b) TYLB with the presence of HA; c) TYLA with the presence of FA; d) TYLB with the presence of FA	77
3.10: Photodegradation of a) TYLA with FA; B) TYLA with HA; c) TYLB with FA; D) TYLB with HA.....	78
3.11: a) Direct and indirect NXP degradation with and without FA (~10 mg/L); b) Direct and indirect NXP degradation with and without HA (~10 mg/L); c) Direct and indirect IBP degradation with and without FA (~10 mg/L); d) Direct and indirect IBP degradation with and without HA (~10 mg/L)	80
3.12: Experimental and model comparisons for UV/H ₂ O ₂ degradation of a) NXP with FA; b) NXP with HA; c) IBP with FA; d) IBP with HA	84
3.13: Overall rate constants (k_d+k_i) as a function of oxidant concentration ([H ₂ O ₂]) and path length (z) of: a) NXP with FA; b) NXP with HA; c) IBP with FA; d) IBP with HA	86
3.14: The UV photodegradation fraction (f_d) as a function of oxidant concentration ([H ₂ O ₂]) and path length (z) of: a) NXP with FA; b) NXP with HA; c) IBP with FA; d) IBP with HA.....	88
4.1: The spectrum of photoproducts of NXP after direct photolysis. a) TIC spectrum; b) spectrum of peak A; c) spectrum of peak B	107
4.2: The spectrum of photoproducts of NXP after indirect photolysis. a) TIC spectrum; b) spectrum of product (VI).....	108
4.3: Possible pathways of NXP under UV and UV/H ₂ O ₂ conditions	109
4.4: The spectrum of photoproducts of IBP after direct photolysis. a) TIC spectrum; b) spectrum of product (XI); c) spectrum of product (X).....	111
4.5: The spectrum of photoproducts of IBP after indirect photolysis. a) TIC spectrum; b) spectrum of product (XII).....	112
4.6: Possible pathways of IBP under UV and UV/H ₂ O ₂ conditions	113
4.7: a) Chromatogram of TYL after 1min UV degradation; b) TIC chromatogram of TYL after 20 min UV treatment; c) Chromatogram of TYL after 1min UV /H ₂ O ₂ degradation.....	117
4.8: Mass spectra of parent compound and by products: a) TYLB; b) TYLB isomer; c) TYLA; d) TYLA isomer	119

ABSTRACT

He, Yang. M.S.E., Purdue University, December, 2013. Photochemical reactions of Naproxen, Ibuprofen and Tylosin. Major Professor: Inez Hua.

Pharmaceuticals and personal care products (PPCPs) include a wide range of compounds that are used extensively and sometimes daily by people. Some PPCPs have been detected in surface water (streams, rivers, lakes) due to incomplete removal in wastewater treatment plants. The water contaminated by PPCPs is harmful to aquatic organisms and human. Naproxen (NXP), ibuprofen (IBP) and tylosin (TYL) are chosen as representative PPCPs in the current research, because they are consumed in large quantities throughout the world and there is limited data about photodegradation of these compounds in aqueous solution at the wavelength of 254 nm.

The combination of ultraviolet light (UV_{254nm}) and hydrogen peroxide (H_2O_2) (UV/H_2O_2) degraded greater than 90% of the initial concentration of NXP and IBP within 3 min ($k = 0.018 \text{ sec}^{-1}$, $k = 0.023 \text{ sec}^{-1}$ for NXP and IBP, respectively). Under direct photolysis (UV_{254nm}) and at pH = 7, 20 min of treatment was required to obtain 90% degradation ($k = 0.0028 \text{ sec}^{-1}$ for NXP, $k = 0.0023 \text{ sec}^{-1}$ for IBP). Under the same conditions, molar absorptivity (ϵ) and quantum yield (ϕ) of each compound were determined (for NXP, $\epsilon = 4240 \text{ M}^{-1}\text{cm}^{-1}$ and $\phi = 0.008$; for IBP, $\epsilon = 299 \text{ M}^{-1}\text{cm}^{-1}$ and $\phi = 0.098$). Overall, degradation rate constants increased with increasing initial H_2O_2 level (0 mM, 1 mM and 3

mM) and increasing pH values (at pH =3, $k = 0.0016 \text{ sec}^{-1}$ for NXP and $k = 0.0015 \text{ sec}^{-1}$ for IBP; at pH =9, $k = 0.0036 \text{ sec}^{-1}$ for NXP and $k = 0.0029 \text{ sec}^{-1}$ for IBP). The presence of nitrate increased the photolysis rate constants of both NXP and IBP slightly due to hydroxyl radical formation from irradiation of nitrate. The rate constants were decreased because of screening light effect from the addition of natural organic matter (NOM): the rate constants were reduced by 18% and 36% for NXP and by 30% and 46% for IBP degradation with fulvic acid (FA) and humic acid (HA), respectively. To understand the mechanism of degradation under the $\text{UV}_{254\text{nm}}/\text{H}_2\text{O}_2$ with NOM, a model was constructed to predict the phototransformation rate constants of NXP and IBP. From the model results, it could be seen that there was a concentration of H_2O_2 corresponding to the maximum enhancement of photolysis of select PPCPs. The mineralization of NXP and IBP was 30% and 32%, respectively.

The degradation behaviors of TYL under $\text{UV}_{254 \text{ nm}}$ and $\text{UV}_{254\text{nm}}/\text{H}_2\text{O}_2$ were quite different from the degradation of NXP and IBP. TYL was present as a mixture of two compounds: TYL A and TYL B. Photoisomerization and photodegradation proceeded at the same time, and photoisomerization reactions predominated. A kinetic model was constructed for determining the kinetic data. Under $\text{UV}_{254\text{nm}}$ condition and at pH = 7, for TYLA, $k_f = 0.066 \text{ sec}^{-1}$, $k_r = 0.016 \text{ sec}^{-1}$, $k_d = 0.00057 \text{ sec}^{-1}$, and for TYLB, rate constant for forward reaction $k_f = 0.067 \text{ sec}^{-1}$, rate constant for backward reaction $k_r = 0.022 \text{ sec}^{-1}$ and degradation rate constant $k_d = 0.00040 \text{ sec}^{-1}$. Solution pH values and the presence of nitrate and NOM did not have any significant influences on the direct photolysis ($\text{UV}_{254\text{nm}}$) of TYL. Also at pH =7, the addition of H_2O_2 did not dramatically affect the photoisomerization reaction, but accelerated the photodegradation of TYL.

Selected major photochemical reaction by-products were identified by Gas Chromatography/Mass Spectroscopy (GC/MS) and Liquid Chromatography/Mass Spectroscopy (LC/MS). For both UV_{254nm} and UV_{254nm}/H₂O₂ conditions, the first step of NXP and IBP photodegradation is decarboxylation, then the intermediates were oxidized to ketone and other products. Possible pathways of NXP and IBP degradation are proposed. For TYL, photoisomerization results from the γ/δ rotation of bond of the ketodiene on the TYL ring.

CHAPTER 1. INTRODUCTION

1.1 Background

Surface water (lakes, rivers, and streams) is a necessary resource for human survival. Annually, the world's population is increasing by approximately 80 million people, which leads to a significant growth in demand for water [1]. It is estimated that, in 2005, in the United States roughly 44,200 million gallons of water were withdrawn each day for domestic use with 66 % of that from surface water, which is 2% more than the estimated amount of water withdraw from surface water in 2000 [2]. Therefore, the safety of surface water is imperative for public health and development.

Surface water receives continuous inputs of anthropogenic chemicals from contaminated by municipal, industrial and agricultural sources. Discharges containing substances from sewage treatment plants, factories and agricultural lands directly enter the water environment via outfall pipes or channels. Especially for pharmaceuticals, both unmetabolized and metabolized forms of drugs can enter surface water through sewage outfalls, or unused or expired drugs may simply be flushed down the drain. Moreover, storm and rain water runoff also bring pollutants to surface water by either dissolving the pollutants or carrying contaminated particles. Researchers and engineers have concentrated on removal of priority pollutants in surface water, such as persistent organic pollutants (POPs), toxic metals and radionuclides [3-5]. More recently, the attention and interests of

the scientific community have begun to shift to pharmaceutical and personal care products (PPCPs), since they have been detected in natural water system throughout the world [6-9].

PPCPs include a wide range of compounds, including shampoo, fragrances, laundry detergents, sun screen, painkillers, pesticides, nourishment (for example, huperzine A as food supplement) and diagnostic agents (e.g., X-ray contrast media) [10]. So, hospitals, farms, veterinary clinics, offices and homes are all sources of PPCPs. There is no doubt that PPCPs provide numerous benefits for treatment and prevention of disease to our society. Therefore, the production and use of PPCPs are in vast quantities. According to the report from National Community Pharmacists Association, in the United States, the annual usage of pharmaceuticals has grown from 2 billion to 3.9 billion tons between 1999 and 2009 [11]. Some pharmaceuticals are consumed in quantities greater than 100 tons every year in the European Union [12]. For example, in 2001, some non-steroidal anti-inflammatory chemicals are consumed in vast quantities [13]. For example, in Germany, the consumption of ibuprofen was 345 tons, acetylsalicylic acid was 836 tons, paracetamol was 622 tons, diclofenac was 86 tons, oral antidiabetic metformin was 517 tons and antiepileptic carbamazepine was 88 tons. Such production and consumption can lead to pollution if the compounds enter natural waters.

For over 30 years, it has been known that certain pharmaceutical compounds, such as nicotine, caffeine, and aspirin, have been known to enter the natural water system via treated wastewater [10]. Compared to other types of pollutants, PPCPs have a feature of comparatively low concentration in water but continual replenishment [13]. PPCPs, even at a low level, have shown to adversely affect the water quality, aquatic animals and human

health [14-16]. Exposure to surface waters contaminated with PPCPs could result in: abnormal reproduction [17-19], higher incidences of cancer [20], and the growth of antibiotic-resistant bacteria [21]. The adverse effects of NXP on human health include causing endocrine disruptions, which lead to change of hormonal actions [22]. IBP has been observed to cause disturbance of amphipoda and cnidarian [23], and negative impacts have been reported for human embryonic cells [24]. Water contaminated by TYL or other veterinary antibiotics could cause allergic reaction and teratogenic and carcinogenic effects [25]. The findings about PPCPs' influence on human health are of concern when considering their occurrence in our water resource. Moreover, some PPCPs are extremely persistent because of continual sewage effluents, which results in long term contamination for aquatic organisms and human.

So far, few classes of pharmaceutical compounds have been investigated. The degradation kinetics and the transformation fate of many PPCPs in the aquatic environment are poorly understood, and few studies concerning toxicology of PPCPs have been completed. In the U.S. and most other countries, there is no environmental monitoring for PPCPs nor are there regulatory limits on surface water concentrations of PPCPs [26]. Furthermore, most wastewater treatment plants (WWTPs) do not have special units to remove PPCPs. The removal of PPCPs in WWTPs generally depends on biological treatment tanks where PPCPs are eliminated by means of sorption on suspended particles or biological degradation [27]. However, many pharmaceuticals are difficult to eliminate in terms of their low biodegradability and highly hydrophilic nature. With incomplete removal in the WWTPs, PPCPs probably enter surface water. Thus, it is necessary to develop alternate technologies in order to effectively purify our scarce water resources.

UV and advanced oxidation process (AOP) technology are employed to decrease PPCPs by many researchers. Such processes as UV/H₂O₂, UV/O₃, UV/TiO₂ and UV/Fe²⁺ have been reported by many researchers [28-30] as ways to successfully degrade a variety of PPCPs. A few studies on investigating effectiveness of UV alone or UV/AOP for the most commonly detected PPCPs have been carried out. A study on degradation of selected PPCPs with UV/H₂O₂ and ozone was conducted by Vogna *et al.*[31]. This study showed that UV/H₂O₂ and ozonation were effective for degrading diclofenac. While in another study also reported by Vogna, UV was not effective for removing carbamazepine [31]. Kim *et al.*[32] conducted a study on UV degradation of 30 representative PPCPs with UV/H₂O₂ system, such as ketoprofen, propranolol, sulfamethoxazole, tetracycline, 17 α -ethinylestradiol (EE2), iopromide and indomethacin), evaluating kinetic rate constants values for these compounds. The average rate constants for all selected PPCPs were enhanced by a factor of 1.3 with the presence of H₂O₂. Canonica *et al.*[33] focused on the photolysis of selected compounds in water treatment plant for disinfection purpose. The authors showed that the decreased kinetic rates of PPCPs were due to dissolved organic matter (DOM) as light absorbers. However, in most studies, possible rate changes resulting from indirect photo-transformation are not taken into consideration. Moreover, the overall rate constants of degradation of PPCPs in complex water matrix are not predicted. There are relatively few publications on the removal of naproxen, ibuprofen and tylosin in aqueous solution at a $\lambda=254$ nm.

Thus, the research in this thesis explores the photoreaction mechanisms of decomposition of selected PPCPs (naproxen, ibuprofen and tylosin) by UV alone and in UV//H₂O₂ system. In addition, the research investigates the effects of different surface

water compositions and we determine the quantum yield for each compound. To precisely predict the photodegradation of selected PPCPs under UV and UV/H₂O₂ condition, a model is constructed. By-products studies and possible pathways are suggested in this thesis.

1.2 Pharmaceuticals and Personal Care Products (PPCPs)

Recently, there is an increasing concern about the occurrence of PPCPs in source for drinking water. These organic compounds are released into aquatic environment as a consequence of their extensive use in medical care, industry, agriculture and consumer goods. The target compounds in this research are naproxen, ibuprofen and tylosin due to their relatively high level to other PPCPs in water and incomplete removal in wastewater treatment plants [6, 34-36].

1.2.1 Naproxen (NXP)

Naproxen, (+)-(S)-2-(6-methoxynaphthalen-2-yl) propanoic acid (molecular formula C₁₄H₁₄O₃), is an anti-inflammatory drug frequently used for reduction of fever, inflammation and pain [37, 38]. It can be bought over the counter.

It has a molecular weight (MW) of 230.26 g/mol, and CAS # 22204-53-1. The structure is illustrated in the Figure 1.1. The solid material is an off-white crystalline powder without odor. It has a boiling point = 403.9 °C and melting point = 143-154 °C at 760mmHg; a density of 1.197 g/cm³ at 25 °C[39]. It is lipid-soluble (e.g. chloroform, dehydrated alcohol), and sparingly soluble in ether; in aqueous solution, the solubility of NXP is low at low pH, and it is soluble in water at high pH. It is reported that the aqueous

solubility of naproxen is $100\mu\text{M}$ at $25\text{ }^\circ\text{C}$. Its half-life is from 3.9 to 15.1 days in the biosolid systems. The pK_a of the chemical is 4.15 and $\log P_{\text{ow}}$ (octanol/water) is 3.18.

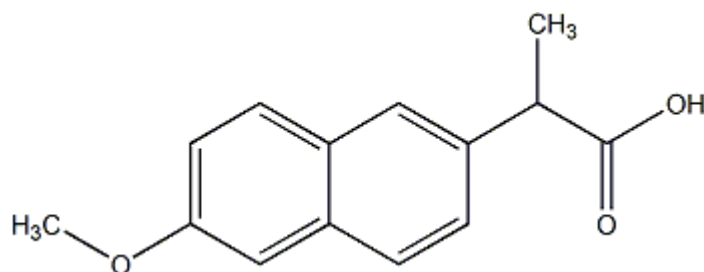


Figure 1.1: Chemical structure of NXP

Naproxen has been detected in natural aqueous environments with range from 0.000043 to $0.0043\ \mu\text{M}$ [35, 40, 41], and in WWTPs effluents with range of 0.00043 to $0.011\ \mu\text{M}$ [40, 42].

1.2.2 Ibuprofen (IBP)

Ibuprofen, (molecular formula $\text{C}_{13}\text{H}_{18}\text{O}_2$), 2-(4-(2-methylpropyl) phenyl) propanoic acid, is an alkybenzene with a carboxylic acid. Ibuprofen is also a non-steroidal anti-inflammatory drug (NSAID) used as pain killer and fever reduction [43].

Ibuprofen's molecular weight is $206.3\ \text{g/mol}$ and CAS #15687-27-1. The structure is illustrated in the Figure 1.2. The appearance of solid material is white or almost white crystalline powder. The appearance of solid material is white or almost white crystalline powder. It has a density of $1.03\ \text{g/cm}^3$; melting point = $75\text{-}78\text{ }^\circ\text{C}$ and boiling point = $157\text{ }^\circ\text{C}$ (4 mmHg). Ibuprofen is almost insoluble in water, with solubility less than $200\ \mu\text{M}$ [44]. The pK_a is 4.8, and log octanol /water partition coefficient (K_{ow}) is 2.48 at pH 7 [45].

It is reported that approximately 70% on a mass basis of ibuprofen ingested by human

is metabolized in the human body. Despite this loss, the concentrations of ibuprofen are detected in WWTP effluent as high as 0.015 mM [45].

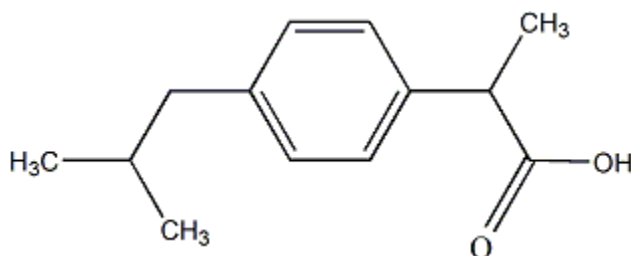


Figure 1.2: Chemical structure of ibuprofen

1.2.3 Tylosin (TYL)

Tylosin (molecular formula C₄₆H₇₇NO₁₇) is a widely use veterinary growth promoter for swine and poultry. Tylosin has been reported to appear in surface water through the U.S. [7].

The reagent form in this study is tylosin tartrate (CAS1405-54-5), a mixture of tylosin A (TYLA, CAS# 8026-48-0) and tylosin B (TYLB, CAS # 11032-98-7). Molecule weight is 916 g/mol for TYLA, and 772 g/mol for TYLB. The appearance of tylosin tartrate is a white crystal. TYLA is the main component, and TYLB is a compound corresponding to loss of one sugar moiety from TYLA. Figure 1.3 illustrates the chemical structure of tylosin compounds.

In aqueous solution, it is stable at pH 5.5~7.5. If the pH is below 4, the compound will be degradation due to acid hydrolysis. pK_a is 7.15 and logK_{ow} is 1.63 [46]. Tylosin tartrate has a density of 1.24 g/cm³, boiling point = 980.7 °C at 760 mmHg and the melting point = 128~132 °C.

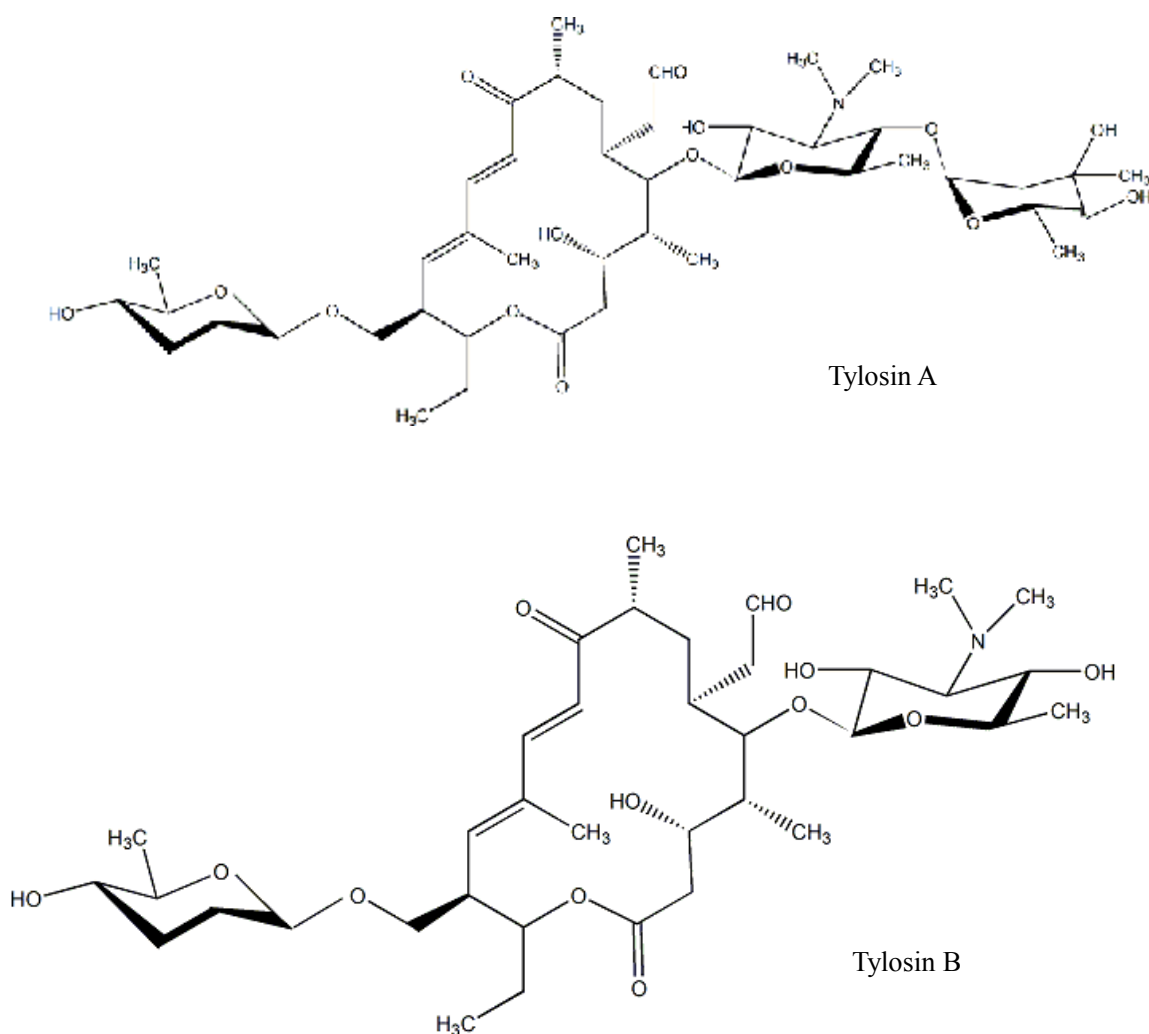


Figure 1.3: Chemical structures of TYL A and TYLB

Tylosin has been reported to appear in surface water through the U.S. [7]. In the report “A First Assessment of Pharmaceuticals and Personal Care Products in the Middle Wabash, River, Indiana” [47], there were three sites in Wabash river selected to represent different concentration in the surface water. Tylosin was detected in all sites with level of $2.52 \pm 1.5 \mu\text{g/L}$, range of $0.05 - 6.1 \mu\text{g/L}$ [47].

1.3 Photochemistry

Photochemistry is the study of chemical reactions and physical processes that occur after molecules absorb light [48]. If a molecule absorbs light, no matter ultraviolet or visible light, electrons are promoted from the ground state to a higher energy state. In other words, the molecule becomes a reactive species. In aqueous solution, photochemical transformations of the target compounds (NXP, IBP and TYL) may occur via two pathways: direct photolysis or indirect photolysis. Direct photolysis occurs when the photochemically excited species undergoes chemical reactions to form products. Indirect photolysis involves transformation of a target chemical resulting from light absorption by other constituents.

Quantitative determination of light absorption is described by two empirical laws, Lambert's law and Beer's law. From these two classic laws, the well-known Beer-Lambert law is developed to demonstrate how the transmission (T) of a photon moves through water or air medium with the amount of light absorbed (A) by a chemical that also exists in the medium [48].

When the photons of light are absorbed by a reactive chemical in the media, the Beer-Lambert Law could be written as

$$A = \epsilon \cdot [C] \cdot l \quad (1.1)$$

The equation means that the absorbance (A) of the transmitted light is proportional to the concentration of the chemical ([C], M) and the chemical molar absorptivity (ϵ) through a specific transmittance path length (l , cm).

1.3.1 Direct photolysis

Generally, in a homogeneous media, the chemicals can react directly with incoming light. Some chromophores that consist of functional groups on the molecule absorb light directly so that the molecules become “excited” as a result of the transition of the electrons. Since the excited state cannot exist for a long time, the excited electrons need to return to the ground state by releasing energy. Therefore, when a compound is in an excited state, there are several chemical or physical processes that the excited compound may undergo. These processes include re-arrangement of chemical bonds (degradation to form some by-products), heat transfer, luminescence, isomerization, and electrons transfer between chemicals.

The quantum yield Φ , that defines the fraction of the total number of photons absorbed at a given wavelength that promote the molecules to excited state, is calculated as [48]:

$$\Phi_{\lambda} = \frac{\text{\#of molecules reacted}}{\text{total\# of molecules excited by absorption of irradiation of wavelength } \lambda} \quad (1.2)$$

We also define the rate of light absorbance at wavelength λ as $I_a(\lambda)$ (units of einstein per second), which is discussed in Appendix A. The product of Φ and $I_a(\lambda)$ denotes the concentration of compound phototransformed over time [48].

Rate of direct photolysis at wavelength λ :

$$-\frac{dC}{dt} = \Phi(\lambda)I_a(\lambda) = \Phi(\lambda)k_a(\lambda)C = k(\lambda)C \quad (1.3)$$

Where k_a (einstein mole⁻¹ sec⁻¹) is the specific rate of light absorption $k_a(\lambda)C = I_a(\lambda)$, and k (sec⁻¹) is the direct photolysis rate constant at wavelength λ . However, no rules are developed for obtaining quantum yields values from chemical structure, so Φ values are generally determined with experimental data.

1.3.2 Indirect photolysis

Some additional photochemical reactions may be initiated by interactions of the target compound with free-radical or reactive species generated through light absorption by oxidants or other species such as natural organic matter, which is referred to as the indirect photolysis. According to Table 1.1, the reactive species are rather strong oxidants compared to $^3\text{O}_2$, so they can oxidize pollutants in parallel to direct photolytic reactions. These reactive species are short-lived and at very low concentrations also because of their high reactivity.

Table 1.1 Standard One-Electron Reaction Potentials, E_{H}^1 in water at 25 °C of some common oxidants [48].

Oxidant	Reaction in water	E_{H}^1/V
$\text{HO}\cdot$	$\text{HO}\cdot + \text{e}^- = \text{HO}^-$	1.9
$\text{O}_3\cdot$	$\text{O}_3\cdot + \text{e}^- = \text{O}_3^-$	1
$^1\text{O}_2$	$^1\text{O}_2 + \text{e}^- = \text{O}_2^-$	0.83
$^3\text{O}_2$	$^3\text{O}_2 + \text{e}^- = \text{O}_2^-$	-0.16
$\text{NO}_3\cdot$	$\text{NO}_3\cdot + \text{e}^- = \text{NO}_3^-$	2.3

As a result, reactions between target organic pollutants and reactive species in solution can form more possible intermediates. The current research focuses on evaluating phototransformation rates of selected PPCPs under the UV and UV/ H_2O_2 condition and suggestion of possible pathway.

1.3.3 Advanced Oxidation Processes (AOPs)

Generally, advanced oxidation processes (AOPs) refer to a series of chemical reactions used to oxidize organic materials in aqueous solution through interaction with hydroxyl radicals ($\cdot\text{OH}$) generated from irradiated oxidants. Oxidants must be

photosensitive for the degradation to occur. In this research, the system where H₂O₂ is exposed to light at $\lambda = 254$ nm can produce $\cdot\text{OH}$, because the energy at this wavelength is sufficient to break bonds within hydrogen peroxide molecules (H₂O₂). The reaction of H₂O₂ at $\lambda = 254$ nm is described as below [49]:



1.3.4 Kinetics

The photolysis reaction rate (k), in which the concentration of a compound decreases over time (t), can generally be assumed to follow the first-order rate law [48, 50]. The pseudo-first order rate constant can be expressed as:

$$d[C]/dt = -k[C] \quad (1.5)$$

Subsequently, integrating of equation above can result in a logarithm of the ratio of $[C]_t/[C]_0$, which plotted with respect to time, is a straight line with a slope of $-k$ representing the rate constant.

1.4 Objectives

1. Determine the reaction conditions that promote the fastest degradation of NXP, IBP and TYL. Several factors include pH, H₂O₂ concentration, nitrate and natural organic matter (fulvic acid and humic acid) are varied.
2. Calculate aqueous phase molar absorptivity and quantum yield of NXP, IBP and TYL, under direct photolysis condition at 254 nm.

3. Identify major degradation products under direct (UV) and indirect (UV/H₂O₂) condition and suggest possible degradation pathways.
4. Model PPCPs photodegradation base on some fundamental parameters to predict the degradation.

The research framework is outlined in the figure below.

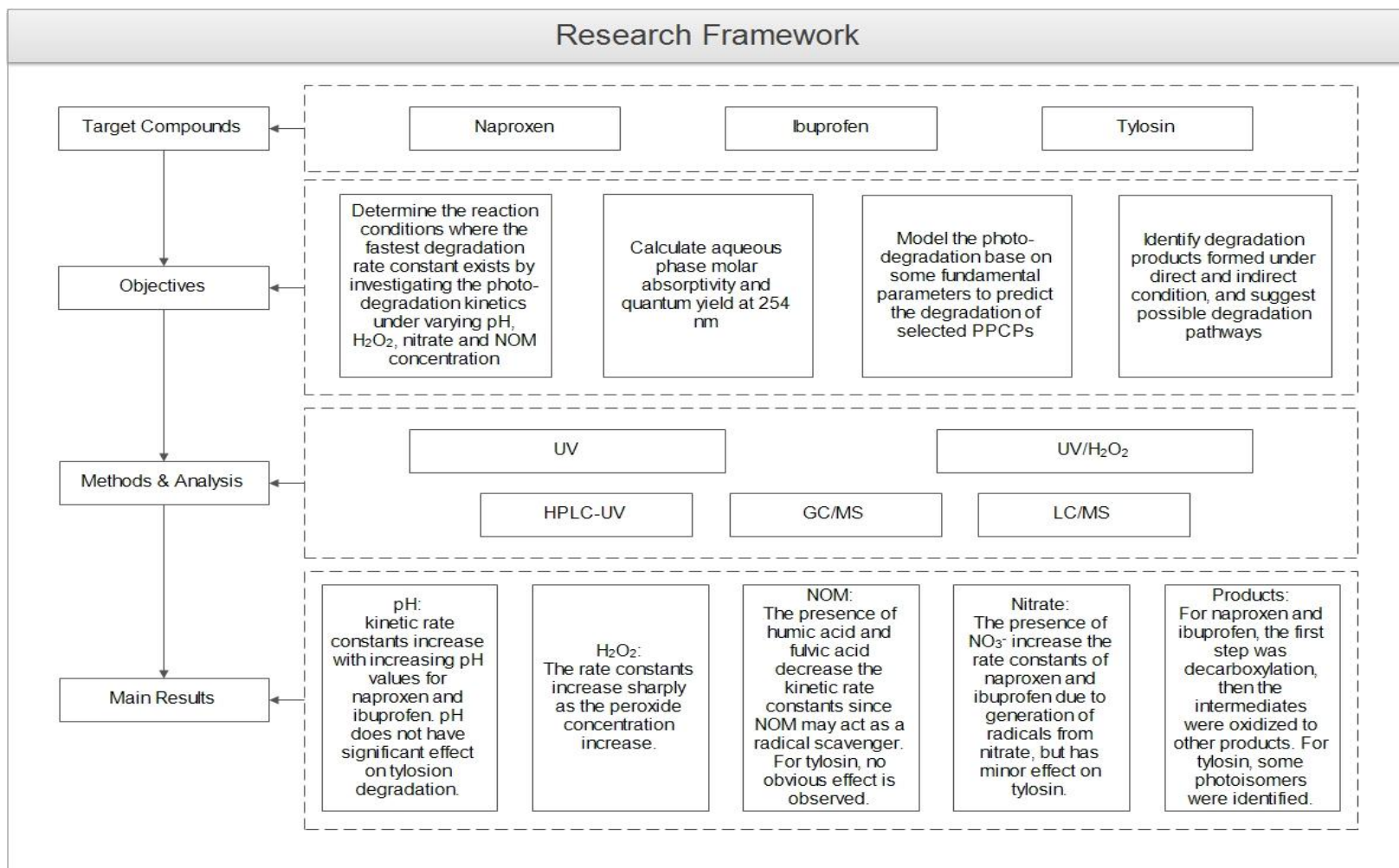


Figure 1.4: Research Framework

List of References

1. Kunzig, R., Population 7 Billion. national geographic, 2011.
<http://ngm.nationalgeographic.com/2011/01/seven-billion/kunzig->.
2. Joan F. Kenny, N.L.B., Susan S. Hutson, Kristin S. Linsey, and a.M.A.M. John K. Lovelace, Estimated Use of Water in the United States in 2005. U.S. Department of the Interior, U.S. Geological Survey, 2005.
3. Olli, J.J., et al., Removal of persistent organic pollutants from Atlantic salmon (*Salmo salar* L.) diets: Influence on growth, feed utilization efficiency and product quality. *Aquaculture*, 2010. **310**(1–2): p. 145-155.
4. Huang, L., C. Xiao, and B. Chen, A novel starch-based adsorbent for removing toxic Hg(II) and Pb(II) ions from aqueous solution. *Journal of Hazardous Materials*, 2011. **192**(2): p. 832-836.
5. Hosseini, A., et al., Review of research on impacts to biota of discharges of naturally occurring radionuclides in produced water to the marine environment. *Science of The Total Environment*, 2012. **438**(0): p. 325-333.
6. Ternes, T.A., Occurrence of drugs in German sewage treatment plants and rivers. *Water Research*, 1998. **32**(11): p. 3245-3260.
7. Kolpin, D.W., et al., Pharmaceuticals, Hormones, and Other Organic Wastewater Contaminants in U.S. Streams, 1999–2000: A National Reconnaissance. *Environmental Science & Technology*, 2002. **36**(6): p. 1202-1211.

8. Nikolaou, A., S. Meric, and D. Fatta, Occurrence patterns of pharmaceuticals in water and wastewater environments. *Analytical & Bioanalytical Chemistry*, 2007. **387**(4): p. 1225-1234.
9. Daughton, C.G. and T.A. Ternes, Pharmaceuticals and Personal Care Products in the Environment: Agents of Subtle Change? *Environmental Health Perspectives*, 1999. **107**: p. 907-938.
10. Tools for tracking antibiotic resistance. 2011. **119**(5): p. A214(4).
11. Tong, A.Y.C., B.M. Peake, and R. Braund, Disposal practices for unused medications around the world. *Environment International*, 2011. **37**(1): p. 292-298.
12. Nikolaou, A., S. Meric, and D. Fatta, Occurrence patterns of pharmaceuticals in water and wastewater environments. *Analytical and Bioanalytical Chemistry*, 2007. **387**(4): p. 1225-1234.
13. Fent, K., A.A. Weston, and D. Caminada, Ecotoxicology of human pharmaceuticals. *Aquatic Toxicology*, 2006. **76**(2): p. 122-159.
14. Heberer, T., Tracking persistent pharmaceutical residues from municipal sewage to drinking water. *Journal of Hydrology*, 2002. **266**(3-4): p. 175-189.
15. Roefer, P., et al., Endocrine-disrupting chemicals in a source water. *Journal (American Water Works Association)*, 2000. **92**(8): p. 52-58.
16. Trussell, R.R., Endocrine disruptors AND THE WATER INDUSTRY. *Journal (American Water Works Association)*, 2001. **93**(2): p. 58-65.
17. Purdom, C.E., et al., Estrogenic Effects of Effluents from Sewage Treatment Works. *Chemistry and Ecology*, 1994. **8**(4): p. 275-285.

18. White, R., et al., Environmentally persistent alkylphenolic compounds are estrogenic. *Endocrinology*, 1994. **135**(1): p. 175-82.
19. Jobling, S., et al., Widespread Sexual Disruption in Wild Fish. *Environmental Science & Technology*, 1998. **32**(17): p. 2498-2506.
20. van der Werf, H.M.G., Assessing the impact of pesticides on the environment. *Agriculture, Ecosystems & Environment*, 1996. **60**(2-3): p. 81-96.
21. Smith, K.E., et al., Quinolone-resistant *Campylobacter jejuni* infections in Minnesota, 1992-1998. *New England Journal of Medicine*, 1999. **340**(20): p. 1525-1532.
22. Suarez, S., J.M. Lema, and F. Omil, Removal of Pharmaceutical and Personal Care Products (PPCPs) under nitrifying and denitrifying conditions. *Water Research*, 2010. **44**(10): p. 3214-3224.
23. Quinn, B., F. Gagné, and C. Blaise, The effects of pharmaceuticals on the regeneration of the cnidarian, *Hydra attenuata*. *Science of The Total Environment*, 2008. **402**(1): p. 62-69.
24. Pomati, F., et al., Effects of a Complex Mixture of Therapeutic Drugs at Environmental Levels on Human Embryonic Cells. *Environmental Science & Technology*, 2006. **40**(7): p. 2442-2447.
25. Halling-Sørensen, B., et al., Occurrence, fate and effects of pharmaceutical substances in the environment- A review. *Chemosphere*, 1998. **36**(2): p. 357-393.
26. Daughton, C.G., Pharmaceuticals and Personal Care Products in the Environment: Overarching Issues and Overview. <http://www.epa.gov/esd/bios/daughton/book-summary.htm>.

27. Nghiem, L.D., A.I. Schäfer, and M. Elimelech, Pharmaceutical Retention Mechanisms by Nanofiltration Membranes. *Environmental Science & Technology*, 2005. **39**(19): p. 7698-7705.
28. Yuan, F., et al., Degradation of selected pharmaceuticals in aqueous solution with UV and UV/H₂O₂. *Water Research*, 2009. **43**(6): p. 1766-1774.
29. Santoke, H., et al., Advanced oxidation treatment and photochemical fate of selected antidepressant pharmaceuticals in solutions of Suwannee River humic acid. *Journal of Hazardous Materials*, 2012. **217-218**: p. 382-390.
30. Wols, B.A.H.-C., C.H.M., Review of photochemical reaction constants of organic micropollutants required for UV advanced oxidation processes in water. *Water Research*, 2012. **46**(9): p. 2815-2827.
31. Vogna, D., et al., Kinetic and chemical assessment of the UV/H₂O₂ treatment of antiepileptic drug carbamazepine. *Chemosphere*, 2004. **54**(4): p. 497-505.
32. Kim, I., N. Yamashita, and H. Tanaka, Photodegradation of pharmaceuticals and personal care products during UV and UV/H₂O₂ treatments. *Chemosphere*, 2009. **77**(4): p. 518-525.
33. Canonica, S., L. Meunier, and U. von Gunten, Phototransformation of selected pharmaceuticals during UV treatment of drinking water. *Water Research*, 2008. **42**(1-2): p. 121-128.
34. Gross, B., et al., Occurrence and fate of pharmaceuticals and alkylphenol ethoxylate metabolites in an effluent-dominated river and wetland. *Environmental Toxicology and Chemistry*, 2004. **23**(9): p. 2074-2083.

35. Tixier, C., et al., Occurrence and Fate of Carbamazepine, Clofibric Acid, Diclofenac, Ibuprofen, Ketoprofen, and Naproxen in Surface Waters. *Environmental Science & Technology*, 2003. **37**(6): p. 1061-1068.
36. Hilton, M.J. and K.V. Thomas, Determination of selected human pharmaceutical compounds in effluent and surface water samples by high-performance liquid chromatography–electrospray tandem mass spectrometry. *Journal of Chromatography A*, 2003. **1015**(1–2): p. 129-141.
37. Daughton, C.G., Cradle-to-Cradle Stewardship of Drugs for Minimizing Their Environmental Disposition While Promoting Human Health. II. Drug Disposal, Waste Reduction, and Future Directions. *Environmental Health Perspectives*, 2003. **111**(5): p. 775-785.
38. Damiani, P., M. Bearzotti, and M.A. Cabezón, Spectrofluorometric determination of naproxen in tablets. *Journal of Pharmaceutical and Biomedical Analysis*, 2002. **29**(1–2): p. 229-238.
39. *Pharmaceuticals and Care Products in the Environment*. ACS Symposium Series. Vol. 791. 2001: American Chemical Society. 420.
40. Stumpf, M., et al., Polar drug residues in sewage and natural waters in the state of Rio de Janeiro, Brazil. *Science of The Total Environment*, 1999. **225**(1–2): p. 135-141.
41. Metcalfe, C.D., et al., Occurrence of neutral and acidic drugs in the effluents of Canadian sewage treatment plants. *Environmental Toxicology and Chemistry*, 2003. **22**(12): p. 2872-2880.

42. Boyd, G.R., et al., Pharmaceuticals and personal care products (PPCPs) and endocrine disrupting chemicals (EDCs) in stormwater canals and Bayou St. John in New Orleans, Louisiana, USA. *Science of The Total Environment*, 2004. **333**(1–3): p. 137-148.
43. Vanesch, A.V., HA, Steyerberg, EW; Offringa M; Habbema, JDF; Derksenlubsen, G, Antipyretic efficacy of ibuprofen and acetaminophen in children with febrile seizures. *Archives of pediatrics & adolescent medicine*, 1995. **149**(6): p. 6.
44. Jacobs, L.E., et al., Fulvic acid mediated photolysis of ibuprofen in water. *Water Research*, 2011. **45**(15): p. 4449-4458.
45. Scheytt, T., et al., 1-Octanol/Water Partition Coefficients of 5 Pharmaceuticals from Human Medical Care: Carbamazepine, Clofibrac Acid, Diclofenac, Ibuprofen, and Propyphenazone. *Water, Air, and Soil Pollution*, 2005. **165**(1-4): p. 3-11.
46. Sepulveda, M.S., A First Assessment of Pharmaceuticals and Personal Care Products in the Middle Wabash River, Indiana. Final Report to the IWRRC, 2010.
47. Sepulveda, M.S., A First Assessment of Pharmaceuticals and Personal Care Products in the Middle Wabash River, Indiana U.S. Geological Survey, 2011.
48. Schwarzenbach, R.P., P.M. Gschwend, and D.M. Imboden, Direct Photolysis, in *Environmental Organic Chemistry*. 2005, John Wiley & Sons, Inc. p. 611-654.
49. Crittenden, J.C., *Water treatment : principles and design*. 2005.
50. *The Kinetics of Environmental Aquatic Photochemistry*. *Analytical Chemistry*, 1989. **61**(3): p. 220A-220A.

CHAPTER 2. UV/H₂O₂ ENHANCED PHOTOCHEMICAL REACTION OF SELECTED PPCPs: KINETICS, MOLAR ABSORPTIVITY AND QUANTUM YIELD

2.1 Introduction

Studying the environmental fate of pharmaceutical and personal care products (PPCPs) is of importance due to their continued and extensive use. It is reported that the total number of pharmaceuticals being used is greater than 3000 worldwide [1], and some individual drugs are consumed in quantities of more than 100 tons per year in the European Union [2]. These PPCPs are released directly or indirectly to environmental waters. For example, some unused and expired drugs are probably disposed to sewage systems, and then enter aquatic environments after going through wastewater treatment processes where there is no specific unit to remove PPCPs [3]. Body lotions or sunscreen may be directly released to waters via swimming or washing, and synthetic pesticides and fertilizers are sprayed onto measured sites on farms, and washed out to rivers by rains [4] or infiltrated into groundwater and eventually connect to surface water.

To obtain the information on their occurrence in aquatic environment, many countries conducted reconnaissance to measure the concentrations of different kinds of PPCPs. The findings are summarized in the Table 2.1. For tylosin, there was relatively little information about the occurrence, since detection and quantification of this

macrolide antibiotic is challenging. As analytical methods have developed, tylosin has been easier to detect and has been found in various streams throughout the U.S [5].

Table 2. 1 Summary of occurrence of PPCPs.

PPCPs	Location	Range of Detection Level ($\mu\text{g/L}$)	Reference
Salicylic acid	Canada	0.05	[6]
	Galicia ,Spain	3.6	[7]
Diclofenac	Switzerland	0.31–0.93	[8]
	Madrid, Spain	1.9	[9]
	Finland	0.17–0.35	[10]
Ibuprofen	Galicia ,Spain	0.9–2.1	[7]
	Switzerland	0.6–0.8	[11]
	United States	0.01–0.02	[12]
Naproxen	Canada	12.5	[6]
	United States	0.023	[12]
	Brazil	0.1–0.54	[13]
	Finland	0.15–1.9	[10]
Clofibric acid	Brazil	0.68–0.88	[13]
	Switzerland	0.15–0.25	[11]
Diazepam	Netherlands	0.1–0.66	[14]
Tylosin	Indiana, United States,	0.05 – 6.1	[15]
	Michigan, United States	0.020-0.030	[16]

There is limited available literature specifically focusing on the degradation and environmental fate of the PPCPs in water environments. Some studies on the elimination efficiency are mainly based on measurements of influent and effluent concentrations in wastewater treatment plants. It is reported that the average removal efficiencies for carbamazepine are 7% to 8% [8], up to 26% for diclofenac [10] and 30% for naproxen [13]. Due to the relatively low removal rate by conventional wastewater treatment plants, it is desirable to develop an easier and efficient method to degrade these pharmaceuticals.

Various technologies have been applied to remove PPCPs. In a paper by Joss *et al.*, diclofenac and naproxen were reported to be partially removed by biological methods [17]. In the experiments conducted by Zwiener *et al.*, ozone could react with a few specific types

of pharmaceuticals. They observed that 97% of diclofenac decomposes, but only 12% of ibuprofen decay after the same time interval [18]. Membrane bioreactors (MBR) were also employed to eliminate some PPCPs, resulting in 50% removal of diclofenac and 80% removal of naproxen [19].

Thus, the current study concentrated on photodegradation of PPCPs in a homogeneous aqueous buffered solution. This chapter is a discussion of the following study goals: evaluate UV and UV/H₂O₂ photochemical degradation kinetics under variable conditions: i) pH (~3, 7, 9) and H₂O₂ concentration (0, 1, 3mM), and ii) for each compound, the molar absorptivity and quantum yield at $\lambda = 254$ nm were determined.

2.2 Materials and Methods

2.2.1 Rayonet 100 UV Reactor

All irradiation experiments were conducted in a Rayonet 100 photochemical reactor (From Southern New England Ultraviolet Company). The photo-reactor was equipped with 8 UV lamps which emitted monochromatic light at a wavelength of 253.7 nm. Each lamp was 26 cm long and 1.4 cm in diameter. The lamps were placed 11 cm equidistantly across the width of the reactor (22 cm). Experimental samples in quartz tubes were positioned vertically on a merry-go-round. The photo-reactor was placed in a laboratory grade fume hood with a blackout curtain to ensure safe operation and no light interference. Additionally, fluorescent lights in the lab remained off during all experiments. Chemical actinometry

(methods discussed in Appendix A) was applied to measure the incident light intensity of the UV reactor.

2.2.2 Chemicals

Naproxen (NXP, grade 98%), ibuprofen (IBP, grade 98%), tylosin tartrate (>98%) and spiramycin (SPI, >98%) were purchased from sigma-Aldrich Chemical Co. and used without further purification. Hydrogen peroxide (H₂O₂, 30% by weight) was purchased from Mallinckrodt Pharmaceuticals and used as received. All solvents (acetonitrile and methanol) and inorganic chemicals (85% H₃PO₄, >98% K₂HPO₄, >99% KH₂PO₄, and >98% Na₃PO₄) were obtained from Mallinckrodt Pharmaceuticals and used as received. Hydrochloric acid (HCl, 0.01N) and sodium hydroxide (NaOH, >97%) were obtained from Fisher Scientific Inc. and used to adjust the pH of solution.

2.2.3 Preparation of aqueous PPCPs solution and standards

Phosphate buffers were prepared at pH values of 2.98, 6.97 and 9.01 by mixing the solid phosphate salts and phosphoric acid. The concentrations of buffer solutions were 3.45mM KH₂PO₄ and 1.55 mM H₃PO₄ for pH = 2.98; 2.30 mM K₂HPO₄ and 2.69 mM KH₂PO₄ for pH = 6.97; and 0.036 mM K₂HPO₄ and 4.96 mM Na₃PO₄ for pH = 9.01. Water for all aqueous solutions was purified through a Barnstead NanoPure system with a background electrolyte resistance to less than 18 M.Ω cm⁻¹.

500 μM stock solutions were prepared by dissolving the parent compounds (NXP, IBP or TYL) in different pH buffer solutions. The stock solutions were kept at 4 °C and

equilibrated to room temperature before use. The working solutions of NXP, IBP and TYL with initial concentrations of 100 μM were prepared by diluting the stock solutions with corresponding buffer solutions, respectively. All solutions were stored at 4°C in the amber flasks and equilibrated to room temperature before experiments.

500 μM NXP was used as internal standard (IS) for IBP, and 500 μM IBP was used as an IS for NXP. A stock solution of 500 μM SPI, used as IS for TYL, was also prepared and stored as described above.

2.2.4 Experimental Procedures

Before each experiment, 2 mL working solution was removed using a volumetric pipette and transferred into a 2 mL HPLC vial to determine the exact initial concentration (C_0) by HPLC. Each 10 mL aliquot of equilibrated aqueous PPCPs solution was transferred into a quartz reaction tube, then all the tubes were suspended on the merry-go-round. At each sampling time, the merry-go-round was stopped, but the lamps were not turned off. The entire 10 mL sample volume from one quartz tube was transferred to an amber vial and 200 μL methanol (as quenching reagent) was added in the vial immediately.

For experiments with H_2O_2 , the appropriate amount of a 30% H_2O_2 was added to the PPCPs working solution by volumetric pipette and mixed thoroughly before irradiation. At subsequent time intervals, a tube containing 10 mL sample was removed from the photoreactor and the solution was transferred to an amber vial. For kinetics calculation, 200 μL methanol was added to the amber vial immediately. 10 mL aliquots of Dark Control (DC, working solution with H_2O_2) and 10 mL aliquots of blank samples (buffered solution

with H₂O₂) were taken for each time point and kept in amber vials. 200 µL of methanol was also added to each DC and blank sample. Dark control samples were covered by aluminum foil while they were in the photoreactor.

Seventeen experiments are described in this chapter, and each experiment is assigned with a qualifier and number, i.e. NXP Exp.1.

2.2.5 Analytical Methods

2.2.5.1 High Performance Liquid Chromatography (HPLC)

Before HPLC analysis, IS was added to each sample. 2 mL of 500 µM IS was added to 10 mL volumetric flask, then 2 mL sample was transferred into the same volumetric flask, and diluted with buffer solution to the volume. The linearity of selected PPCPs was evaluated over the range 5-100 µM in buffer solution containing 100 µM of IS. The standard curves were plots of the PPCPs-IS peak area ratio (f) vs. PPCPs concentration. For TYL experiments, the concentrations of TYLA_{iso} and TYLB_{iso} were calibrated using the relative HPLC response (peak areas), assuming a 1:1 transformation of TYLA/B to its isomer. Samples were transferred into ~2 mL amber HPLC vials, labeled and stored at 4°C until analysis.

Quantification of PPCPs concentration was obtained with Shimadzu HPLC (UV detector: SPD 10Ai; Autosampler: SIL 10A; 10 Pump: LC 10A). Compounds separation was achieved by using a Restek revers-phase C18 column (150 mmx3.2mmID, 3µM), with a guard column (7.5x4.6 mm) from Grace Company. For NXP and IBP, an isocratic elution

was performed with 45%:55% mixture of phosphate buffer (pH3): acetonitrile at a constant flow rate of 1.0 mL min⁻¹. For tylosin, the mobile phase A was water with 0.1% formic acid solution, and the mobile phase B was acetonitrile. A gradient elution with 90% A and 10% B for the first 10 min, and 60% A and 40% B during 10-35 min was adopted. The percentages of each solvent discussed in this section were by volume. The flow rate was 1 mL min⁻¹. The injection volume was 20 µL for all samples. Based on absorption spectra of each compound in buffered solution, the UV detector was set at 230 nm for NXP, 223 nm for IBP, 289 nm for TYL, and 232 nm for SPI, respectively.

2.2.5.2 UV-vis spectrometer

UV spectrum profiles of the compounds were obtained by Cary 100 UV-vis spectrophotometer in a 1 cm quartz cuvette.

2.3 Kinetics

2.3.1 Results and Discussion

All pseudo-first order kinetics rate constants (k) of NXP and IBP presented in this chapter were determined from weighted least-squares analysis of the raw experimental data. For TYLA and TYLB, the kinetic rate constants are estimated by a model that will be discussed in Section 2.3.2.2. Table 2.2 summarizes the rate constants for the experiments. Figure 2.1 depicts a representative photo-degradation of selected PPCPs.

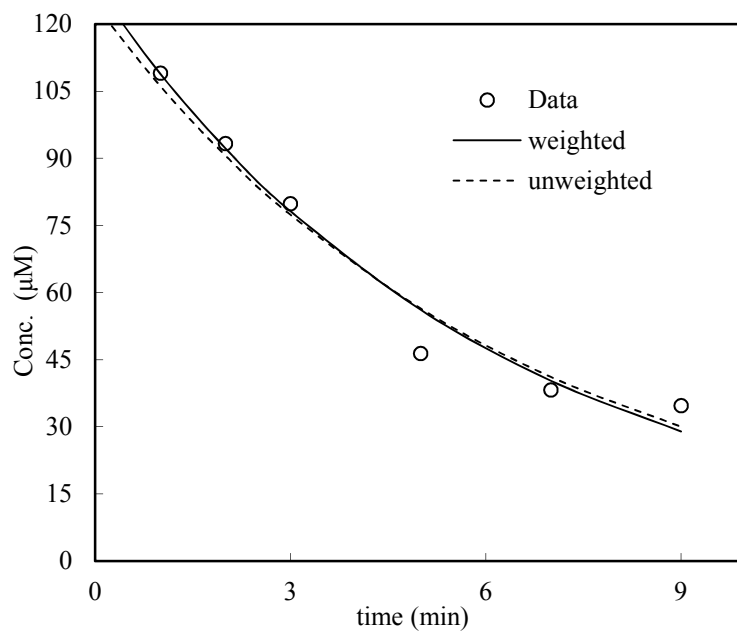


Figure 2.1: Degradation of Naproxen (NXP Exp.1) at $\text{pH} = 7$ within 9 minutes

Table 2.2 NXP, IBP and TYL degradation rate constants.

	Exp #	C _o (μM)	pH	H ₂ O ₂ (mM)	k (sec ⁻¹)
Naproxen (NXP)	1	108.83	7	0	0.0028 (R ² =0.98)
	2	103.81	3	0	0.0016 (R ² =0.96)
	3	98.52	9	0	0.0036 (R ² =0.97)
	4	123.99	7	1	0.0094 (R ² =0.95)
	5	127.41	7	3	0.018 (R ² =0.99)
Ibuprofen (IBP)	1	106.32	7	0	0.0023 (R ² =0.99)
	2	114.55	3	0	0.0015 (R ² =0.98)
	3	100.05	9	0	0.0029 (R ² =0.97)
	4	118.17	7	1	0.013 (R ² =0.99)
	5	117.68	7	3	0.023 (R ² =0.99)
Tylosin (TYL)	1	TYLA: 64.36 TYLB: 33.64	7	0	k _f =0.064 k _r =0.017 k ₁ =0.00018 k ₂ =0.00095 k _f =0.068 k _r =0.022 k ₁ =0.00018 k ₂ =0.00073
	2	TYLA:64.59 TYLB: 33.57	5	0	k _f =0.065 k _r =0.015 k ₁ =0.0002 k ₂ =0.00088 k _f =0.067 k _r =0.022 k ₁ =0.00018 k ₂ =0.00075

Table 2 Cont'd

3	TYLA: 64.39 TYLB: 33.56	9	0	$k_f=0.063$ $k_r=0.017$ $k_1=0.00018$ $k_2=0.00095$ $k_f=0.067$ $k_r=0.022$ $k_1=0.00018$ $k_2=0.00068$
4	TYLA: 64.35 TYLB: 33.63	7	1	$k_f=0.065$ $k_r=0.016$ $k_1=0.011$ $k_2=0.016$ $k_f=0.068$ $k_r=0.023$ $k_1=0.0088$ $k_2=0.015$
5	TYLA: 67.36 TYLB: 38.36	7	3	$k_f=0.063$ $k_r=0.016$ $k_1=0.018$ $k_2=0.029$ $k_f=0.068$ $k_r=0.022$ $k_1=0.032$ $k_2=0.027$

2.3.2 Effects of pH

pH is well known to influence the photo-degradation processes of many micro-pollutants. Canonic *et al.* [20] found that the photolysis rate constants of sulfamethoxazole, iopromide and diclofenac are strongly dependent on pH, but pH is not important for 17 α -ethinylestradiol photo-transformation. Lee *et al.* [21] observed that the pH values had a significant effect on the both photo-degradation rate constant and photoproducts formation of *N*-nitrosodimethylamine. Other researchers revealed the effect of pH on the photolysis of antibiotics such as sulfonamide and fluoroquinolone [22-24]. Speciation of NXP, IBP

and TYL will be determined by the solution pH and the dissociation constants ($pK_a=4.15$, 4.9 and 7.15 for NXP, IBP and TYL, respectively) [5, 20, 25].

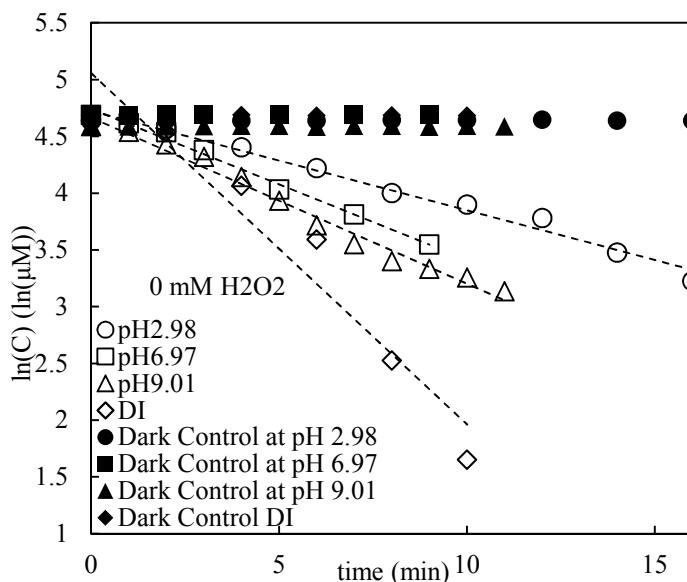


Figure 2.2: Direct photo-degradation of naproxen (NXP Exp.1, 2, 3) in buffer solutions ((pH = 2.98, 6.97 and 9.01) and deionized water (DI water, pH = 5.86))

2.3.2.1 Naproxen and ibuprofen degradation at different pH values

Here, NXP was prepared in buffered solution to investigate the influences of pH (pH 2.98, 6.97 and 9.01) on compound decomposition under direct photolysis system (UV/0 mM H_2O_2). Additional experiments were conducted without buffer at initial pH values of ~ 5.9 . Under direct photo-degradation condition (UV/0 mM H_2O_2), as shown in in Figure 2.2, the obvious NXP degradation was observed at all pH values. The kinetic rate constants were found to increase with the increase of pH values from 3 to 9. The pseudo-first order kinetic rate constant at pH of 9 was ~ 2.3 times greater than that at pH of 3.

For IBP experiments, aqueous solution was prepared in buffered solution at pH of 2.94, 6.97 and 9.07. Figure 2.3 and Table 2.2 show that the fastest rate constant, $k = 0.0029 \text{ sec}^{-1}$, was obtained at pH 9.07, and direct photolysis rate constant at pH 7 was only slightly slower, $k = 0.0023 \text{ sec}^{-1}$. The rate constant $k = 0.0016 \text{ sec}^{-1}$ at pH of 3.

In kinetic figures, dark control and blank time points demonstrate that temperature and species in buffer solution do not have any influence of the direct photolysis of NXP and IBP.

Table 2.3 pH values of unbuffered NXP and IBP solution

Time (min)	NXP pH	IBP pH
0	5.86	5.59
2	6.28	6.33
4	6.45	6.11
6	6.51	6.23
8	6.56	6.48
10	6.47	6.48
12	6.54	6.23
14	6.49	6.28
16	~	6.3

The higher rate constants under neutral/ base environment suggested that NXP and IBP photo-degradation preferred a basic condition. The unbuffered experiments could support this conclusion. Table 2.3 showed the pH increases over time for the DI experiments (NXP Exp6. and IBP Exp 6.), and Figure 2.2 and Figure 2.3 indicated that the rate constant of DI experiments were higher than that at pH 3. For both NXP and IBP, the anionic species was dominant when $\text{pH} = 7$ or 9 . The direct photolysis of NXP and IBP were driven by the deprotonated fraction having a $\pi \rightarrow \pi^*$ conjugation system that was more

reactive [26]. This finding is in agreement with other studies, which showed that deprotonated species would favor the photolysis [27, 28].

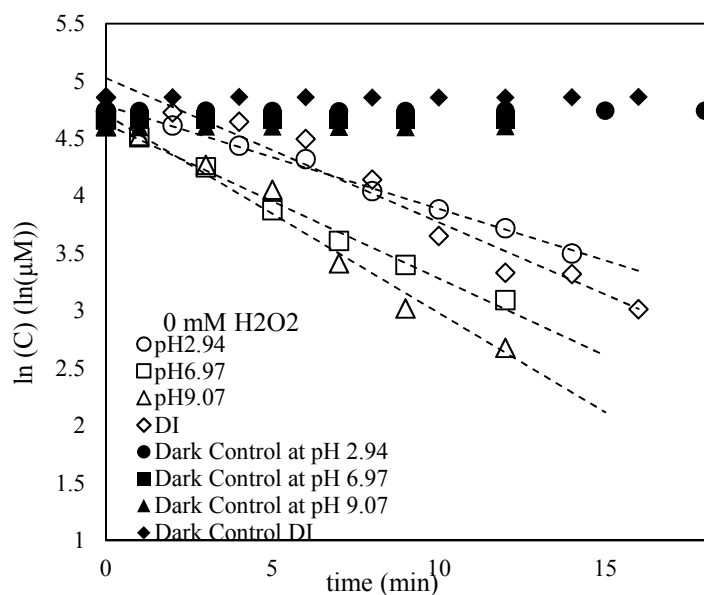
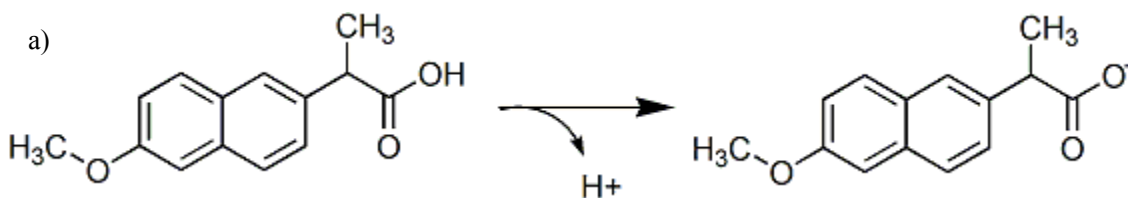


Figure 2.3: Direct photo-degradation of ibuprofen (IBP Exp. 1, 2, 3) in buffer solutions ((pH = 2.94, 6.97 and 9.07) and deionized water (DI water, pH = 5.59)

As displayed in the Figure 2.4 a) and b), NXP and IBP ionized within the pH range of this study, except for pH 3, so the speciation of parent compounds were a factor influencing the degradation process, and the increased rate constants of NXP and IBP at pH 7 and pH 9 were likely attributable to the direct photolysis at the chromophores enhanced by deprotonated fraction with relatively high molar absorptivity.



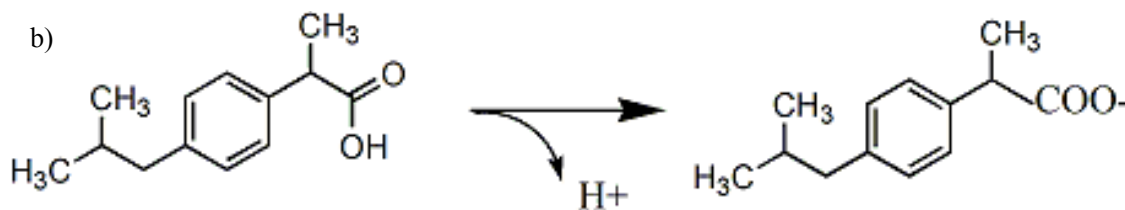


Figure 2.4: a) protonated (neutral) and deprotonated (negative charged) speciation of NXP with $pK_a = 4.15$; b) protonated (neutral) and deprotonated (negative charged) speciation of IBP with $pK_a = 4.9$

2.3.2.2 Tylosin degradation at different pH values

It is reported that TYL aqueous solution is stable at pH 4 to 9, because an acid hydrolysis product is produced at low pH values [29]. In this study, TYL working solutions were prepared in pH buffered solution (pH = 5.06, 6.98 and 9.05) to examine the role of pH on the photolytic reactions of TYL under direct photolysis condition (UV/0 mM H_2O_2). As illustrated in Figure 2.6, degradations of TYLA and TYLB are observed at all pH levels, and the rate constants are independent of pH. According to LC/MS data (discussed in Chapter Four), photoisomers of TYLA and TYLB are formed after 1 minute of UV irradiation. After 20 min, only lower molecular weight (400 to 600 m/z) fragments are detected, indicating the parent compounds have been transformed into smaller chain (fewer carbon-carbon bonds) compounds. Mass spectra data and Figure 2.6 profiles indicate rapid photoisomerization and a slower photodegradation occur during the photolysis of TYLA and TYLB. The photoisomerization (k_f and k_r) and photodegradation (k_1 and k_2) are depicted below (Figure 2.5), and the rate constants are calculated from experimental data

by combining two rate expressions and solving a second-order-differential equation (Eq.2.7).

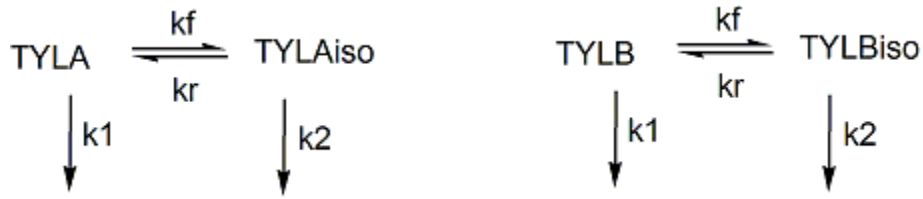


Figure 2.5: TYLA and TYLB undergo photoisomerization and photodecomposition

Equation 2.1 is the rate expression for either TYLA or TYLB:

$$\frac{dC}{dt} = -k_f C + k_r C_{iso} - k_1 C \quad (2.1)$$

Equation 2.2 is the rate expression for each isomer:

$$\frac{dC_{iso}}{dt} = -k_r C_{iso} + k_f C - k_2 C_{iso} \quad (2.2)$$

Rearranging Eq. (2.1) yields:

$$C_{iso} = \frac{1}{k_r} \left(\frac{dC}{dt} + k_f C + k_1 C \right) \quad (2.3)$$

Take the second derivative of Eq. (2.1) to obtain:

$$\frac{d^2 C}{dt^2} = -k_f \frac{dC}{dt} + k_r \frac{dC_{iso}}{dt} - k_1 \frac{dC}{dt} \quad (2.4)$$

Rearrange Eq. (2.4):

$$\frac{dC_{iso}}{dt} = \frac{1}{k_r} \left(\frac{d^2 C}{dt^2} + k_f \frac{dC}{dt} + k_1 \frac{dC}{dt} \right) \quad (2.5)$$

Plug Eq. (2.3) and (2.5) into Eq. (2.2) to obtain one equation with one unknown:

$$\frac{1}{k_r} \left(\frac{d^2 C}{dt^2} + k_f \frac{dC}{dt} + k_1 \frac{dC}{dt} \right) = -k_r \frac{1}{k_r} \left(\frac{dC}{dt} + k_f C + k_1 C \right) + k_f C - k_2 \frac{1}{k_r} \left(\frac{dC}{dt} + k_f C + k_1 C \right) \quad (2.6)$$

Rearrange Eq. (2.6):

$$\frac{d^2 C}{dt^2} + (k_f + k_r + k_1 + k_2) \frac{dC}{dt} + (k_r k_1 + k_f k_1 + k_1 k_2) C = 0 \quad (2.7)$$

The analytical solution to Eq. (2.7) is: $C_t = e^{st}$, where C_t = concentration of TYLA or TYLB at any time, t , and S is a real number such that:

$$s^2 + (k_1 + k_2 + k_f + k_r)s + (k_f k_2 + k_r k_1 + k_1 k_2) = 0 \quad (2.8)$$

There are two roots to the equation for S [18]:

$$S_{1,2} = \frac{-k_1 - k_2 - k_f - k_r \pm \sqrt{(k_1 + k_2 + k_f + k_r)^2 - 4(k_r k_1 + k_f k_2 + k_1 k_2)}}{2} \quad (2.9)$$

Then, the concentration of TYL at any time, t , is:

$$C = A_1 e^{s_1 t} + A_2 e^{s_2 t} \quad (2.10)$$

Solve for A_1 and A_2 by utilizing the initial conditions:

$$t=0, C=C_0$$

$$t=0, \left(\frac{dC}{dt}\right)_{t=0} = (-k_1 - k_f)C_0.$$

$$\text{When } t=0, A_1 + A_2 = C_0 \quad (2.11)$$

$$\text{When } t=0, A_1 S_1 + A_2 S_2 = (-k_1 - k_f)C_0 \quad (2.12)$$

$$\text{So, } A_2 = \frac{-k_1 - k_f - s_1}{s_2 - s_1} C_0 \quad (2.13)$$

$$A_1 = \frac{k_1 + k_f + s_2}{s_2 - s_1} C_0 \quad (2.14)$$

The phototransformation rate constants are tabulated in the Table 2.2. Figure 2.7 is the comparison of the photochemical reactions of TYLA/B, showing that pH plays a minor role in the photolysis. Photoisomerization, a major initial step, is promoted by rotation around a bond of the chromophore, which is not pH dependent. Moreover, from Figure 2.6, the concentration of TYLA/B isomer was observed to increase significantly within 1 minute and then decrease in a slower time scale. The rate of concentration increase of

TYLA/B_{iso} indicated that initially, the photoisomerization was much faster than the photodegradation.

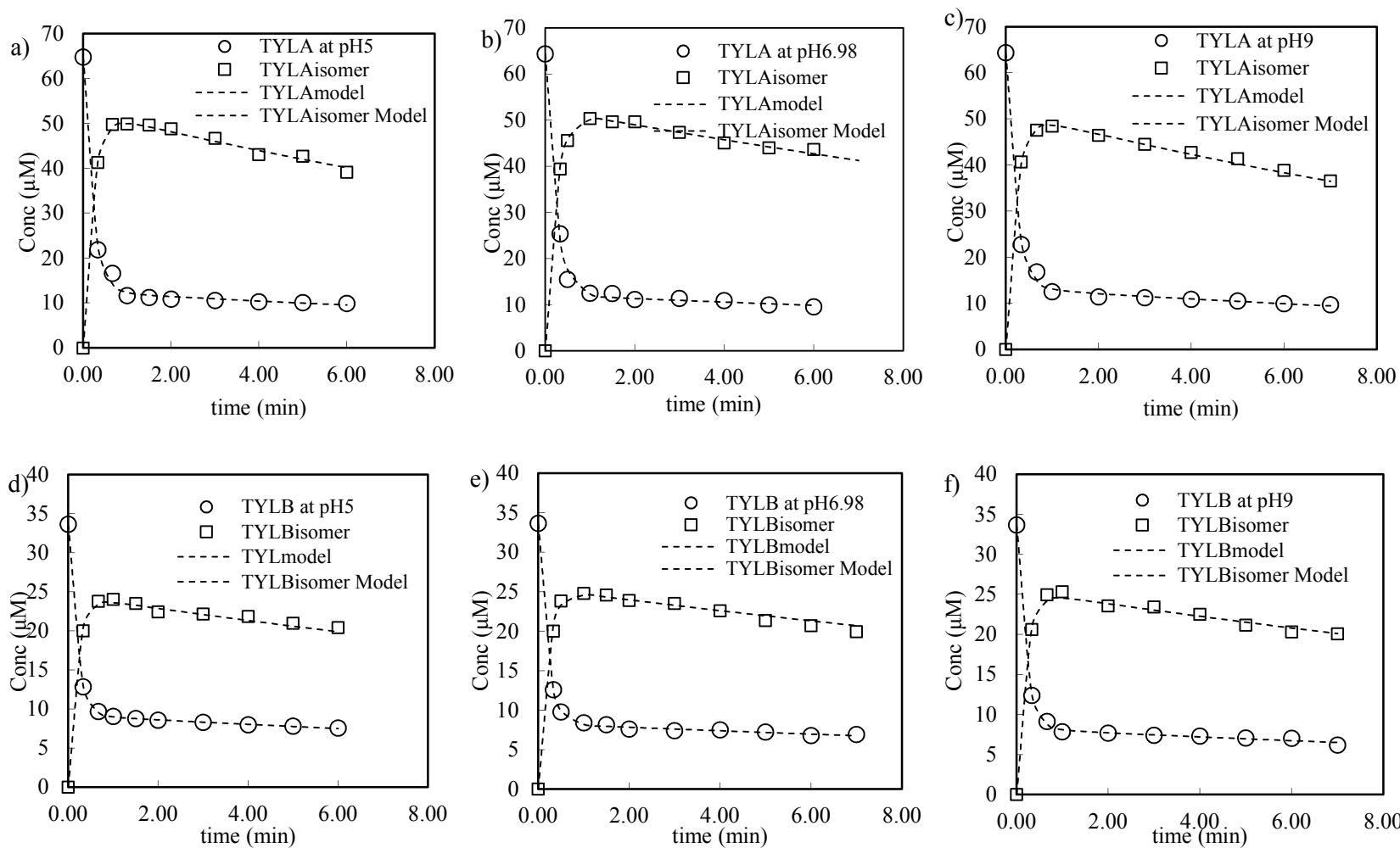


Figure 2.6: Direct photolysis of a) TYLA at pH = 5.06; b) TYLA at pH = 6.98; c) TYLA at pH = 9.05; d) TYLB at pH = 5.06; e) TYLB at pH = 6.98; f) TYLB at pH = 9.05

Moreover, Werner *et al.* [5] observed a similar mechanism for photoisomerization of TYLA under simulated solar system. They mention in their research work that photoisomerization is much quicker than photodegradation, which is the same as we assume, and reported $k_f = k_r = 0.028 \text{ sec}^{-1}$ at pH =7 with light intensity of $5.3 \times 10^{-4} \text{ Einstein m}^{-2} \text{ sec}^{-1}$. In our study, TYL was irradiated with a greater photon flux ($3.5 \times 10^{-2} \text{ Einstein m}^{-2} \text{ sec}^{-1}$). However, our observed rate constant is the same order of magnitude as previously published values.

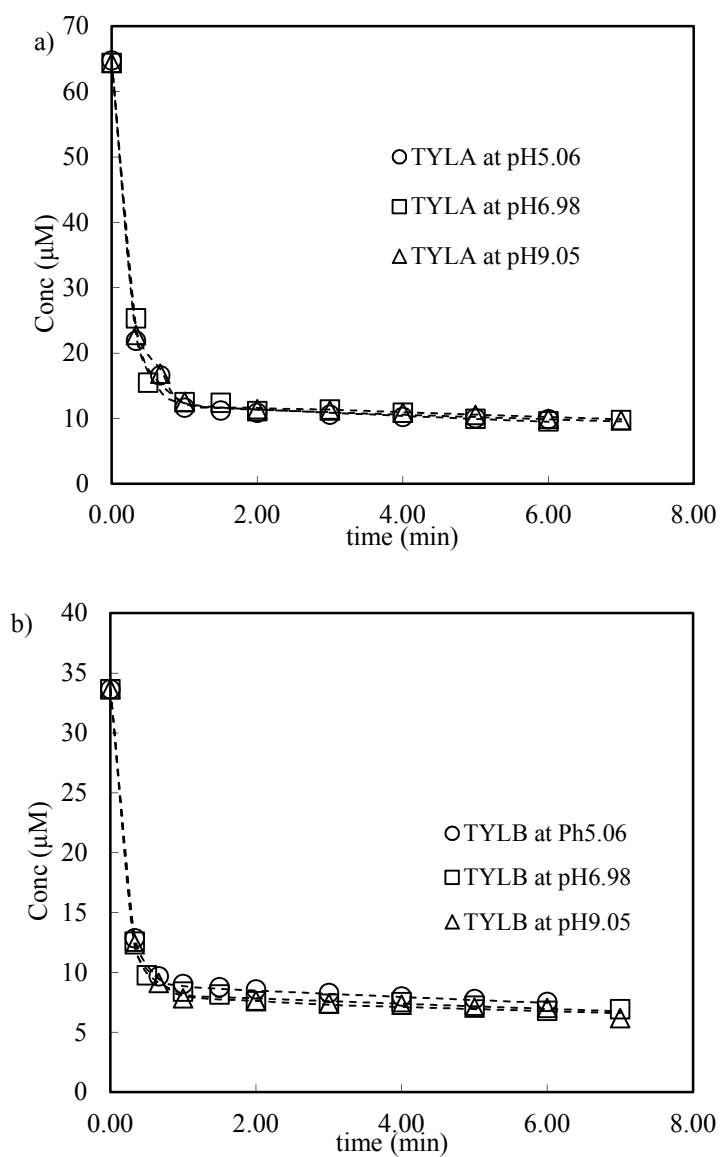


Figure 2.7: Comparison of photolysis at different pH a) TYLA; b) TYLB

2.3.3 Effects of Hydrogen Peroxide (H₂O₂)

UV/H₂O₂ has been applied to remove PPCPs in recent years [18, 31]. This system is able to overcome some disadvantages of other UV based AOP technologies. When ozone/UV technology is applied to treat bromide containing water, it produces bromate ion, and treatment is required for the off-gas and to strip VOCs [32]. For Fenton technology, the main disadvantage is the production of large amounts of ferric hydroxide after treatment [33]. The UV/H₂O₂ process does not cause any of these disadvantages.

2.3.3.1 Naproxen and ibuprofen degradation with hydrogen Peroxide (H₂O₂)

Several experiments were conducted to investigate how the H₂O₂ concentrations influence the photolysis of NXP and IBP. NXP and IBP aqueous solutions were prepared in pH 7 phosphate buffer, with the addition of 0, 1 and 3 mM H₂O₂ (it is assumed that H₂O₂ was in excess), respectively.

Figure 2.8 depicts and Table 2.2 lists NXP kinetic rate constants with $k = 0.018 \text{ sec}^{-1}$ as the fastest, which was due to the highest initial concentration of H₂O₂ (3 mM). This was roughly 6.3 times faster than rate constants obtained from direct photolysis (UV/0 mM H₂O₂, $k = 0.0028 \text{ sec}^{-1}$), and 1.86 times faster than indirect photolysis with less oxidant (UV/1 mM H₂O₂, $k = 0.0094 \text{ sec}^{-1}$) at the same pH.

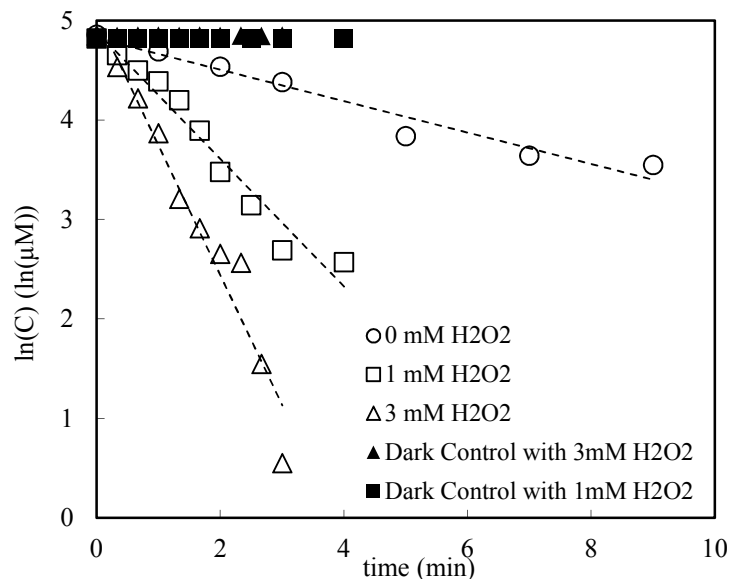


Figure 2.8: NXP degradation with increasing oxidant [$\text{H}_2\text{O}_2=0, 1, 3 \text{ mM}$] at $\text{pH} = 7$

As indicated in Figure 2.9 and Table 2.2, the addition of H_2O_2 also accelerated the IBP decomposition process, which was similar to the behavior of NXP. The direct photolysis rate constant (UV/0 mM H_2O_2) k was 0.0023 sec^{-1} , and the addition of 1 mM H_2O_2 enhanced the rate constant up to 0.013 sec^{-1} . The fastest rate constant k was 0.023 sec^{-1} obtained under the condition of 3 mM H_2O_2 .

Comparing the direct photolysis of NXP with IBP suggests that NXP is more reactive via photodegradation because the rate constants of NXP are larger than those for IBP, which may be related to molar absorptivity. For UV/ H_2O_2 experiments, the rate constants of NXP were smaller than the constants of IBP at all levels of the oxidant. The possible reason was that the free-radical process pre-dominated during the photolysis of NXP and IBP, and the IBP was more susceptible to attack by $\cdot\text{OH}$.

The figures and table revealed that the presence of H_2O_2 accelerated the photochemical decomposition of NXP and IBP. These enhancements could be attributed to

the degradation of H_2O_2 , which yielded reactive hydroxyl radicals $\cdot\text{OH}$. Furthermore, it was clear that the rate constants at 3 mM H_2O_2 were greater than those at 1 mM H_2O_2 , because higher oxidant level resulted in a higher concentration.

These results are consistent with conclusions in other publication of hydroxyl radical $\cdot\text{OH}$, where the presence of H_2O_2 promoted photo-catalytic processes such as UV/ TiO_2 , UV/ H_2O_2 , and UV/Solar for several PPCPs. Cao *et al.*[34] conducted several UV experiments with suspended TiO_2 , finding TiO_2 enhanced the photo-degradation of phenobarbital. Huang *et al.* [35] added 2.53 mM H_2O_2 into UV system and recorded an enhancement factor > 1.49 enhancement for phenol degradation. He *et al.* [36] observed a two-fold rate increase for microcystin-LR with the assistance of oxidant (peroxide). Jung *et al.* [37] found that the addition of 10 mM H_2O_2 increased kinetic rate constants up to six fold for degradation of amoxicillin. Köhler *et al.* [38] also agreed that the addition of oxidant enhanced Ciprofloxacin degradation, and Wol *et al.* [39] reported similar experimental results for Atrazine, Clofibric acid, Ketoprofen and several PPCPs they investigated. More recent studies confirm the increase in PPCPs degradation rate constants with the addition of oxidant to a variety of advanced oxidation processes (AOP).

In this study, higher concentrations of H_2O_2 resulted in faster degradation rates. However, it is noteworthy that some researchers observed that the addition of H_2O_2 did not necessarily enhance the photo-degradation. Nienow *et al.* [40] reported in their research paper (UV/ H_2O_2 system) about a pesticide, lindane, that the high amount of H_2O_2 decreased photo-degradation of the compounds. In their work, the relatively smaller kinetics rate constants occurred with the presence of 30 mM H_2O_2 compared with rate constants

obtained at 1-5 mM H₂O₂. They attributed this result to scavenging of hydroxyl radical by H₂O₂:

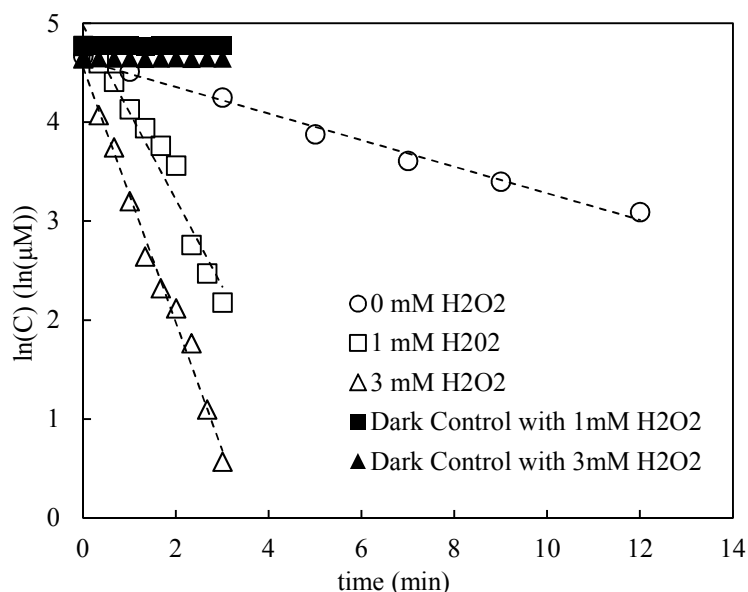
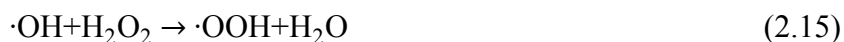


Figure 2.9: IBP degradation with increasing oxidant [H₂O₂=0, 1,3 mM] at pH = 7

2.3.3.2 Hydrogen Peroxide (H₂O₂) effect on Tylosin

TYL aqueous solutions were prepared in pH=7 phosphate buffer, with the addition of 0, 1 and 3 mM H₂O₂. Figure 2.10 displays the phototransformation of TYLA/B under UV/H₂O₂ condition. Even though the reaction of target compound with $\cdot\text{OH}$ is a second-order reaction, the model derived in the 2.3.2.2 in this thesis can be applied to calculate the rate constants under UV/H₂O₂, because the concentration of H₂O₂ is in excess, and thus $\cdot\text{OH}$ reaches a constant, steady-state concentration. The second-order rate constant and the $\cdot\text{OH}$ ($k_{\text{OH}}[\cdot\text{OH}]$) can be combined into a pseudo-first order rate constant that is time invariant.

From Figure 2.11 and Table 2.2 it can be seen that the addition of H_2O_2 accelerates the photodegradation. The greater the initial concentration of H_2O_2 , the greater the enhancement in rate. Photodegradation rate constants (k_1 and k_2) were increased by two orders of magnitude for both TYLA/B and its isomer with addition of 3 mM H_2O_2 , while photoisomerization reaction rate constants were not affected dramatically. In this case, although k_f and k_r were still larger than k_1 and k_2 , the role of oxidation of TYLA/B was enhanced, which made the phototransformation profiles of TYLA/B close to the profile of a first-order reaction.

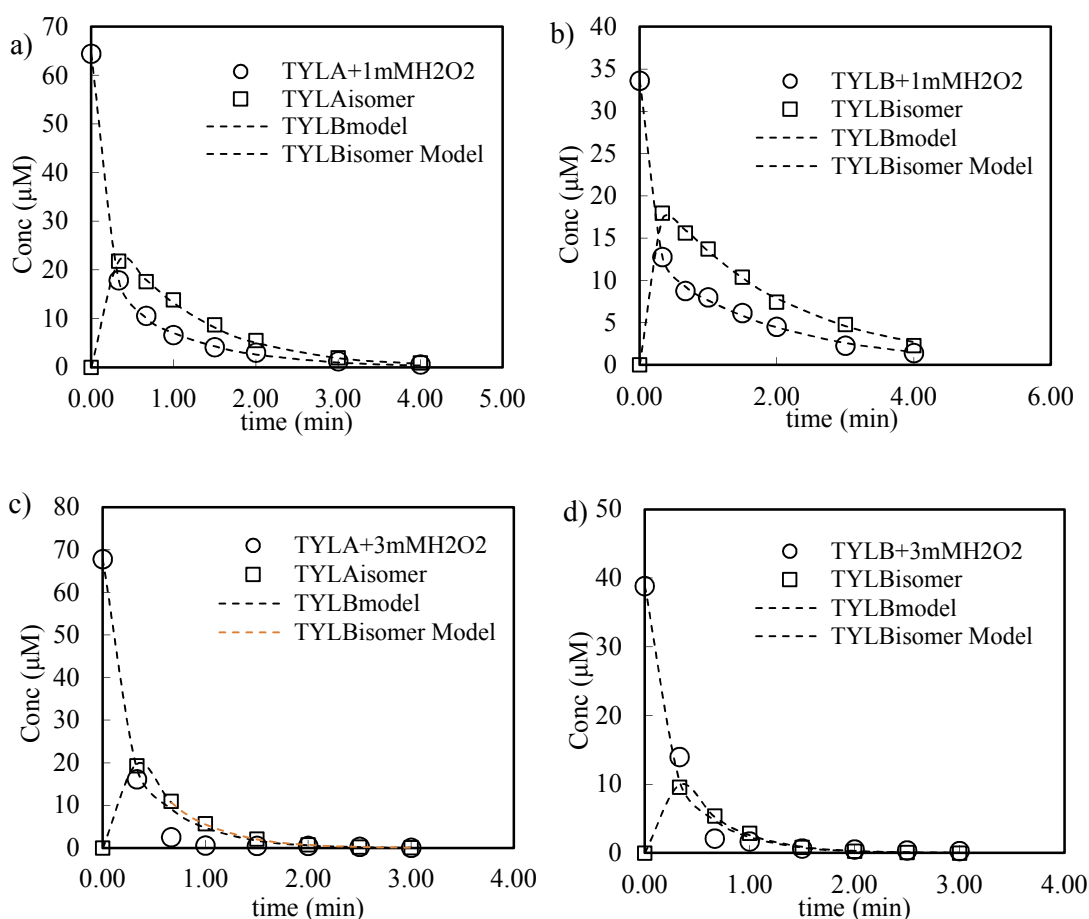


Figure 2.10: Indirect photolysis of a) TYLA with 1mM H_2O_2 ; b) TYLB with 1mM H_2O_2 ; c) TYLA with 3mM H_2O_2 ; d) TYLB with 3mM H_2O_2

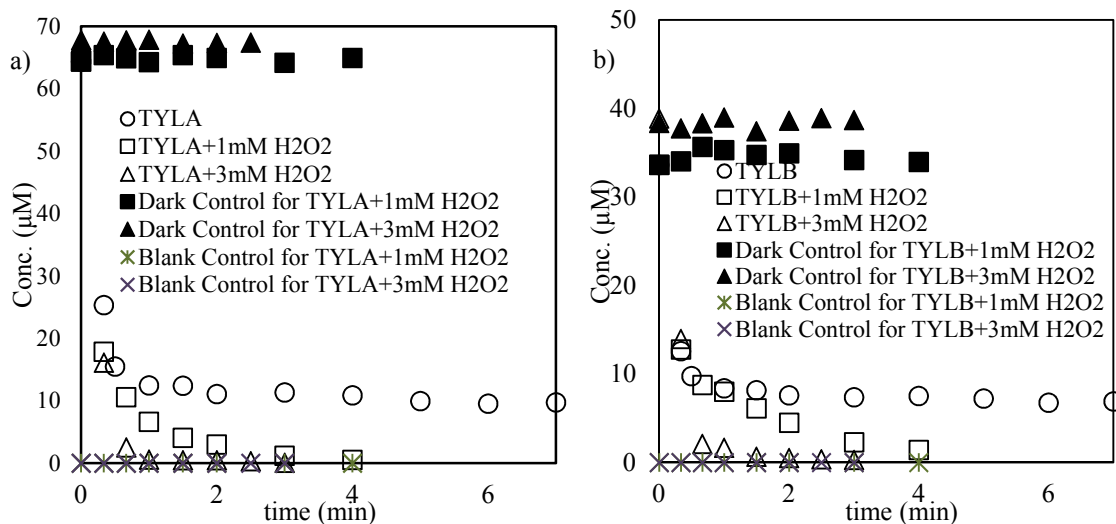


Figure 2.11 Comparison of indirect photolysis of a) TYLA; b) TYLB

2.4 Direct photolysis Molar Absorptivity (ϵ) and Quantum Yield (ϕ)

2.4.1 Molar absorptivity (ϵ)

Molar absorptivity is an intrinsic property of the molecule, which reflects how strongly a molecule absorbs light at a given wavelength [41]. Molar absorptivity is directly related to the chromophore (s) on the molecule.

For NXP, the chromophore is the naphthalene with the methoxy group system, so the strong peak appears around 230 nm [42]. For IBP, the chromophore is a benzene ring. Figure 2.12 shows that NXP and IBP had a strong absorbance at 230 nm and 223 nm, respectively. TYL has a ketodiene chromophore, which is unique among the macrolides [5].

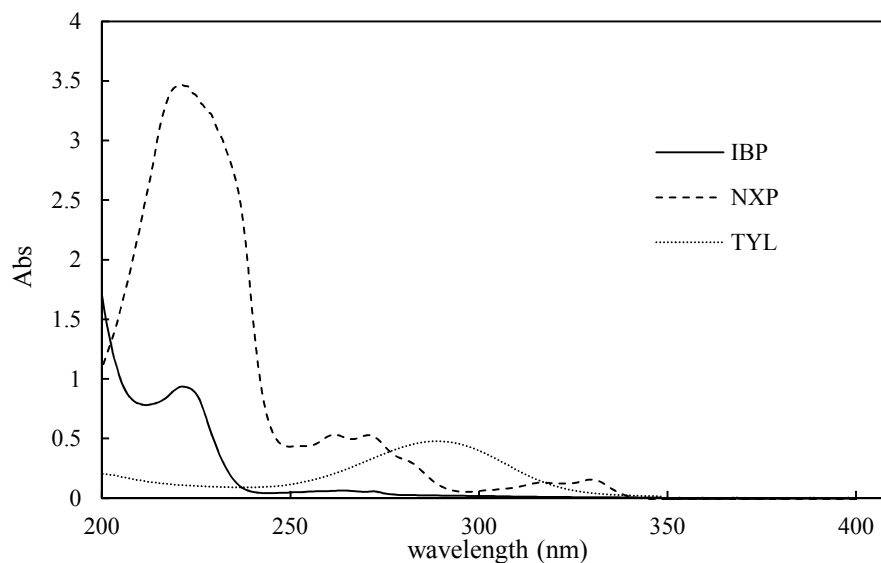


Figure 2.12: UV-vis spectrum of Naproxen, Ibuprofen and tylosin in buffered solution (100 μM , pH = 7)

Molar absorptivity depends on wavelength. In this study, molar absorptivity at 254 nm was determined in order to evaluate the potential for direct photolysis at that wavelength. The absorbance of buffered (pH = 7) solution of NXP, IBP and TYL was measured at the following concentrations: 0 μM , 20 μM , 40 μM , 60 μM , 80 μM and 100 μM . According to Beer-Lambert Law (Eq 2.16), molar absorptivity can be determined from the slope of linear regression of absorbance against the corresponding molar concentration.

$$A = \epsilon Cl \quad (2.16)$$

Figure 2.13 a), b) and c) show the linear regression profiles of target compounds' absorbance dissolved in water, resulting in a slope, molar absorptivity ϵ , of 4240.30 $\text{M}^{-1}\text{cm}^{-1}$ for NXP, 299.05 $\text{M}^{-1}\text{cm}^{-1}$ for IBP, respectively. The molar absorptivity $\epsilon_B = 2400 \text{M}^{-1}\text{cm}^{-1}$ and molar absorptivity $\epsilon_A = 3815 \text{M}^{-1}\text{cm}^{-1}$ are determined by additional Eq. (2.17).

$$A = \epsilon_B C_B l + \epsilon_A C_{BA} l \quad (2.17)$$

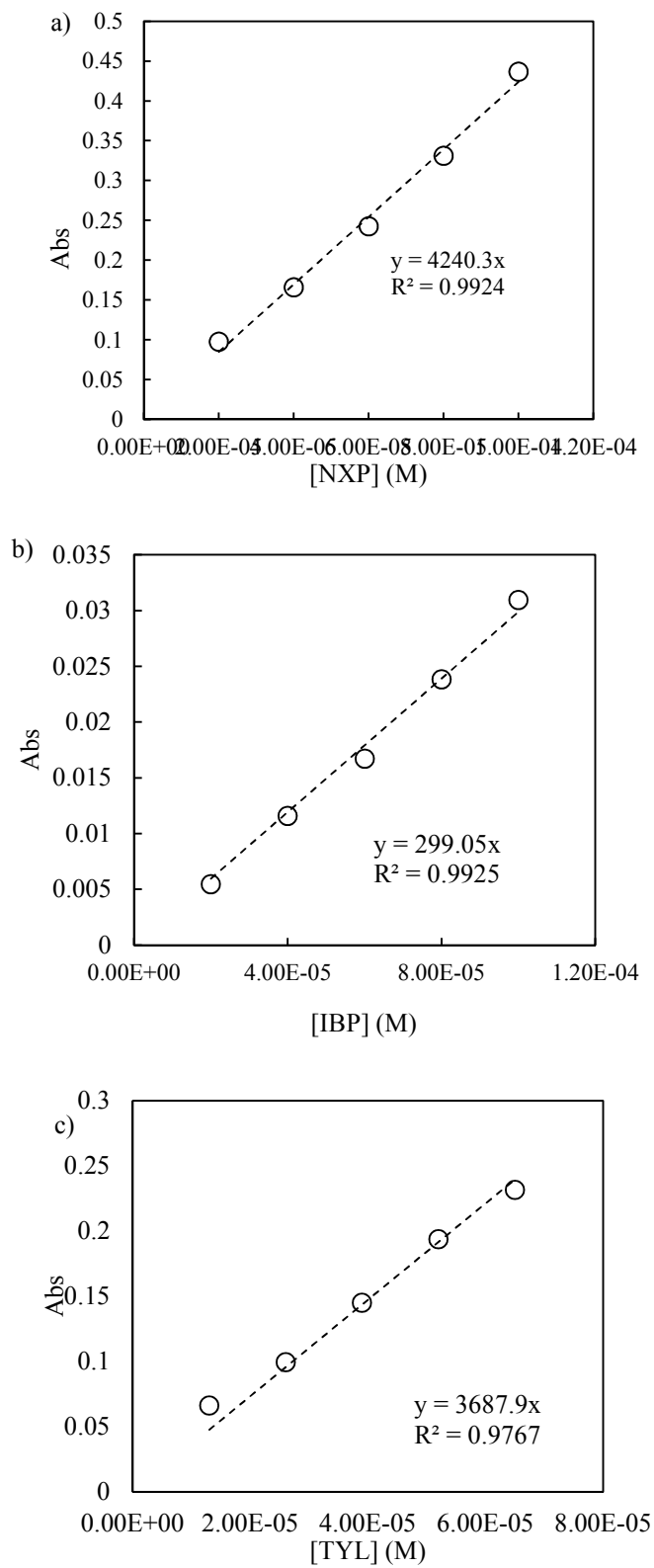


Figure 2.13: Linear regression analysis of a) NXP; (b) IBP; c) TYL

2.4.2 Quantum Yield ϕ

Quantum yield, ϕ , is a parameter describing the ratio of the number of molecules of compounds transformed to the number of photons absorbed by the compounds at a particular wavelength. Quantum yield is determined by Eq (2.18) [41],

$$\phi_{\text{direct}(254\text{nm})} = k/2.303I\epsilon l \quad (2.18)$$

where k is the direct photolysis rate constant of target compound, I is the photon flux ($I = 7.2 \times 10^{-5}$ einstein/sec) determined by potassium ferrioxalate actinometry for the photoreactor in this study, ϵ is the molar absorptivity reported in section 2.4.1, and l (0.69 cm) is the path length of the quartz tube. Table 2.4 displays the values of quantum yield of NXP, IBP and TYL.

$$\text{pH} = \text{pKa} + \log [A^-] / [HA] \quad (2.19)$$

where HA is the cationic form of compound and A^- is the anionic form of compound [26]. pKa values are 4.1, 4.9, and 7.15 for NXP, IBP, TYLA and TYLB, so the ratio of A^-/HA is 741 and 117 for NXP and IBP at pH = 6.97, and 0.76 for TYLA/B at pH = 6.98, respectively. Since ϕ was calculated at pH \approx 7, the values presented here are quantum yield of anionic species of NXP and IBP and cation species of TYLA and TYLB.

Quantum yield is a function of molar absorptivity. As we can see, the quantum yield of NXP was much lower than the quantum yield of IBP. This could explain why the kinetic rate constant of IBP was slightly lower than NXP, although the molar absorptivity of IBP was significantly lower.

Table 2.4 Quantum Yield of anionic species of NXP and IBP and cation species of TYL at 254 nm

	pH	Φ_{exp}	Φ_{cal}
NXP	6.97	0.0080	0.0076
IBP	6.97	0.0978	0.0923
TYLA	6.98	0.2131 ^a	
TYLB	6.98	0.3439 ^a	

The relatively high Φ_f indicates that TYLA/B is much easier to be excited with the rotation of bond within the compound than NXP and IBP. In this study, only photoisomerization of TYLA/B quantum yield Φ_f is calculated, because there is no information on pure TYLA/B isomer's molar absorptivity spectrum. Furthermore, it is not possible to determine the quantum yields of both pure TYLA/B and the isomer, since the observed photochemical loss reflected by k_d is the sum of TYLA/B and its isomer. As expected, if both TYLA/B and the isomer are excited by photons, the photodegradation quantum yield should be the same for TYLA/B and its isomer, because they have the same chromophore.

Since the quantum yield values of NXP and IBP presented were determined with Eq. 2.18 including the kinetic rate constants calculated under the assumption of first order decay, it is necessary to validate the quantum yield values. Euler's method was employed:

$$\frac{dC}{dt} = \Phi I(A/V)(1 - e^{-\epsilon Cl}) \quad (2.20)$$

Where $I(A/V)$ is the incident light intensity normalized to the reaction volume, in units of einsteins per volume (determined by chemical actinometry). For each time point, the initial guess on the initial concentration of the target compound and quantum yield were variables, and minimized the sum of residuals squared between the experimental and calculated values of concentrations at each time point using Solver in Excel applied to Eq.

(2.20). The calculated quantum yield values were also listed in the Table 2.4. Figure 2. 14 a) and b) indicated that good agreement between the experimental data and calculated data using Euler's equation. The slight difference of the experimental data and calculated one may resulted the different initial concentration of the compounds.

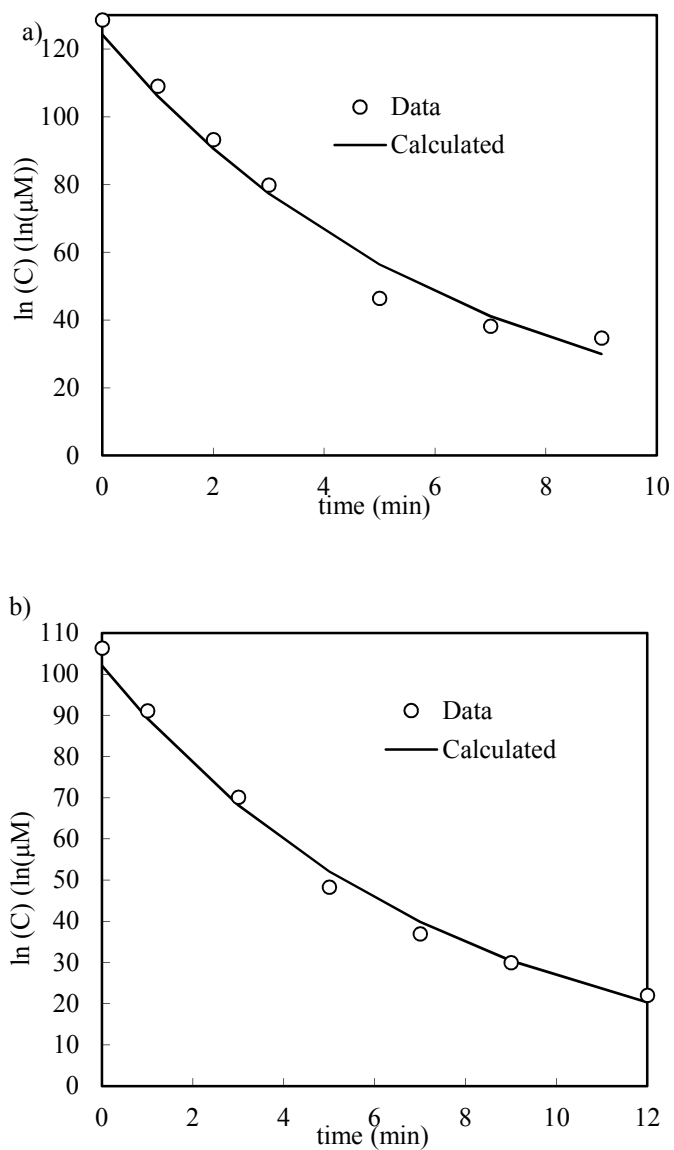


Figure 2.14: a) comparison of the calculated data vs. the experimental data for NXP; b) comparison of the calculated data vs. the experimental data for IBP

List of References

1. Richardson, S.D., Water Analysis: Emerging Contaminants and Current Issues. *Analytical Chemistry*, 2009. **81**(12): p. 4645-4677.
2. Nikolaou, A., S. Meric, and D. Fatta, Occurrence patterns of pharmaceuticals in water and wastewater environments. *Analytical and Bioanalytical Chemistry*, 2007. **387**(4): p. 1225-1234.
3. Halling-Sørensen, B., et al., Occurrence, fate and effects of pharmaceutical substances in the environment- A review. *Chemosphere*, 1998. **36**(2): p. 357-393.
4. Zhang, X. and M. Zhang, Modeling effectiveness of agricultural BMPs to reduce sediment load and organophosphate pesticides in surface runoff. *Science of The Total Environment*, 2011. **409**(10): p. 1949-1958.
5. Werner, J.J., et al., Environmental Photochemistry of Tylosin: Efficient, Reversible Photoisomerization to a Less-Active Isomer, Followed by Photolysis. *Journal of Agricultural and Food Chemistry*, 2007. **55**(17): p. 7062-7068.
6. Metcalfe, C.D., et al., Occurrence of neutral and acidic drugs in the effluents of Canadian sewage treatment plants. *Environmental Toxicology and Chemistry*, 2003. **22**(12): p. 2872-2880.
7. Carballa, M., et al., Behavior of pharmaceuticals, cosmetics and hormones in a sewage treatment plant. *Water Research*, 2004. **38**(12): p. 2918-2926.

8. Heberer, T., Occurrence, fate, and removal of pharmaceutical residues in the aquatic environment: a review of recent research data. *Toxicology Letters*, 2002. **131**(1–2): p. 5-17.
9. Quintana, J.B., S. Weiss, and T. Reemtsma, Pathways and metabolites of microbial degradation of selected acidic pharmaceutical and their occurrence in municipal wastewater treated by a membrane bioreactor. *Water Research*, 2005. **39**(12): p. 2654-2664.
10. Lindqvist, N., T. Tuhkanen, and L. Kronberg, Occurrence of acidic pharmaceuticals in raw and treated sewages and in receiving waters. *Water Research*, 2005. **39**(11): p. 2219-2228.
11. Tauxe-Wuersch, A., et al., Occurrence of several acidic drugs in sewage treatment plants in Switzerland and risk assessment. *Water Research*, 2005. **39**(9): p. 1761-1772.
12. Thomas, P.M. and G.D. Foster, Determination of Nonsteroidal Anti-inflammatory Drugs, Caffeine, and Triclosan in Wastewater by Gas Chromatography–Mass Spectrometry. *Journal of Environmental Science and Health, Part A*, 2004. **39**(8): p. 1969-1978.
13. Stumpf, M., et al., Polar drug residues in sewage and natural waters in the state of Rio de Janeiro, Brazil. *Science of The Total Environment*, 1999. **225**(1–2): p. 135-141.
14. van der Hoeven, N., Current Issues in Statistics and Models for Ecotoxicological Risk Assessment. *Acta Biotheoretica*, 2004. **52**(3): p. 201-217.

15. Sepulveda, M.S., A First Assessment of Pharmaceuticals and Personal Care Products in the Middle Wabash River, Indiana. Report as of FY2010 for 2010IN242B.
16. Song, W., et al., Determination of amprolium, carbadox, monensin, and tylosin in surface water by liquid chromatography/tandem mass spectrometry. *Rapid Communications in Mass Spectrometry*, 2007. **21**(12): p. 1944-1950.
17. Joss, A., et al., Removal of pharmaceuticals and fragrances in biological wastewater treatment. *Water Research*, 2005. **39**(14): p. 3139-3152.
18. Zwiener, C. and F.H. Frimmel, Oxidative treatment of pharmaceuticals in water. *Water Research*, 2000. **34**(6): p. 1881-1885.
19. Michael, I., et al., Urban wastewater treatment plants as hotspots for the release of antibiotics in the environment: A review. *Water Research*, 2013. **47**(3): p. 957-995.
20. Canonica, S., L. Meunier, and U. von Gunten, Phototransformation of selected pharmaceuticals during UV treatment of drinking water. *Water Research*, 2008. **42**(1-2): p. 121-128.
21. Lee, C., et al., UV Photolytic Mechanism of N-Nitrosodimethylamine in Water: Dual Pathways to Methylamine versus Dimethylamine. *Environmental Science & Technology*, 2005. **39**(7): p. 2101-2106.
22. Boreen, A.L., W.A. Arnold, and K. McNeill, Photochemical Fate of Sulfa Drugs in the Aquatic Environment: Sulfa Drugs Containing Five-Membered Heterocyclic Groups. *Environmental Science & Technology*, 2004. **38**(14): p. 3933-3940.

23. Y. Lester, I.G., D. Avisar and H. Mamane, Photodegradation of sulphadimethoxine in water by medium pressure UV lamp. *Water Science & Technology*, 2008. **58**(5): p. 1147–1154.
24. Mella, M., E. Fasani, and A. Albini, Photochemistry of 1-Cyclopropyl-6-fluoro-1,4-dihydro-4-oxo-7-(piperazin-1-yl)quinoline-3-carboxylic Acid (=Ciprofloxacin) in Aqueous Solutions. *Helvetica Chimica Acta*, 2001. **84**(9): p. 2508-2519.
25. Jacobs, L.E., et al., Fulvic acid mediated photolysis of ibuprofen in water. *Water Research*, 2011. **45**(15): p. 4449-4458.
26. Fang, J.-Y., L. Ling, and C. Shang, Kinetics and mechanisms of pH-dependent degradation of halonitromethanes by UV photolysis. *Water Research*, 2013. **47**(3): p. 1257-1266.
27. Xu, Y., et al., Photodegradation kinetics of p-tert-octylphenol, 4-tert-octylphenoxy-acetic acid and ibuprofen under simulated solar conditions in surface water. *Chemosphere*, 2011. **85**(5): p. 790-796.
28. Real, F.J., et al., Kinetics of the Chemical Oxidation of the Pharmaceuticals Primidone, Ketoprofen, and Diatrizoate in Ultrapure and Natural Waters. *Industrial & Engineering Chemistry Research*, 2009. **48**(7): p. 3380-3388.
29. Lewicki, J., TYLOSIN A review of pharmacokinetics, residues in food animals and analytical methods. 66th meeting of the Joint FAO/WHO Expert Committee on Food Additives (JECFA), 2006.
30. Zwillinge, D., *CRC Standard Mathematical Tables and Formulae*. 2011.

31. Ternes, T.A., et al., Removal of Pharmaceuticals during Drinking Water Treatment. *Environmental Science & Technology*, 2002. **36**(17): p. 3855-3863.
32. von Gunten, U. and J. Hoigne, Bromate Formation during Ozonization of Bromide-Containing Waters: Interaction of Ozone and Hydroxyl Radical Reactions. *Environmental Science & Technology*, 1994. **28**(7): p. 1234-1242.
33. Boonrattanakij, N., M.-C. Lu, and J. Anotai, Iron crystallization in a fluidized-bed Fenton process. *Water Research*, 2011. **45**(10): p. 3255-3262.
34. Cao, H., et al., Photocatalytic degradation kinetics and mechanism of phenobarbital in TiO₂ aqueous solution. *Chemosphere*, 2013. **90**(4): p. 1514-1519.
35. Huang, C.-R. and H.-Y. Shu, The reaction kinetics, decomposition pathways and intermediate formations of phenol in ozonation, UVO₃ and UVH₂O₂ processes. *Journal of Hazardous Materials*, 1995. **41**(1): p. 47-64.
36. He, X., et al., Efficient removal of microcystin-LR by UV-C/H₂O₂ in synthetic and natural water samples. *Water Research*, 2012. **46**(5): p. 1501-1510.
37. Jung, Y.J., et al., Removal of amoxicillin by UV and UV/H₂O₂ processes. *Science of The Total Environment*, 2012. **420**(0): p. 160-167.
38. Köhler, C., et al., Elimination of pharmaceutical residues in biologically pre-treated hospital wastewater using advanced UV irradiation technology: A comparative assessment. *Journal of Hazardous Materials*, 2012. **239–240**(0): p. 70-77.
39. Wols, B.A. and C.H.M. Hofman-Caris, Review of photochemical reaction constants of organic micropollutants required for UV advanced oxidation processes in water. *Water Research*, 2012. **46**(9): p. 2815-2827.

40. Nienow, A.M., et al., Hydrogen peroxide-assisted UV photodegradation of Lindane. *Chemosphere*, 2008. **72**(11): p. 1700-1705.
41. Schwarzenbach, R.P., P.M. Gschwend, and D.M. Imboden, Direct Photolysis, in *Environmental Organic Chemistry*. 2005, John Wiley & Sons, Inc. p. 611-654.
42. Moore, D.E. and P.P. Chappuis, A Comparative Study of The Photochemistry of The Non-Steroidal Anti-inflammatory Drugs, Naproxen, Benoxaprofen and Indomethacin. *Photochemistry and Photobiology*, 1988. **47**(2): p. 173-180.

CHAPTER 3. THE ROLES OF NITRATE AND NOM ON PHOTODEGRADATION AND MODELING THE PHOTOCHEMICAL FATE OF NAPROXEN, IBUPROFEN AND TYLOSIN

3.1 Introduction

In the previous chapter, the selected PPCPs (naproxen, ibuprofen and tylosin) photodegradation rate constants were reported under direct (UV) and indirect (UV/H₂O₂) photolysis conditions. Effects of pH and oxidant H₂O₂ concentration were evaluated, and results indicated that i) neutral and basic conditions enhanced the direct photolysis of naproxen and ibuprofen, but pH has no significant influence on the phototransformation of TYLA and TYLB; ii) the presence of oxidant H₂O₂ accelerated the photodegradation of NXP, IBP, TYLA, and TYLB, but photoisomerization process was not affected. The effects of other dissolved constituents commonly detected in surface water were not discussed.

Several photochemically mediated pathways generate hydroxyl radical ($\cdot\text{OH}$) in natural aquatic system, including irradiation of nitrate and nitrite [1], photo-Fenton reactions [2, 3] and dissolved humic acid [4]. Jacob *et al.*[5] conducted a series of experiments to study how the $\cdot\text{OH}$, nitrate and fulvic acid affect the degradation of caffeine under sunlight, and observed that indirect photolysis rate constants increased because of enhanced $\cdot\text{OH}$ produced by irradiated fulvic acid and nitrate. Megyeri *et al.* [6] reported that the dissolved oxygen enhanced the photochemical reaction of ibuprofen under solar

irradiation, but no effect was found on the phototransformation of ketoprofen. Guerand *et al.* [7] investigated the effects of different types of natural organic matter (NOM) on sulfadimethoxine and triclocarban. They reported that Suwannee River fulvic acid had no effects on sulfadimethoxine, but enhanced the degradation of triclocarban. In contrast, Pony Lake and Old Woman Creek fulvic acid accelerated the photolysis of sulfadimethoxine and triclocarban. In more recent papers, to better understand the mechanism of photochemical reaction, some kinetic models were introduced to study the degradation of clofibric acid, carbamazepine and iohexol and other pharmaceuticals. [8, 9].

The research in this chapter evaluates the phototransformation of the target compounds under the following conditions, i) photolysis in the presence of nitrate ($\sim 320 \mu\text{M}$) in UV system, ii) photolysis with Suwannee River Fulvic acid (FA) and Suwannee River Humic acid (HA) ($\sim 10 \text{ mg/L}$) in both of UV and UV/H₂O₂ system. A kinetic model will be applied to understand the mechanism of these photochemical reactions, and the extent of mineralization will also be calculated in this chapter.

3.2 Materials and Methods

Most materials and methods are the same as those described in chapter two except for amendments to the solution preparation, experimental and analytical methods, all of which are described in the following sections.

3.2.1 Chemicals and Preparation of Aqueous PPCPs Solution

Suwannee River Humic acid (HA 2S101H) and fulvic acid (FA 1S101H) as a surrogate for Natural Organic Matter (NOM), were obtained from the International Humic Soil Society (IHSS), and used without further purification. Sodium nitrate (NaNO_3), potassium iodide (KI), sodium chloride (NaCl) and starch were purchased from Sigma-Aldrich Chemical Co. and Mallinckrodt Inc, respectively. 0.1 M sodium bicarbonate standard solution and carbon dioxide buffer solution (0.1 M Sodium Citrate) were received from Thermo Fisher Scientific Inc.

500 μM stock solutions of three PPCPs were prepared by dissolving the target compounds in pH 7 buffer solutions in amber volumetric flasks. Working solution was prepared by diluting stock solution to 100 μM and adding the appropriate amount of HA, FA or nitrate. Magnetic stir bar was added to each amber volumetric flask and the flask was placed on the magnetic stir plate to mix for 24 hours. All solutions were stored at 4°C in the amber flasks.

3.2.2 Experimental Procedures

Before each irradiation experiment, 2 mL working solution was transferred into a ~2 mL amber HPLC vial to determine the initial concentration (C_0) of the compound by HPLC. Each 10 mL aliquot of equilibrated aqueous PPCPs solution was transferred into a quartz reaction tube; all tubes were suspended on the merry-go-round. At each sampling time, the merry-go-round was stopped, but the lamps were not turned off. The entire 10 mL samples from one quartz tube was transferred to an amber vial, and 200 μL methanol (quenching

reagent) was added immediately. Before HPLC analysis, IS was added to each samples as described in the chapter two.

For experiments under UV/H₂O₂ condition, the appropriate amount of 30% H₂O₂ solution was added to the PPCPs working solution and mixed well before irradiation. 10 mL aliquots of Dark Control (working solution with H₂O₂) and 10 mL aliquots of blank samples (buffer solution) were taken for each time point and kept in amber vials.

In order to build a kinetic model, some fundamental parameters also needed to be measured after irradiation. An iodometric method (discussed in Appendix B) was employed to measure the residual concentration of H₂O₂ over time. The concentration of bicarbonate (HCO₃⁻) and carbonate (CO₃²⁻) were analyzed by Carbon Dioxide Ion Selective Electrode (ISE).

3.2.3 Analytical Methods

3.2.3.1 High Performance Liquid Chromatography (HPLC)

Preparation of samples with IS and measurement of PPCPs concentration were the same as methods described in section 2.2.5.1 of this thesis.

3.2.3.2 Carbon Dioxide Ion Selective Electrode (ISE)

Quantification of inorganic carbon species was achieved with a Carbon Dioxide Ion Selective Electrode (ISE) which measures free carbon dioxide in aqueous solution. The

analytical procedure requires a calibration curve: 5 mL carbon dioxide buffer was added into 50 mL of 0.001M sodium bicarbonate standard solution, and mixed thoroughly. The mV value was recorded when a sF reading displayed for each standard concentration (0.001 M and 0.01 M). The calibration curve was obtained by linearly correlating the concentration of standard to mV readout (calibration curve is displayed in Appendix C). For photolyzed samples, 5 mL sample was diluted to 50 mL, and then 5 mL carbon dioxide buffer was transferred into 50 mL samples. After thorough mixing, the mV value was recorded. The purpose of carbon dioxide buffer solution is to adjust pH values of standard solution and the sample solution, so that all carbonate species can be converted to CO₂. The carbon dioxide concentration was determined by using calibration curve above. The calibration curve needed to be verified every two hours.

3.3 Results and Discussion

In this section, the effects of nitrate (NO₃⁻) and natural organic matter (NOM, FA and HA) on photochemical reactions were evaluated. All kinetic rate constants for NXP and IBP reported here are pseudo-first-order calculated from weighted least squares analysis of original experimental data. The kinetic results of TYL are from the Eq. (2.8) discussed in the Chapter Two. A total of fifteen experiments were completed, and rate constants (Table 3.1) were calculated from plots.

Table 3.1 Summary of experiments

Compound	Exp #	C_o (μM)	pH	H_2O_2 (mM)	Other variables	k (sec^{-1})
Naproxen (NXP)	1	101.1	7	0	$\sim 323 \mu\text{M}$ NO_3^-	0.0029 ($R^2=0.98$)
	2	122.42	7	0	$\sim 10 \text{ mg/L}$ FA	0.0023 ($R^2=0.98$)
	3	125.34	7	0	$\sim 10 \text{ mg/L}$ HA	0.0018 ($R^2=0.98$)
	4	96.79	7	1	$\sim 10 \text{ mg/L}$ FA	0.0080 ($R^2=0.95$)
	5	101.71	7	1	$\sim 10 \text{ mg/L}$ HA	0.0065 ($R^2=0.93$)
Ibuprofen (IBP)	1	105.96	7	0	$\sim 318 \mu\text{M}$ NO_3^-	0.0030 ($R^2=0.98$)
	2	104.98	7	0	$\sim 10 \text{ mg/L}$ FA	0.0016 ($R^2=0.98$)
	3	99.24	7	0	$\sim 10 \text{ mg/L}$ HA	0.0013 ($R^2=0.97$)
	4	95.82	7	1	$\sim 10 \text{ mg/L}$ FA	0.011 ($R^2=0.99$)
	5	97.33	7	1	$\sim 10 \text{ mg/L}$ HA	0.010 ($R^2=0.99$)

Table 3.1 Cont'd

Tylosin (TYL)	1	TYLA: 64.30 TYLB: 34.59	7	0	~320 μ M NO ₃	$k_f=0.068$ $k_r=0.019$ $k_1=0.00032$ $k_2=0.00098$ $k_f=0.068$ $k_r=0.026$ $k_1=0.00033$ $k_2=0.00011$
	2	TYLA: 64.36 TYLB: 32.56	7	0	~10 mg/L FA	$k_f=0.063$ $k_r=0.015$ $k_1=0.00027$ $k_2=0.00085$ $k_f=0.055$ $k_r=0.021$ $k_1=0.00018$ $k_2=0.00063$
	3	TYLA: 61.73 TYLB: 33.92	7	0	~10 mg/L HA	$k_f=0.059$ $k_r=0.015$ $k_1=0.00018$ $k_2=0.0007$ $k_f=0.053$ $k_r=0.021$ $k_1=0.00018$ $k_2=0.00058$

3.3.1 Effect of nitrate (NO_3^-) on photolysis kinetics

Nitrate (NO_3^-) exists in natural waters with a representative range of 0-485 μM . In some studies, NO_3^- was reported to enhance or suppress the phototransformation of some organic pollutants [10-12], but there is relatively little literature evaluating effects of NO_3^- on NXP, IBP and TYL photolysis at 254 nm.

3.3.1.1 Effect of nitrate (NO_3^-) on photolysis kinetics of naproxen and ibuprofen

100 μM NXP working solution was prepared by diluting the 500 μM stock solution with buffered solution (pH=7) and adding 0.0027g NaNO_3 (323 μM NO_3^-) in a 100 mL volumetric flask. Figure 3.1 displays the photochemical reaction process, and Table 3.1 lists the $k = 0.0030 \text{ sec}^{-1}$, which is 7.14% greater than that observed for direct photolysis ($k = 0.0028 \text{ sec}^{-1}$).

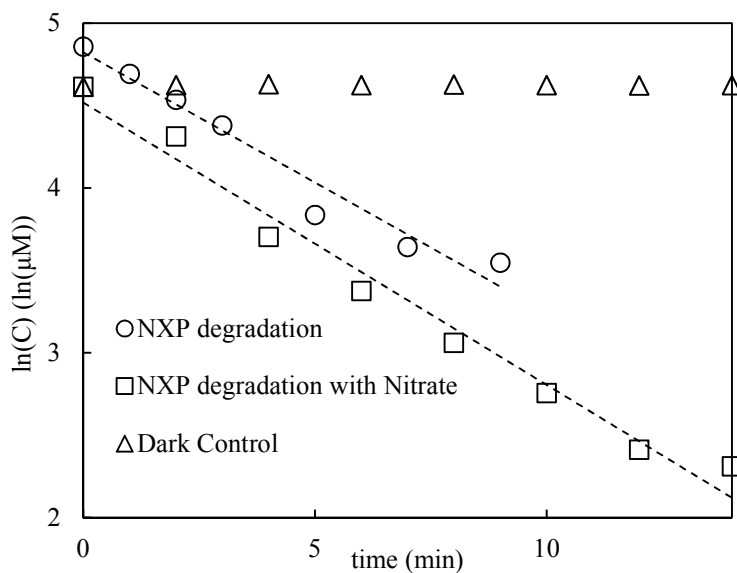


Figure 3.1: NXP photodegradation with NO_3^- (323 μM) at pH = 7

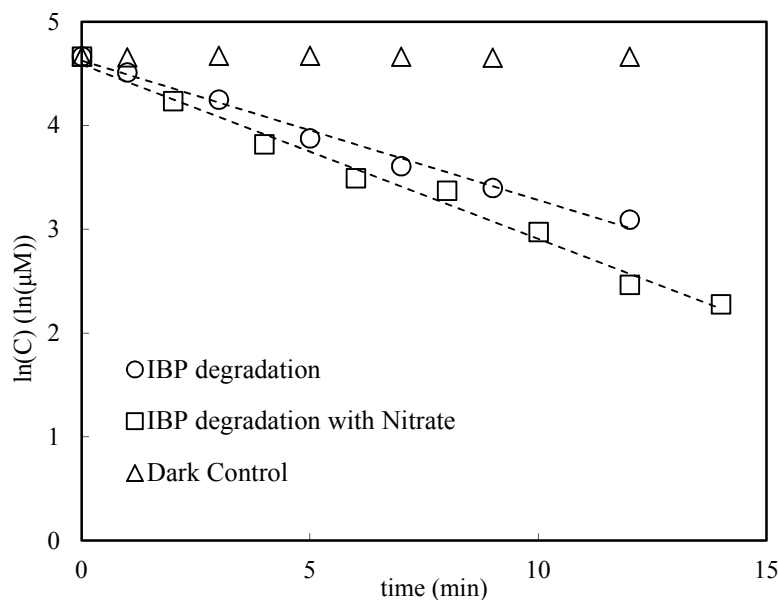


Figure 3.2: IBP photodegradation with NO_3^- ($312 \mu\text{M}$) at pH 7

A $500 \mu\text{M}$ IBP stock solutions were prepared in buffered solution (pH =7) and diluted to $100 \mu\text{M}$ with the addition of 0.0026g NaNO_3 ($312 \mu\text{M NO}_3^-$). As Figure 3.2 and Table 3.1 display, IBP photolysis with NO_3^- ($k=0.0030 \text{ sec}^{-1}$) was faster than the IBP direct photolysis ($k=0.0023 \text{ sec}^{-1}$), indicating that the irradiated NO_3^- played a role on the photochemical process.

According to previous literatures, the NO_3^- species generally behaves as a paradox in photochemical systems, since either it could compete with the target compounds by absorbing light, or generate reactive oxygen species via sensitization (Eqs. (3.1)-(3.5)) [13].





In our case, the experimental results of the photolysis of NXP and IBP demonstrated that the sensitization effects of NO_3^- overweighed the effects caused by the absorption of light by NO_3^- . The photolysis of NO_3^- produced some reactive species so that the photochemical processes of NXP and IBP were enhanced, but not very significantly. To explain why NO_3^- just a minor effect on the photolysis, literatures reported by Mack and Bolton are good reference. They demonstrated that the quantum yield of $\cdot\text{OH}$ generation by photolysis of NO_3^- was relatively low at $\lambda < 302 \text{ nm}$ [14].

The results presented here agree with previous studies about NXP and IBP photolysis in sunlight or other wavelengths. Xu *et al.* [15] found the presence of NO_3^- increased the degradation rate of ibuprofen in a simulated solar reactor. Vione *et al.* [16] also reported that the reaction rate constant of naproxen under natural sunlight increased due to the presence of NO_3^- .

Comparing NXP experimental data with IBP experimental results, it can be seen that NO_3^- has a more significant influence on the degradation of IBP (~30% increase in rate constant) than that of NXP (~7% increase in rate constant). The possible explanation is that IBP is more susceptible to $\cdot\text{OH}$: in the absence of NO_3^- the rate constant for indirect photolysis is substantially greater than the rate constant for direct photolysis. In contract, direct photolysis dominates the NXP degradation process as evidenced the close values of the rate constants for direct and indirect photolysis in the absence of NO_3^- .

3.3.1.2 Effect of nitrate (NO_3^-) on photolysis kinetics of tylosin

Photolytic experiments in the presence of $320 \mu\text{M NO}_3^-$ were completed for TYLA and TYLB. From Figure 3.3, the presence of NO_3^- enhances both the photoisomerization and photodegradation process. For both TYLA and TYLB, k_f and k_r were slightly increased, but k_1 and k_2 were increased up to 0.0032 sec^{-1} and 0.00098 sec^{-1} for TYLA, 0.00033 sec^{-1} and 0.011 sec^{-1} for TYLB. The role of NO_3^- in the photochemical reaction of TYL is the same as the behavior in the photolytic reaction of NXP and IBP: $\cdot\text{OH}$ formed from the irradiation of NO_3^- enhances the photochemical process. The reason why NO_3^- has no significant effect on the rapid photoisomerization process is likely that the quantum yield of $\cdot\text{OH}$ produced by photolysis of NO_3^- is much smaller than the quantum yield of forward and backward photoisomerization. The variation of TYLA/B isomer (shown in Figure 3.4) was the same as we discussed in previous section: the level was increased, and then decreased.

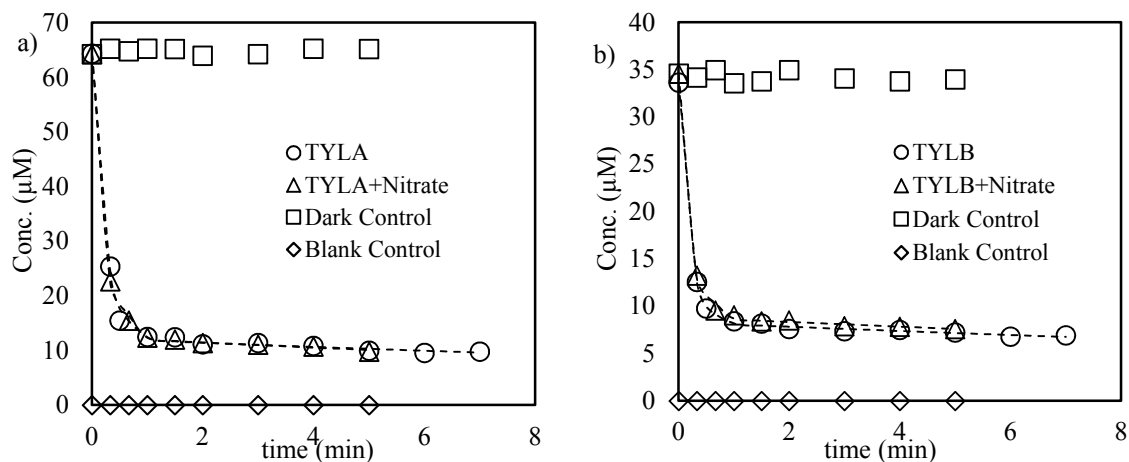


Figure 3.3: Photodegradation with NO_3^- ($320 \mu\text{M}$) at $\text{pH} = 7$ of a) TYLA; b) TYLB

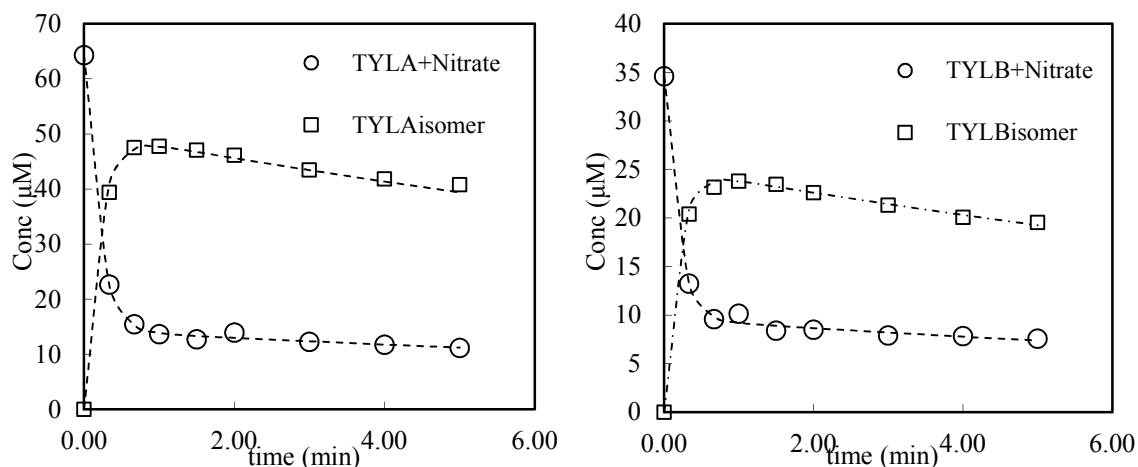


Figure 3.4: a) Phototransformation with the presence of nitrate of a) TYLA and TYLAiso; b)TYLB and TYLBiso.

3.3.2 Effect of Natural organic matter (NOM) on photolysis kinetics

Photochemical processes in natural aquatic environments are more complicated than in reagent grade water because of the presence of some natural organic matter (NOM) and other photosensitive constituents [17]. The exact chemical structures of NOM vary according to soil types, locations and other factors (for example, see Table 3.2) [17]. Humic substances are recognized as the largest portion of NOM in natural aquatic environment at concentrations ranging from 0.3 to 30 mg of C/L and represented as HA and FA with respect to their aqueous solubility [18]. FA has a relatively smaller molecular weight and a larger fraction of oxygen-containing than HA [18].

In previous research, irradiation of NOM produces some reactive species that react with the target compounds, which in turn enhances the photodegradation. However, in some other papers, the presence of NOM may inhibit the photochemical reactions, resulting

in a decreased kinetic rate constant, because high level of NOM can attenuate the ability of photon penetrating the aqueous solution [19]. In this study, 10 mg/L of HA and 10 mg/L FA were added in the PPCPs solution to examine the role of NOM on the phototransformation.

Table 3.2 Elemental analysis data for FA and HA from different sources

	Element Analysis					
	Source	C	H	O	N	S
Suwannee River FA ^a	Terrestrial	52.4	4.3	42.2	0.7	0.4
Suwannee River HA ^a	Terrestrial	52.6	4.3	42.0	1.2	0.5
Pony Lake FA	Microbial	49.6	6.1	37.4	6.5	2.4
Lake Fryxel FA	Microbial	55	5.5	34.9	3.1	1.3
Old Woman Creek FA	Mixed	-	-	-	-	-

^a FA and HA used in this research.

3.3.2.1 Effect of NOM on photolysis of NXP and IBP

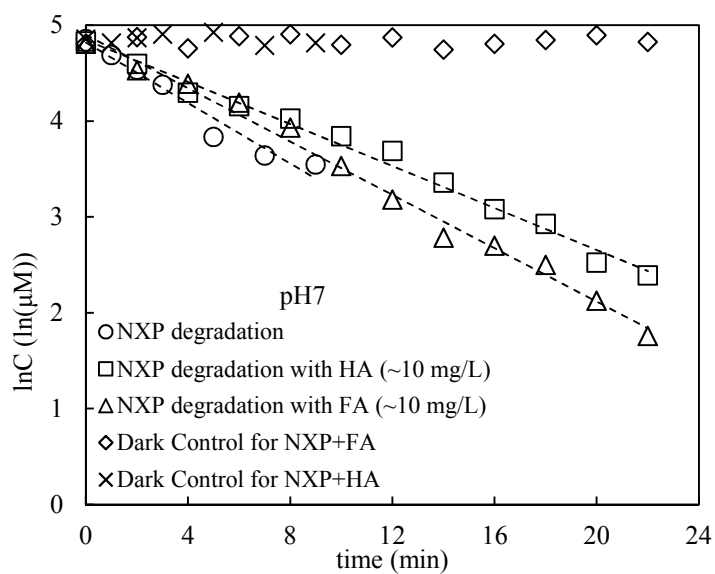


Figure 3.5: NXP photodegradation with FA (~10 mg/L) and HA (~10 mg/L) (NXP Exp.7 and 8, pH = 7)

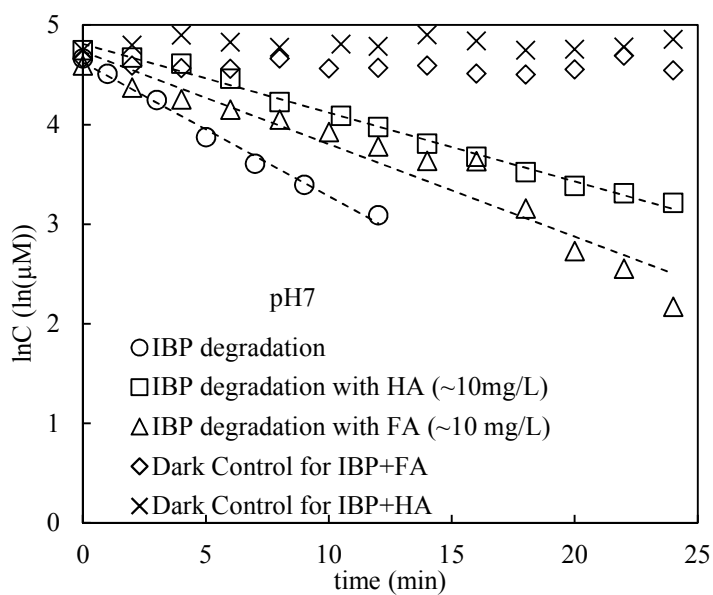


Figure 3.6: IBP photodegradation with FA (~10 mg/L) and HA (~10 mg/L) (NXP Exp. 7 and 8, pH = 7)

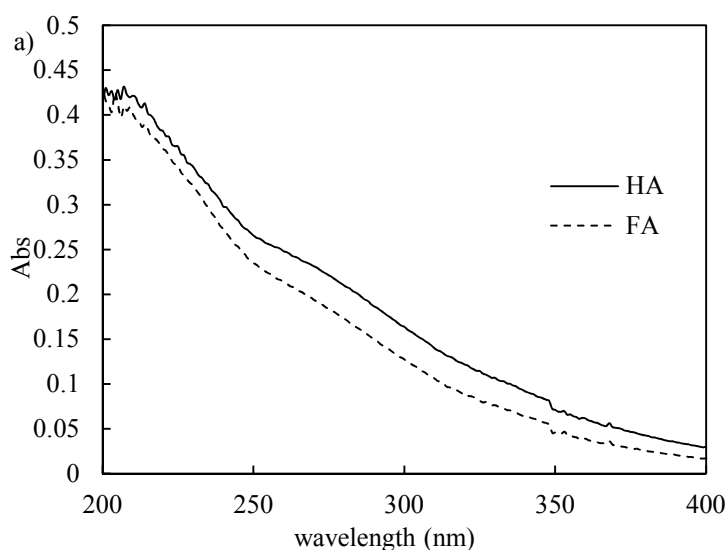
Experiments were performed with 100 μM NXP and IBP working solution with 10 mg/L HA and FA, respectively. The kinetic rate constants obtained in the presence of FA and HA are listed in Table 3.1, and the degradation profiles were described in Figure 3.5 and Figure 3.6. The addition of NOM resulted in a decrease in rate constants for both of NXP and IBP. For NXP experiment with FA, the direct photolysis rate constant was reduced by 18%, (0.0028 sec^{-1} to 0.0023 sec^{-1}). With the addition of HA in NXP solution, the decrease was with a factor of 36%. The photodegradation rate constants of IBP were 0.0016 sec^{-1} (~30% reduction) and 0.0013 sec^{-1} (~43% reduction) in the presence of FA and HA, respectively.

These findings are in contrast to previous literatures studies, which reported that HA or FA promoted the photolysis of NXP, IBP and other pharmaceuticals. Guerard *et al.* [7] observed a large photo-enhancement of sulfadimethoxine and triclocarban degradation in the presence of Pony Lake FA (~10 mgC/L) and Old Women Creek FA (~10 mgC/L) at a wavelength of 280 nm. Jacob *et al.* and Peuravuori *et al.* reported that IBP photochemical reaction proceeded faster in Pony Lake FA (5.45 mgC/L) and in the condition of ~10 mg/L humic materials under UVA-vis (315-400nm) [20, 21]. The variations in chemical makeup of NOM involved and different wavelengths used in these studies are probably responsible for these differences.

NOM consists of a complex mixture of macromolecules with different functional groups including carboxy-, phenoxy-, hydroxyl- and carbonyl-substituents [22]. The various functional groups could be phototransformed to phenoxy, peroxy and oxyl or other radicals after irradiation, which promotes the photolytic reaction of pollutants. On the other hand, the highly aromatic NOM (such as FA and HA used in this study) allows it to absorb

more light leading to a relatively larger molar absorptivity, which inhibit the photoreaction of the target compounds [23].

In our case, the light screening effects seem to be the major effect on the photochemical reactions of NXP and IBP. Figure 3.6 shows several UV-vis spectra. The absorbance values of both FA and HA increase with the decreasing wavelength, and they have relatively high absorbance at wavelengths < 300 nm, (Figure 3.7a)). Comparisons of the absorbance of NXP (or IBP) with or without FA /HA (Figure 3.7b), and c)) demonstrated that the absorbance values were elevated in the NOM solutions at the wavelength of 254 nm. For example, a 10 mg/L FA solution had an absorbance of 0.23, while a 100 μ M IBP solution exhibited an absorbance of only 0.052, confirming the presence of NOM could interfere with the light absorption by the target pollutants. The possible reason that HA had a larger influence on the both NXP and IBP was greater light absorbance of HA compared to that of FA at 254 nm, as indicated in the Figure 3.7. Also, the absorbance values of IBP was significantly increased in the presence of HA and FA.



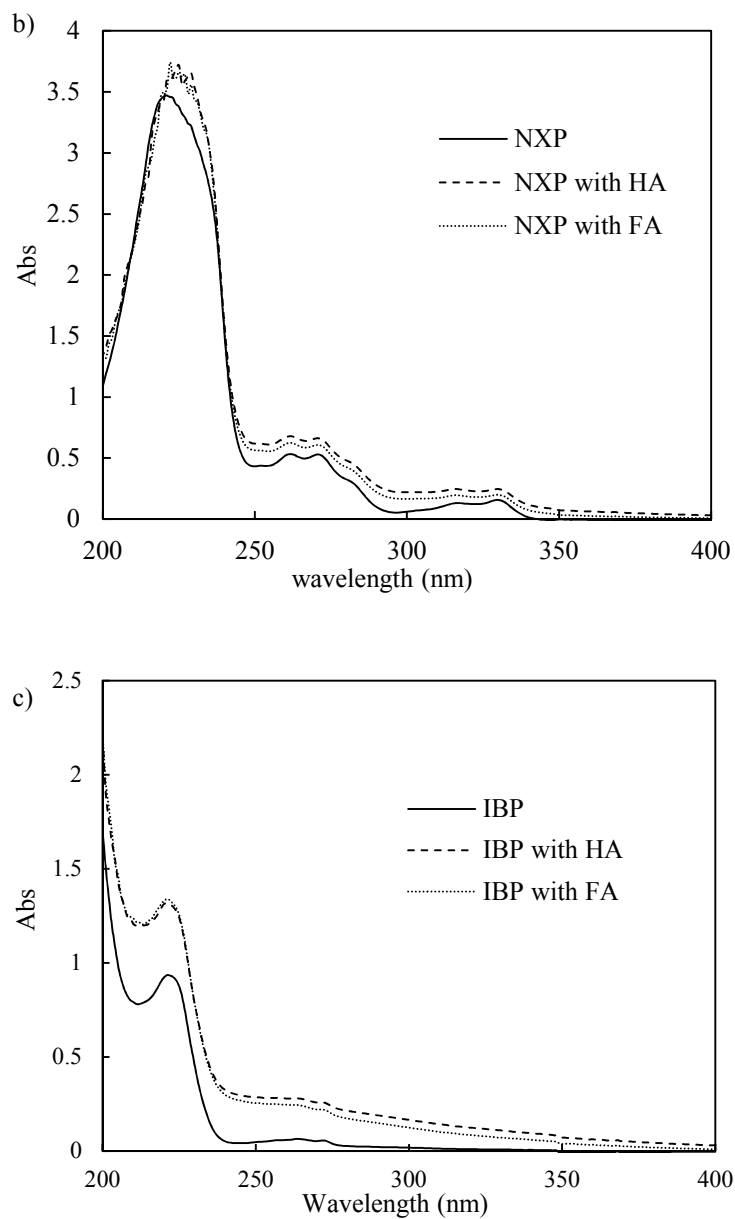


Figure 3.7: UV-vis spectra of a) 10 mg/L HA (—) and 10 mg/L FA (---); b) 100 μ M NXP solution (—), 100 μ M NXP solution with 10 mg/L HA (---) and 100 μ M NXP solution with 10 mg/L FA (\cdots); c) 100 μ M IBP solution (—), 100 μ M IBP solution with 10 mg/L HA (---) and 100 IBP μ M solution with 10 mg/L FA (\cdots)

Light screening effects on the NXP and IBP photolytic degradation can be calculated with a parameter, screening factor S_λ (Eq. 3.6):

$$S_\lambda = \frac{1 - 10^{-D_\lambda \alpha_\lambda z_{\text{mix}}}}{2.3 z_{\text{mix}} D_\lambda \alpha_\lambda} \quad (3.6)$$

Where S_λ is defined as the screening factor, D_λ and z_{mix} are equal to 1 for the solution in the quartz tubes and α_λ is the attenuation coefficient of the medium, obtained from the solution absorbance [22].

$$A_\lambda = [\alpha_\lambda + \epsilon_\lambda C] l \quad (3.7)$$

As Beer-Lambert law described, A_λ is the absorbance values of the solution, ϵ_λ is the molar absorptivity of the target compounds, C is the concentration of the compounds, and l is the path length. Thus, the photolysis rate constants obtained with the addition of FA and HA could be corrected by the light screening factor:

$$k_{\text{corr}} = k_{\text{obs}}^{\text{NOM}} / S_\lambda \quad (3.8)$$

Where $k_{\text{obs}}^{\text{NOM}}$ is the rate constant obtained from experimental data (listed in Table 3.1) and k_{corr} is the rate constants corrected by light screening factor. With the IBP + FA solution as an example, $A_\lambda = 0.25$, $\epsilon_\lambda = 299 \text{ M}^{-1} \text{ cm}^{-1}$, $C = 104.98 \text{ } \mu\text{M}$ and $l = 0.69 \text{ cm}$. All these data are plugged in Eq. (3.7) to get α_λ , subsequently obtain light screening factor by Eq. (3.6).

As Table 3.3 shows, the k_{corr} match the direct photolysis rate constants of NXP and IBP in buffered solution (no FA or HA), which illustrates that the decrease in rate constants due to the presence of NOM could be explained completely by the light screening effect.

Table 3.3 Experimental and light screening corrected rate constants for photodegradation of selected PPCPs at 254 nm

	$k_{\text{exp}} (\text{sec}^{-1})$	S_{λ}	$k_{\text{corr}} (\text{sec}^{-1})$
NXP	0.0028		
NXP+HA	0.0018	0.65	0.0028
NXP+FA	0.0023	0.79	0.0029
IBP	0.0023		
IBP+HA	0.0013	0.60	0.0022
IBP+FA	0.0016	0.71	0.0022

3.3.2.2 Effect of NOM on photolysis of TYL

A 100 μM working solution was used to examine the role of NOM on the photodegradation of TYL. As we discussed in the section 3.3.2.1, the presence of NOM increase the absorbance values of TYL solutions at $\lambda = 254 \text{ nm}$ (Figure 3.8). A light screening factor due to FA and HA can be calculated by Eq. (3.6), respectively.

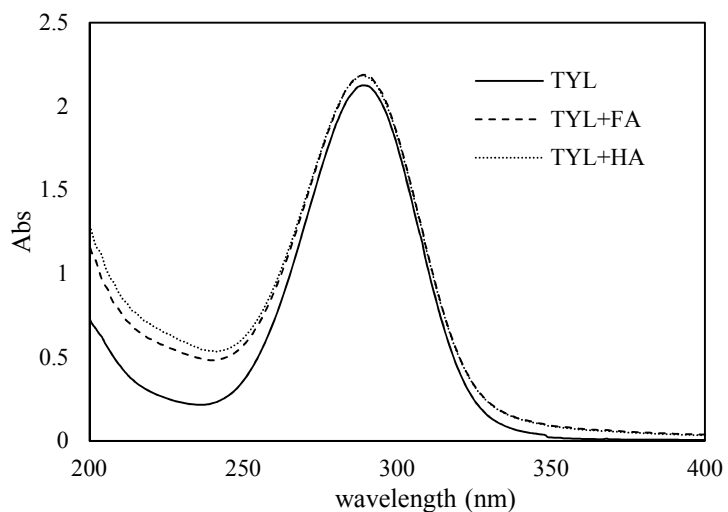
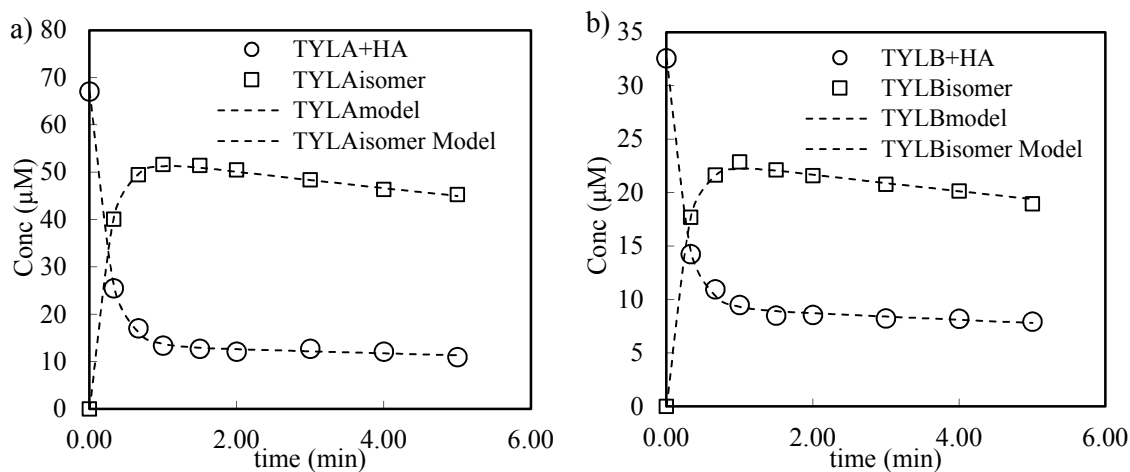


Figure 3.8: UV-vis spectra of 100 μM TYL solution (—), 100 μM TYL solution with 10 mg/L FA (---) and 100 TYL μM solution with 10 mg/L HA (⋯)

Table 3.4 Light screening factors

	S_λ
FA	0.81
HA	0.78

The kinetic rate constants obtained in the presence of FA and HA are listed in Table 3.1, and the degradation profiles were described in Figure 3.9 and Figure 3.10. From kinetic data and figures, the presence of FA and HA decreased the k_f , k_r , k_1 and k_2 for TYLA/B respectively, and HA had greater influence on the rate constants. Less than 10% reduction of k_f and less than 6% reduction of k_r are observed for TYLA, and 20% decrease of k_f and 5% decrease of k_r were reported for TYLB. The light screening effect can be responsible for the decrease in rate constants (light screening factors are listed in Table 3.4). Since the S_λ is calculated based on the absorbance of isomer mixture, the corrected photodegradation rate constant for each isomer is not available. The influence of HA on the photodegradation process is larger than FA, which has been discussed in the last section. In addition, TYLA/B isomer was present at detectible concentration with 1 minute of irradiation and then degraded within 1 to 5 minute, indicating that the photoisomerization reaction was rapid and the major step at the beginning of irradiation.



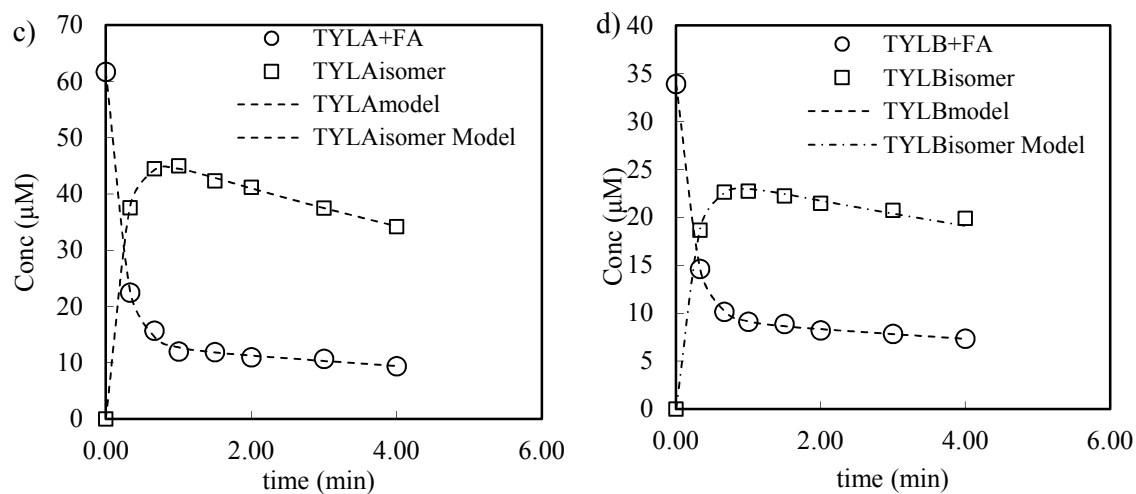


Figure 3.9: photodegradation a) TYLA with the presence of HA; b) TYLB with the presence of HA; c) TYLA with the presence of FA; d) TYLB with the presence of FA

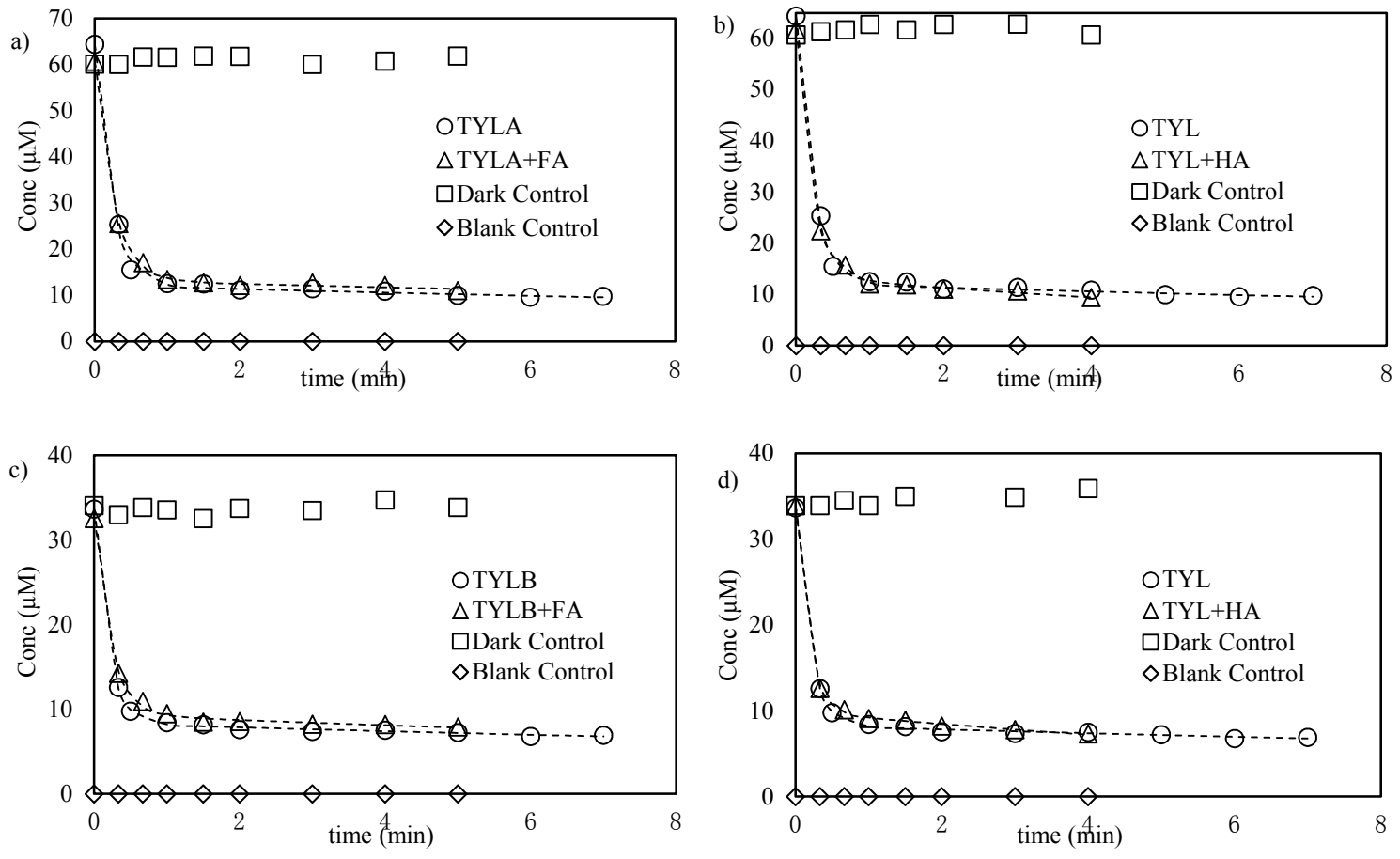
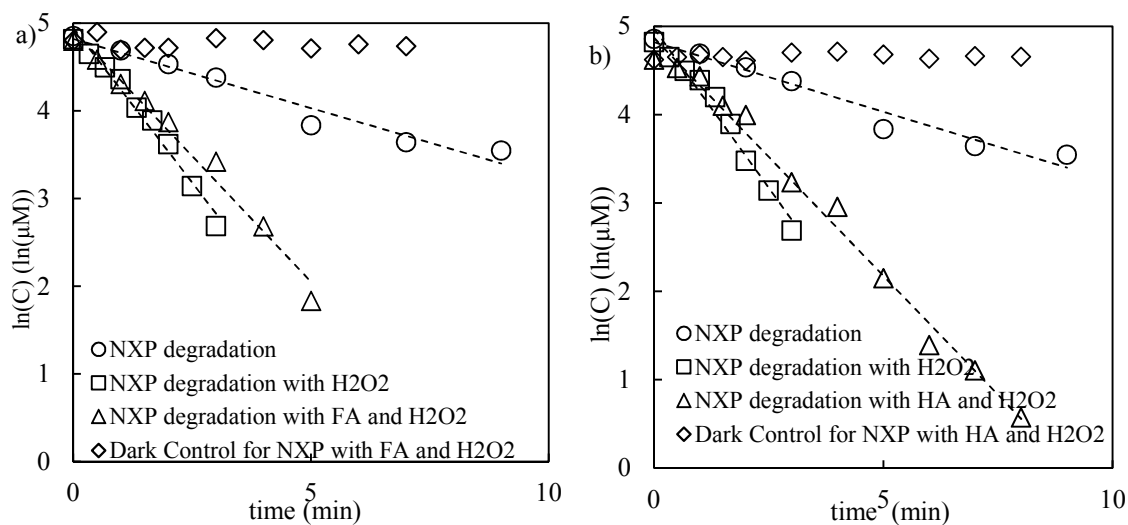


Figure 3.10: Photodegradation of a) TYLA with FA; B) TYLA with HA; c) TYLB with FA; D) TYLB with HA

3.3.3 Model predictions of UV/H₂O₂ process

3.3.3.1 NXP and IBP degradation model

In this section, NXP and IBP working solutions were prepared in pH = 7 buffer solution with the addition of NOM (~10 mg/L HA and FA, respectively). As shown in the Figure 3.11 a), b), c) and d), the presence of HA or FA decreased the rate constants under the UV and UV/H₂O₂ condition compared to no addition, because NOM reduced the ability of light penetrating water and scavenges ·OH produced from the photolysis of H₂O₂. Thus, the degradation with HA under UV/H₂O₂ condition is a complicated process. To understand the mechanism of the degradation, some fundamental parameters were measured and applied to a model prediction for degradation rate constants of the PPCPs in UV/H₂O₂ system.



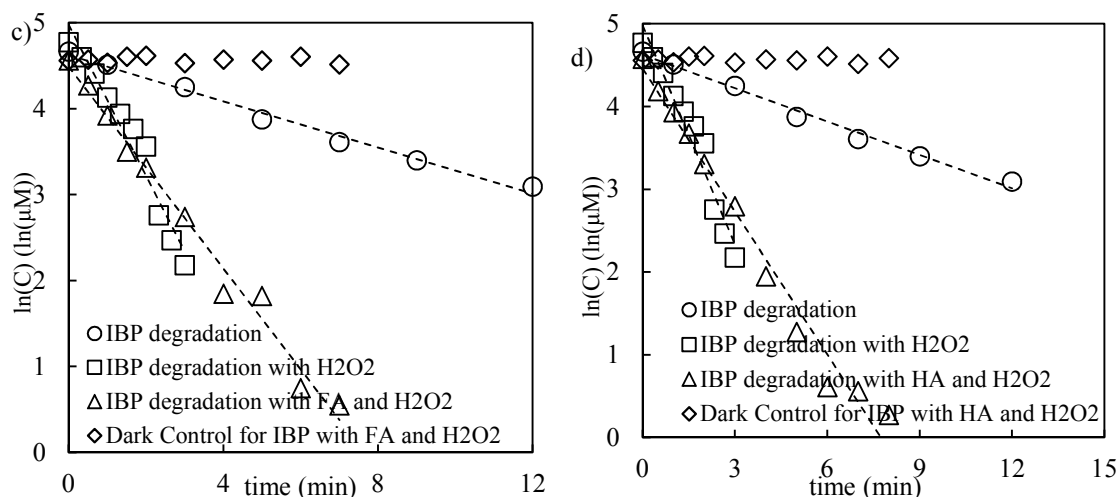


Figure 3.11: a) Direct and indirect NXP degradation with and without FA (~ 10 mg/L); b) Direct and indirect NXP degradation with and without HA (~ 10 mg/L); c) Direct and indirect IBP degradation with and without FA (~ 10 mg/L); d) Direct and indirect IBP degradation with and without HA (~ 10 mg/L)

In Figure 3.11, it can be seen that the presence of NOM decreases the degradation rate constants of NXP and IBP. In section 3.3.2.1, we discussed that NOM inhibited the photochemical reactions of target compounds due to its light screening effect, but in this section, the function of NOM is not the same. As illustrated in the Figure 3.11, the degradation in the presence of NOM under UV/ H_2O_2 condition is still faster than direct photolysis (UV alone). Although NOM scavenges $\cdot\text{OH}$, there is sufficient $\cdot\text{OH}$ production to react with NXP or IBP. It is reported that the second-order rate constant of $\cdot\text{OH}$ reacting with HA is 1.9×10^4 [24]. Thus, the NOM had different influences on the direct and indirect photolysis of PPCPs.

The overall reaction rate constant for degradation of selected PPCPs in the UV/H₂O₂ system can be contributed by both direct UV photolysis and UV/H₂O₂ oxidation process [25, 26]:

$$-\frac{d[\text{PPCPs}]}{dt} = (k_d + k_i)[\text{PPCPs}] \quad (3.9)$$

where k_d is rate constant for direct photolysis (obtained in Chapter Two); and k_i is the rate constant for indirect photolysis. The latter rate constant is the function of rate constant for the reaction of the target compound with $\cdot\text{OH}$ and the steady-state concentration of $\cdot\text{OH}$:

$$k_i = k_{\cdot\text{OH}/\text{PPCPs}}[\cdot\text{OH}]_{\text{ss}} \quad (3.10)$$

Table 3.5 Second-order-rate constant of $\cdot\text{OH}$ with the selected PPCPs [8, 9]

	$k_{\cdot\text{OH}/\text{PPCPs}} (\times 10^9 \text{ M}^{-1}\text{s}^{-1})$
NXP	8.61
IBP	6.67

Since the concentration of H₂O₂ (1 mM) was in excess relative to NXP and IBP, we can assume the concentration of $\cdot\text{OH}$ reached steady-state during the experiment. $[\cdot\text{OH}]_{\text{ss}}$ can be presented as the ratio between the generation rate and consumption rate of hydroxyl radical ($\cdot\text{OH}$)

$$[\cdot\text{OH}]_{\text{ss}} = \frac{K_{a,\text{H}_2\text{O}_2} \phi_{\text{OH}}(\lambda) [\text{H}_2\text{O}_2] f_{\text{H}_2\text{O}_2}}{\sum_i k_{\text{OH}/\text{S}} [\text{S}]_i} \quad (3.11)$$

$$K_{a,\text{H}_2\text{O}_2} = \frac{E_p^0(\lambda) \varepsilon_{\text{H}_2\text{O}_2}(\lambda) \left[1 - 10^{-(a(\lambda) + \varepsilon_{\text{H}_2\text{O}_2}(\lambda) [\text{H}_2\text{O}_2])z} \right]}{(a(\lambda) + \varepsilon_{\text{H}_2\text{O}_2}(\lambda) [\text{H}_2\text{O}_2])z} \quad (3.12)$$

$$f_{\text{H}_2\text{O}_2} = \frac{\varepsilon_{\text{H}_2\text{O}_2} [\text{H}_2\text{O}_2]}{\varepsilon_{\text{H}_2\text{O}_2} [\text{H}_2\text{O}_2] + \varepsilon_{\text{PPCPs}} [\text{PPCPs}]} \quad (3.13)$$

Where the ϕ_{OH} is 1 mol/Einstein, the quantum yield describing the generation of hydroxyl radical ($\cdot OH$) by irradiation of H_2O_2 [27]; k_{a,H_2O_2} is the specific rate of light absorbed by H_2O_2 ; $f_{H_2O_2}$ is defined as the fraction of light absorbed by H_2O_2 ; $\epsilon_{H_2O_2}$ is $18.7 M^{-1} cm^{-1}$ at $\lambda = 254$ nm, the molar absorptivity for H_2O_2 [27]. Since $\cdot OH$ can react non-selectively with any substrates in aqueous solution [28], NOM, CO_3^{2-} , HCO_3^- and H_2O_2 act as the $\cdot OH$ scavengers, and oxidation of PPCPs also consume $\cdot OH$. The main scavengers and rate constants are listed in Eq. (3.14) and Table 3.6.

$$\sum_i k_{OH/S}[S]_i = k_{OH/DOM}[DOM] + k_{OH/CO_3^{2-}}[CO_3^{2-}] + k_{OH/HCO_3^-}[HCO_3^-] + k_{OH/HPO_4^{2-}}[HPO_4^{2-}] + k_{OH/H_2PO_4^-}[H_2PO_4^-] + k_{OH/PPCPs}[PPCPs] + k_{OH/H_2O_2}[H_2O_2] \quad (3.14)$$

In our research, the concentrations of HA, FA, HPO_4^{2-} and $H_2PO_4^-$ remained constant during the short photolysis period. The carbonate species level were determined by ion selective electrode (ISE), and residual concentrations of H_2O_2 was verified by the iodometric method (discussed in Appedix B).

Table 3.6 Most significant $\cdot OH$ scavengers and rate constants

Name	$k_{OH} (M^{-1}s^{-1})$	Ref.
Suwannee River FA	2.06×10^8	[29]
Suwannee River HA	2.5×10^4	[30]
Carbonate	3.9×10^8	[29]
Bicarbonate	8.5×10^6	[29]
Hydrogen phosphate ion	1.5×10^5	[31]
Bihydrogen phosphate ion	2.0×10^4	[31]
Hydrogen peroxide	2.7×10^7	[9]

In Figure 3.12 a), b), c) and d), dashed lines represent the model results calculated from Eq. (10)-(13). The model agreed with NXP and IBP experimental data. The agreement

was excellent for IBP degradation, but the prediction slightly underestimated the degradation rate for NXP.

Thus, the UV/H₂O₂ model described above could be applied to predict the photolysis rate constants for NXP and IBP under different experimental conditions by varying the parameters (concentration of oxidant ([H₂O₂]) and path length (z)). From Figure 3.13 a), b), c) and d), it was obvious that there was a concentration of H₂O₂ corresponding to the maximum enhancement of overall rate constant (k_d+k_i). This is because the photolysis of H₂O₂ is a reversible reaction where hydroxyl radical ($\cdot\text{OH}$) is produced and H₂O₂ also acts as $\cdot\text{OH}$ scavenger. This finding agreed with the conclusion in Sharpless's report [32]. The influence of path length (z) was also investigated because that the path length should affect the light absorbed by H₂O₂ and target compounds. Figure 3.13 illustrated that the overall rate constant was enhanced with a higher concentration of H₂O₂ and a shorter optical path length. The higher second-order rate constant of $\cdot\text{OH}$ with NXP is responsible for higher rate constant obtained by NXP.

Figure 3.14 represents the UV photodegradation fraction that illustrates the relative importance of direct photolysis and indirect photolysis of selected PPCPs under different experimental conditions. The UV photodegradation fraction ($f_d=k_d/(k_d+k_i)$) was defined as the ratio of direct photolysis (k_d) to the overall photolysis rate constant (k_d+k_i). As shown in Figure 3.14, the relatively sharpest decrease in direct photolysis with an increase of the oxidant was obtained for IBP degradation. This is attributed to the low molar absorptivity of IBP, which meant that direct photolysis did not have an important influence on the degradation of IBP when $\cdot\text{OH}$ is present.

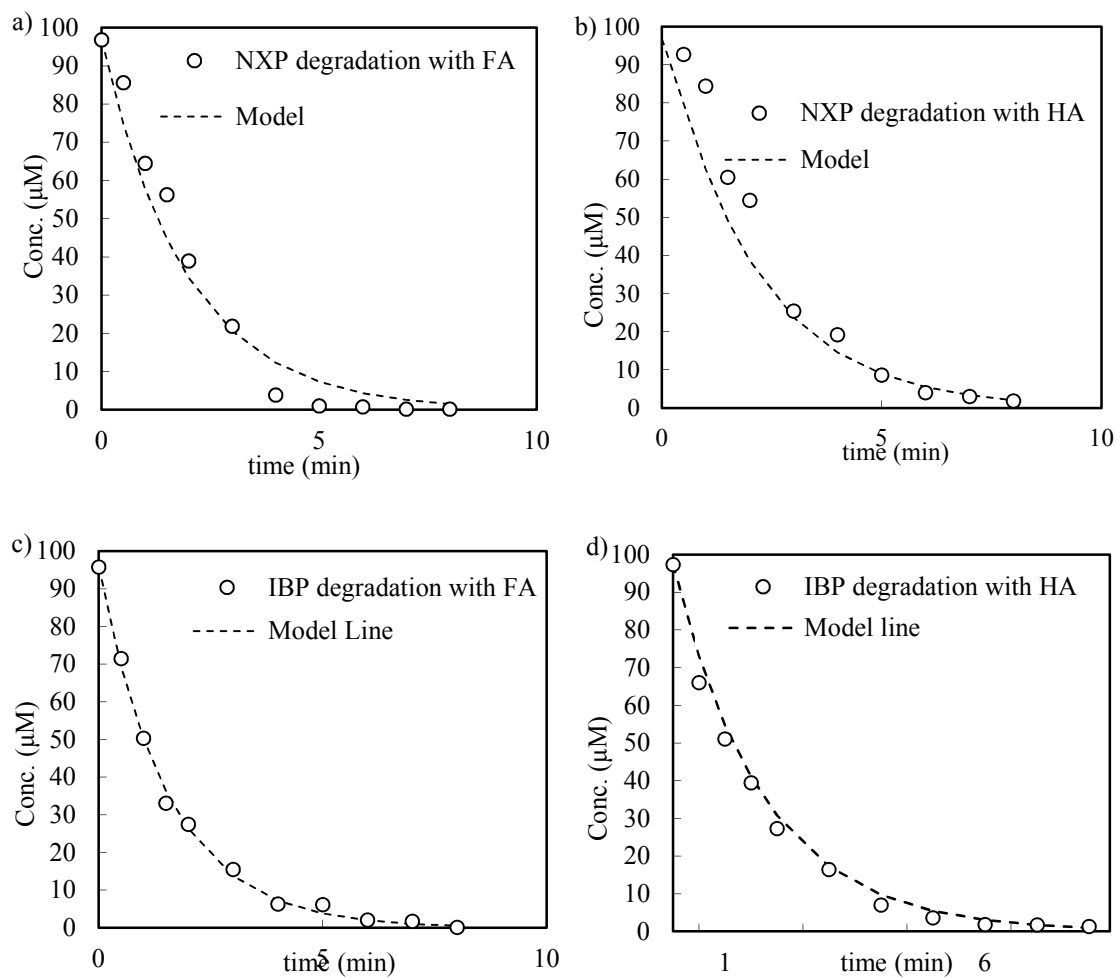
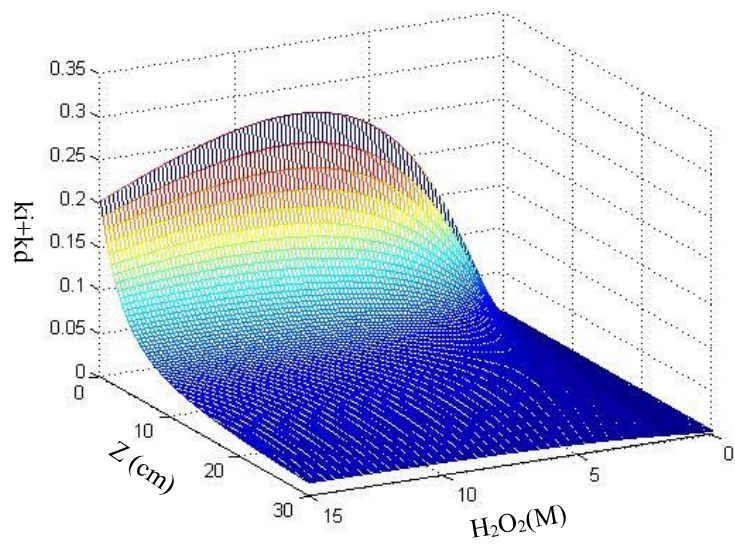
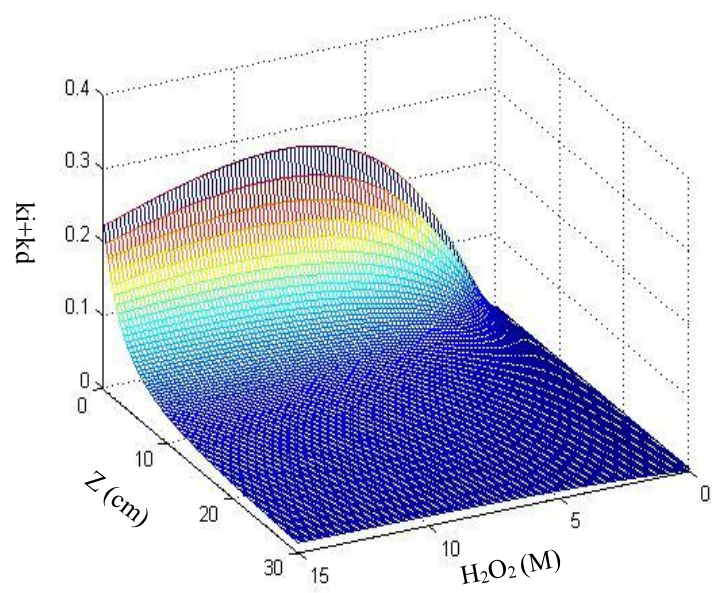


Figure 3.12: Experimental and model comparisons for UV/H₂O₂ degradation of a) NXP with FA; b) NXP with HA; c) IBP with FA; d) IBP with HA

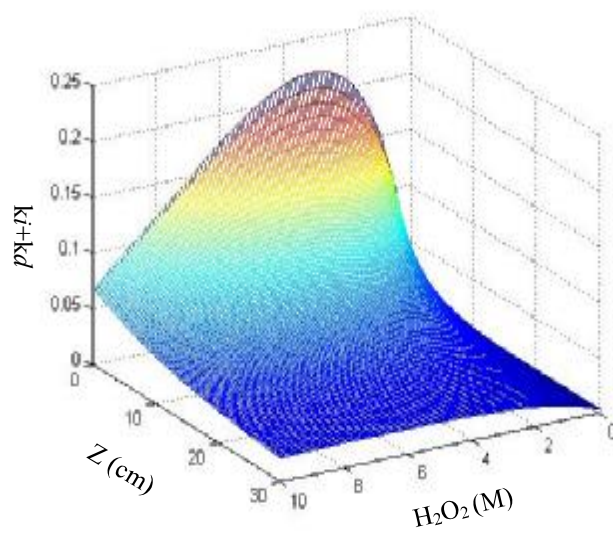
a)



b)



c)



d)

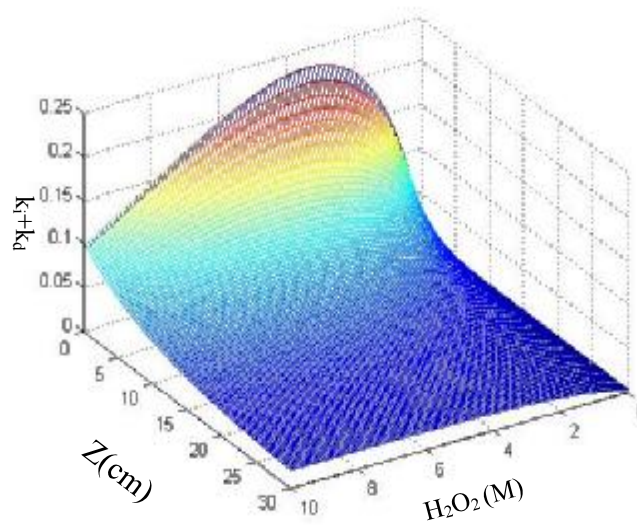
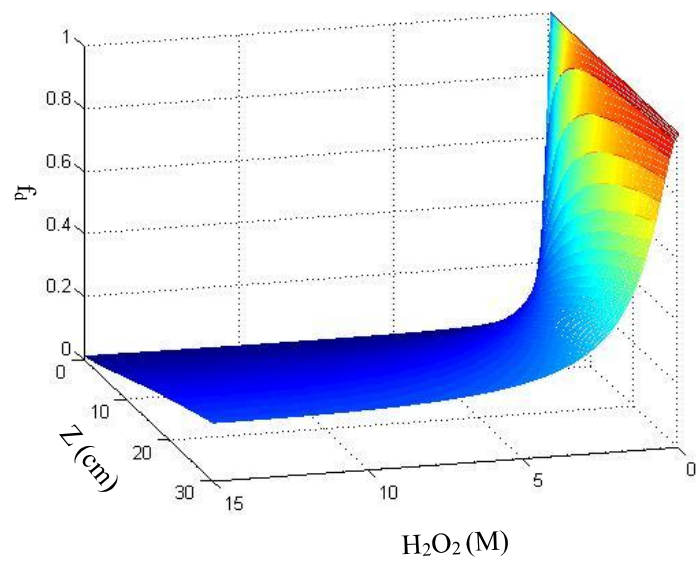
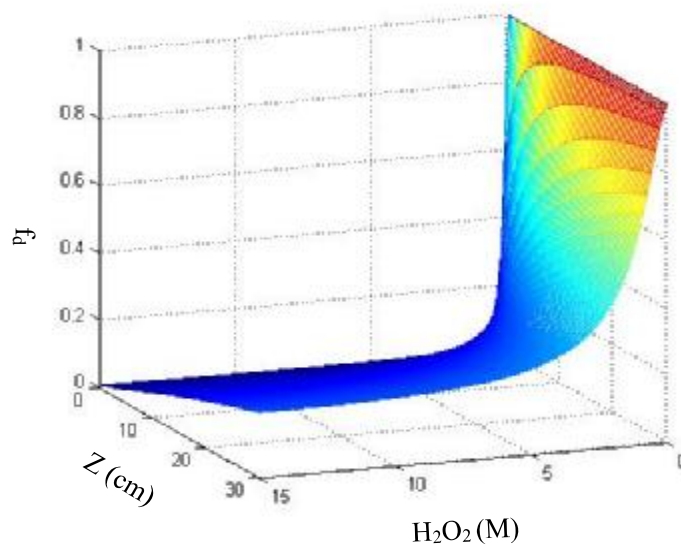


Figure 3.13: Overall rate constants (k_d+k_i) as a function of oxidant concentration ($[H_2O_2]$) and path length (z) of: a) NXP with FA; b) NXP with HA; c) IBP with FA; d) IBP with HA

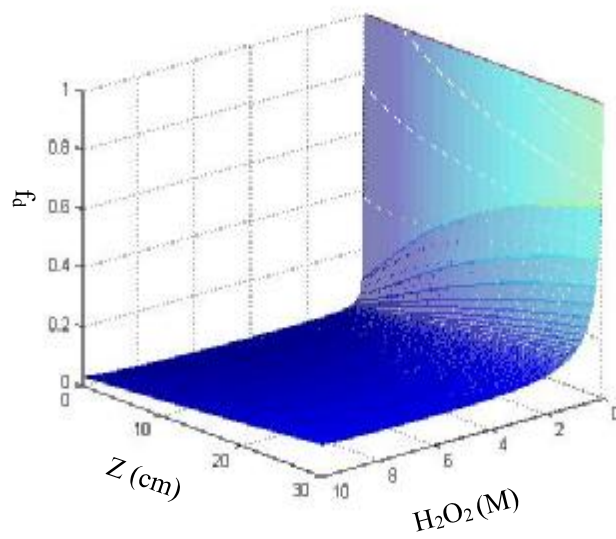
a)



b)



c)



d)

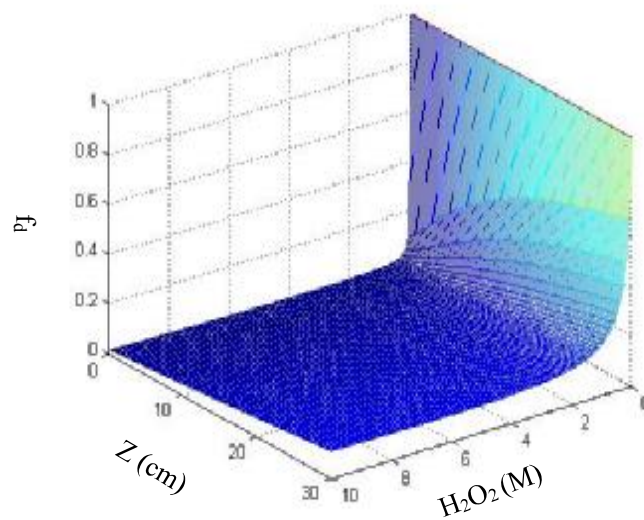


Figure 3.14: The UV photodegradation fraction (f_d) as a function of oxidant concentration ($[H_2O_2]$) and path length (z) of: a) NXP with FA; b) NXP with HA; c) IBP with FA; d) IBP with HA

3.3.3.2 The extent of NXP, IBP and TYL mineralization

Mineralization of organic pollutants in surface water is desirable, because inorganic carbon does not pose toxicity issues to aquatic organisms or humans.

A set of experiments were conducted to determine the time-dependent mineralization of NXP, IBP and TYL during the photolysis under UV/H₂O₂ (1mM). The carbon species (dissolved CO₂, HCO₃⁻ and CO₃²⁻) were determined by ISE in aqueous solution. The principles and use of ISE have been discussed in 3.2.3.2 and Appendix C.

According to carbon mass balance in a closed aqueous solution, the concentration of each carbonate species is calculated by Eq. (3.15) to (3.20):

$$C_T = \text{H}_2\text{CO}_3^* + \text{HCO}_3^- + \text{CO}_3^{2-} \quad (3.15)$$

$$\text{H}_2\text{CO}_3^* = \text{HCO}_3^- + \text{H}^+ \quad k_1 = 10^{-6.35} \quad (3.16)$$

$$\text{HCO}_3^- = \text{CO}_3^{2-} + \text{H}^+ \quad k_2 = 10^{-10.33} \quad (3.17)$$

$$[\text{HCO}_3^-] = \frac{C_T}{1.257} \quad (3.18)$$

$$[\text{CO}_3^{2-}] = 0.00035 C_T \quad (3.19)$$

$$[\text{H}_2\text{CO}_3^*] = C_T - [\text{HCO}_3^-] - [\text{CO}_3^{2-}] \quad (3.20)$$

First, any initial carbonate species, C_0 , need to be measured in the equilibrated aqueous solution before experiment (grey cell in the Table 3.7). C_T represents the total concentration of dissolved CO₂ after irradiation, and is calculated by the values from ISE (C_{ISE}) minus C_0 ($C_T = C_{\text{ISE}} - C_0$). $C\%$ is the ratio of inorganic carbon to the total carbon of NXP, IBP and TYL, denoting the mineralization efficiency. Thus, ~30% of the carbon in each NXP and IBP is in converted to inorganic carbon after 5~6 minutes of treatment, and only ~14% of carbon in TYL is converted to inorganic carbon.

Table 3.7 Extent of mineralization of NXP, IBP and TY

	time(min)	E	logC _{ISE}	C _{ISE} (M)	C _T	HCO ₃ ⁻ (M)	CO ₃ ⁻ (M)	H ₂ CO ₃ (M)	C%
NXP	0	-53.6	-3.97	1.19E-03					
	0.5	-52.8	-3.95	1.24E-03	4.59E-05	3.65E-05	1.63082E-08	9.38E-06	3.38
	1	-51.9	-3.93	1.29E-03	9.97E-05	7.93E-05	3.54082E-08	2.04E-05	7.34
	1.5	-50.4	-3.90	1.38E-03	1.95E-04	1.55E-04	6.91057E-08	3.98E-05	14.33
	2	-49.5	-3.88	1.44E-03	2.55E-04	2.03E-04	9.05024E-08	5.21E-05	18.76
	2.5	-49.3	-3.88	1.46E-03	2.69E-04	2.14E-04	9.53823E-08	5.49E-05	19.77
	3	-49.0	-3.87	1.48E-03	2.89E-04	2.30E-04	1.02789E-07	5.91E-05	21.31
	3.5	-48.3	-3.86	1.53E-03	3.39E-04	2.70E-04	1.20486E-07	6.93E-05	24.98
	4	-47.3	-3.84	1.60E-03	4.13E-04	3.29E-04	1.46807E-07	8.45E-05	30.43
	5	-47.2	-3.83	1.61E-03	4.21E-04	3.35E-04	1.49508E-07	8.60E-05	30.99
IBP	0	-53.8	-3.97	1.18E-03					
	0.5	-53.6	-3.97	1.19E-03	1.12E-05	8.91E-06	3.98152E-09	2.29E-06	0.81
	1	-52.1	-3.93	1.28E-03	9.87E-05	7.85E-05	3.50747E-08	2.02E-05	7.10
	1.5	-50.5	-3.90	1.38E-03	1.99E-04	1.58E-04	7.07655E-08	4.07E-05	14.32
	2	-49.9	-3.89	1.42E-03	2.39E-04	1.90E-04	8.48617E-08	4.88E-05	17.17
	2.5	-49.7	-3.89	1.43E-03	2.52E-04	2.01E-04	8.96501E-08	5.16E-05	18.14
	3	-49.7	-3.89	1.43E-03	2.52E-04	2.01E-04	8.96501E-08	5.16E-05	18.14

	3.5	-48.8	-3.87	1.49E-03	3.15E-04	2.50E-04	1.11767E-07	6.43E-05	22.62
	4	-48.0	-3.85	1.55E-03	3.72E-04	2.96E-04	1.32234E-07	7.61E-05	26.76
	5	-47.4	-3.84	1.60E-03	4.17E-04	3.32E-04	1.481E-07	8.52E-05	29.97
	6	-47.2	-3.83	1.61E-03	4.32E-04	3.44E-04	1.53489E-07	8.83E-05	31.06
	time(min)	E	logC	C(M)		HCO ₃ ⁻ (M)	CO ₃ ⁻ (M)	H ₂ CO ₃ (M)	C%
	0	-58.3	-4.12	8.28E-04					
	0.3	-57.3	-4.10	8.73E-04	4.48E-05	3.57E-05	1.59264E-08	9.16E-06	1.05
	0.67	-56.7	-4.09	9.01E-04	7.29E-05	5.80E-05	2.58932E-08	1.49E-05	1.71
	1	-56.2	-4.08	9.25E-04	9.70E-05	7.71E-05	3.44432E-08	1.98E-05	2.27
TYL	1.5	-55.8	-4.07	9.45E-04	1.17E-04	9.28E-05	4.14474E-08	2.39E-05	2.73
	2	-55.6	-4.06	9.55E-04	1.27E-04	1.01E-04	4.50053E-08	2.59E-05	2.97
	2.5	-52.9	-4.00	1.10E-03	2.73E-04	2.17E-04	9.68968E-08	5.58E-05	6.39
	3	-49.2	-3.91	1.34E-03	5.10E-04	4.06E-04	1.81141E-07	1.04E-04	11.94
	4	-48.1	-3.89	1.42E-03	5.90E-04	4.69E-04	2.09524E-07	1.21E-04	13.81

List of References

1. Zafiriou, O.C. and M.B. True, Nitrite photolysis in seawater by sunlight. *Marine Chemistry*, 1979. **8**(1): p. 9-32.
2. Zepp, R.G., B.C. Faust, and J. Hoigne, Hydroxyl radical formation in aqueous reactions (pH 3-8) of iron(II) with hydrogen peroxide: the photo-Fenton reaction. *Environmental Science & Technology*, 1992. **26**(2): p. 313-319.
3. Southworth, B.A. and B.M. Voelker, Hydroxyl Radical Production via the Photo-Fenton Reaction in the Presence of Fulvic Acid. *Environmental Science & Technology*, 2003. **37**(6): p. 1130-1136.
4. Page, S.E., W.A. Arnold, and K. McNeill, Assessing the Contribution of Free Hydroxyl Radical in Organic Matter-Sensitized Photohydroxylation Reactions. *Environmental Science & Technology*, 2011. **45**(7): p. 2818-2825.
5. Jacobs, L.E., et al., Photosensitized degradation of caffeine: Role of fulvic acids and nitrate. *Chemosphere*, 2012. **86**(2): p. 124-129.
6. Szabó, R.K., et al., Phototransformation of ibuprofen and ketoprofen in aqueous solutions. *Chemosphere*, 2011. **84**(11): p. 1658-1663.
7. Guerard, J., et al., The role of fulvic acid composition in the photosensitized degradation of aquatic contaminants. *Aquatic Sciences*, 2009. **71**(2): p. 160-169.
8. Pereira, V.J., K.G. Linden, and H.S. Weinberg, Evaluation of UV irradiation for photolytic and oxidative degradation of pharmaceutical compounds in water. *Water Research*, 2007. **41**(19): p. 4413-4423.

9. Yuan, F., et al., Degradation of selected pharmaceuticals in aqueous solution with UV and UV/H₂O₂. *Water Research*, 2009. **43**(6): p. 1766-1774.
10. Jiao, S., et al., Aqueous photolysis of tetracycline and toxicity of photolytic products to luminescent bacteria. *Chemosphere*, 2008. **73**(3): p. 377-382.
11. Trovó, A.G., et al., Photodegradation of sulfamethoxazole in various aqueous media: Persistence, toxicity and photoproducts assessment. *Chemosphere*, 2009. **77**(10): p. 1292-1298.
12. Ge, L., et al., Aquatic Photochemistry of Fluoroquinolone Antibiotics: Kinetics, Pathways, and Multivariate Effects of Main Water Constituents. *Environmental Science & Technology*, 2010. **44**(7): p. 2400-2405.
13. Walse, S.S., et al., Role of Dissolved Organic Matter, Nitrate, and Bicarbonate in the Photolysis of Aqueous Fipronil. *Environmental Science & Technology*, 2004. **38**(14): p. 3908-3915.
14. Mack, J. and J.R. Bolton, Photochemistry of nitrite and nitrate in aqueous solution: a review. *Journal of Photochemistry and Photobiology A: Chemistry*, 1999. **128**(1-3): p. 1-13.
15. Xu, Y., et al., Photodegradation kinetics of p-tert-octylphenol, 4-tert-octylphenoxyacetic acid and ibuprofen under simulated solar conditions in surface water. *Chemosphere*, 2011. **85**(5): p. 790-796.
16. Vione, D., et al., Modelling the photochemical fate of ibuprofen in surface waters. *Water Research*, 2011. **45**(20): p. 6725-6736.

17. Grandbois, M., D.E. Latch, and K. McNeill, Microheterogeneous Concentrations of Singlet Oxygen in Natural Organic Matter Isolate Solutions. *Environmental Science & Technology*, 2008. **42**(24): p. 9184-9190.
18. Corin, N., P. Backlund, and M. Kulovaara, Degradation products formed during UV-irradiation of humic waters. *Chemosphere*, 1996. **33**(2): p. 245-255.
19. Santoke, H., et al., Advanced oxidation treatment and photochemical fate of selected antidepressant pharmaceuticals in solutions of Suwannee River humic acid. *Journal of Hazardous Materials*, 2012. **217–218**(0): p. 382-390.
20. Jacobs, L.E., et al., Fulvic acid mediated photolysis of ibuprofen in water. *Water Research*, 2011. **45**(15): p. 4449-4458.
21. Peuravuori, J. and K. Pihlaja, Phototransformations of selected pharmaceuticals under low-energy UVA–vis and powerful UVB–UVA irradiations in aqueous solutions—the role of natural dissolved organic chromophoric material. *Analytical & Bioanalytical Chemistry*, 2009. **394**(6): p. 1621-1636.
22. Schwarzenbach, R.P., P.M. Gschwend, and D.M. Imboden, Direct Photolysis, in *Environmental Organic Chemistry*. 2005, John Wiley & Sons, Inc. p. 611-654.
23. Canonica, S. and M. Freiburghaus, Electron-Rich Phenols for Probing the Photochemical Reactivity of Freshwaters. *Environmental Science & Technology*, 2001. **35**(4): p. 690-695.
24. T, K., Abiotic Hydrolysis of Pesticides in the Aquatic Environment. *Rev. Environ. Contam. Toxicol.*, 2002. **174**: p. 79-261.

25. García Einschlag, F.S., et al., Evaluation of the Efficiency of Photodegradation of Nitroaromatics Applying the UV/H₂O₂ Technique. *Environmental Science & Technology*, 2002. **36**(18): p. 3936-3944.
26. Wu, C., H. Shemer, and K.G. Linden, Photodegradation of Metolachlor Applying UV and UV/H₂O₂. *Journal of Agricultural and Food Chemistry*, 2007. **55**(10): p. 4059-4065.
27. Nienow, A.M., et al., Hydrogen peroxide-assisted UV photodegradation of Lindane. *Chemosphere*, 2008. **72**(11): p. 1700-1705.
28. Wols, B.A. and C.H.M. Hofman-Caris, Review of photochemical reaction constants of organic micropollutants required for UV advanced oxidation processes in water. *Water Research*, 2012. **46**(9): p. 2815-2827.
29. George V. Buxton, C.L.G., W. Phillips Helman, and Alberta B. Ross Critical Review of rate constants for reactions of hydrated electrons, hydrogen atoms and hydroxyl radicals *Journal of Physical and Chemical Reference Data*, 1988. **17**(2).
30. Larson, R.A. and R.G. Zepp, Reactivity of the carbonate radical with aniline derivatives. *Environmental Toxicology and Chemistry*, 1988. **7**(4): p. 265-274.
31. Maruthamuthu, P.N., P, Phosphate radicals. Spectra, acid-base equilibria, and reactions with inorganic compounds. *J. Phys. Chem.*, 1978. **82**(6).
32. Sharpless, C.M. and K.G. Linden, Experimental and Model Comparisons of Low- and Medium-Pressure Hg Lamps for the Direct and H₂O₂ Assisted UV Photodegradation of N-Nitrosodimethylamine in Simulated Drinking Water. *Environmental Science & Technology*, 2003. **37**(9): p. 1933-1940.

CHAPTER 4. DIRECT AND INDIRECT PHOTOTRANSFORMATION OF PPCPs: PRODUCTS AND PROPOSED REACTION PATHWAYS

4.1 Introduction

In the preceding chapter, selected photodegradation rate constants were determined during treatment with: i) UV light and ii) UV plus H₂O₂. The effects of variable parameters, such as pH values, H₂O₂ concentration, NO₃⁻ and NOM (FA and HA), were examined. The results demonstrated that i) pH neutral and basic conditions could enhance the rate of direct photolysis of NXP and IBP, and pH has little influence on the photodegradation of TYL; ii) the photolysis of NO₃⁻ could produce ·OH to increase the direct rate constants for NXP and IBP, but did not affect the photoreactions of TYL; iii) the presence of NOM decreased the direct photolytic reaction rate constants due to light screening effect, but did not have any effects on TYL; iv) the irradiation of H₂O₂ could generate ·OH to increase the degradation of NXP and IBP, but H₂O₂ could otherwise act as the ·OH scavenger; v) the addition of H₂O₂ had little influence on photoisomerization, but promoted the decay of TYL. Also, a kinetic model was employed to predict the photodegradation of NXP and IBP under UV/H₂O₂ condition. These kinetic results provided information on how fast the PPCPs degraded, but not on how the compounds degraded.

Several previous investigations into the degradation products of NXP, IBP and TYL were conducted, but the experimental conditions were quite different from those in this

study (for example, pH, light source, solution, oxidant etc.). Especially for TYL, most products reported were metabolic products in animals, but not comparable to photochemical products in aqueous solution. Szabó *et al.* reported that during irradiation at 185 nm, the presence of dissolved oxygen enhanced the degradation of ibuprofen, and they identified four products as 1-ethyl-4-(2-methylpropyl)-benzene, 1-ethenyl-4-(2-methylpropyl)-benzene, 1-(1-hydroxyethyl)-4-isobutyl-benzene and 4-(2-methylpropyl) acetophenone [1]. Jacobs *et al.* found that FA accelerated the direct photolysis of IBP under natural sunlight condition, and provided information on degradation products: 1-(4-isobutylphenyl) ethanol, isobutylacetophenone, and a phenol derivative [2]. Isidori *et al.* [3] carried out experiments to investigate NXP's photoproducts in a solar reactor, and studied the ecotoxicity of the parent compound and products under solar system. The photoderivatives were not genotoxic nor mutagenic.

To address this knowledge gap, we undertook a study of the nature of the phototransformation of selected PPCPs by identifying selected by-products with Gas Chromatography/ Mass Spectrometry (GC/MS) and Liquid Chromatography/ Mass Spectrometry (LC/MS).

4.2 Materials and Methods

Most materials and methods are the same as those described in Chapter Two and Chapter Three, except for some amendments to the solution preparation, and experimental and analytical methods, all of which are described in the following sections.

4.2.1 Preparation of aqueous PPCPs solution

To identify the intermediates and byproducts of phototransformation of NXP, IBP and TYL in aqueous solution under UV and UV/H₂O₂ experimental conditions, a working solution with a higher initial concentration (500 µM) was used than in the kinetic studies. Three PPCPs aqueous solutions were prepared in pH 7 buffered solution.

4.2.2 Experimental Procedures

To identify photochemical products of NXP and IBP study, all sample analyses were completed with a GC/MS. 500 mL working solution (NXP or IBP) was transferred to a 660 mL quartz tube, which was positioned in the Rayonet 100 reactor. For experiments under UV/H₂O₂ condition, the appropriate amount of oxidant was added to the tube and the contents mixed thoroughly. The irradiation times were up for 30 min for direct photolysis (UV alone) and 20 min for ·OH (UV/1 mM H₂O₂). After irradiation, 500 mL of solution was transferred into a beaker for pH adjustment. 0.01M HCl was used to adjust pH to 3 so that the neutral form of compound was dominant in the solution. 20 mL DCM was added to the sample in a capped vial. Then the solution containing DCM and sample was placed on a Glas-col Rotator and extracted for 24 hours at 30 rpm rotation speed. The resulting extracts were transferred to an amber vial, and concentrated to 5 mL with a nitrogen gas sparge. The condensed sample was stored at 4 °C until analysis.

The product study for TYL was carried out under the following conditions. For direct photolysis, 500 µM TYL solution was transferred into a 660 mL quartz tube and irradiated in the photoreactor. Five mL aliquot was removed from the reactor at 1 min, and other 5

mL aliquot was removed at 20 min. Samples at 1min and 20 min were run on the LC/MS. Under UV/H₂O₂ condition, the appropriate amount of oxidant was added to the tube and contents mixed thoroughly. After 1 min irradiation, 5 mL solution was removed and kept in an amber vial. All samples were kept at 4 °C until analysis. All samples were analyzed with LC/MS.

4.2.3 Analytical Methods

4.2.3.1 Gas Chromatography/ Mass Spectrometry (GC/MS)

All gas chromatography/mass spectrometry analysis was completed using an Agilent 5975C (Agilent Labs, Santa Clara, CA) instrument. The electron impact was used to ionize the samples. Typical electron energy was 70eV with the ion source temperature at 250 °C. The chemical separations were achieved using a 30 meter DB-5 capillary column (250 µm ID X 0.25 µm). The column temperature was set at 100 °C, held for 0.1 minutes prior to ramping the temperature to 320 °C at 10 °C per minute. The flow rate was 1mL/ min, and the injector temperature was 250 °C.

25 µL of PPCPs sample in DCM was mixed with 25µL of Sylon BFT [BSTFA + TMCS; 99:1 (v : v)] (Sigma Aldrich, St. Louis, MO) and allowed to stand for 15 minutes before analysis.

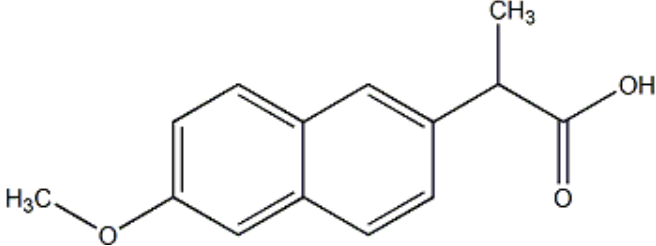
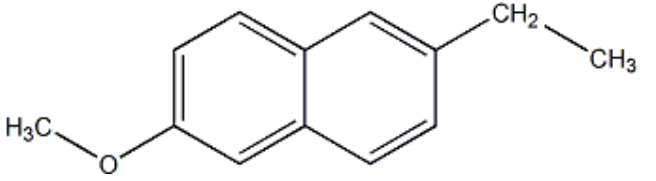
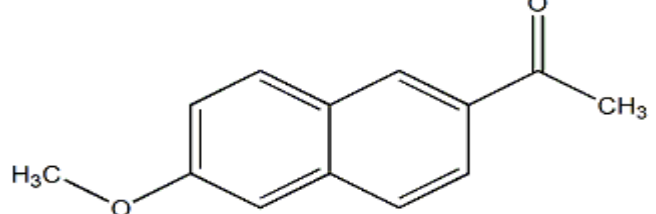
4.2.3.2 Liquid Chromatography/ Mass Spectrometry (LC/MS)

The LC/MS experiments were completed on an Agilent 6320 Ion Trap (Agilent Labs, Santa Clara, CA) liquid chromatography/mass spectrometer with electrospray ionization (ESI). The samples dissolved in the phosphate buffer were injected into a 10 microliter injection loop prior to separation on a Zorbax SB-C18 column, 3mm X 150mm, (Agilent Labs, Santa Clara, CA). The LC mobile phases were: A - 0.02% acetic acid and B - acetonitrile. The samples were separated using a 0.3 microliter per minute flow rate with the following gradient: 90% A; 10% B to 10 minutes, then 60% A; 40% B to 30 minutes and finally 40% A; 60% B to 50 minutes. All percentages of solvent were volume percent. The capillary voltage was set a 2.5 kV with a capillary current of approximately 4 nA. The nebulizer pressure was set at 50 psi and the drying gas flow at 5liters/minute. The drying gas temperature was set at 250 °C and the vaporizing temperature at 150 °C. The skimmer voltage is set at 40 volts. The UV detector was set at 289 nm for these studies.

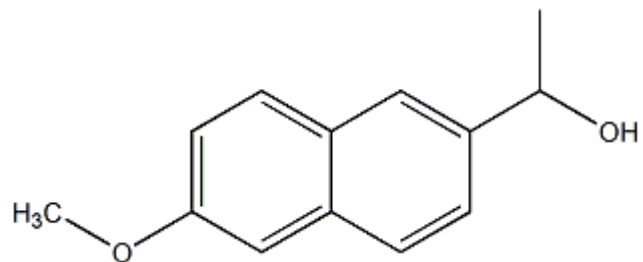
4.3 By-Product Study Results and Discussion

Several photoproducts accumulated during the photolysis of NXP, IBP and TYL under UV and UV/H₂O₂ conditions. Table 4.1 summarizes these photoproducts.

Table 4.1 Photoproducts of NXP, IBP and TYL

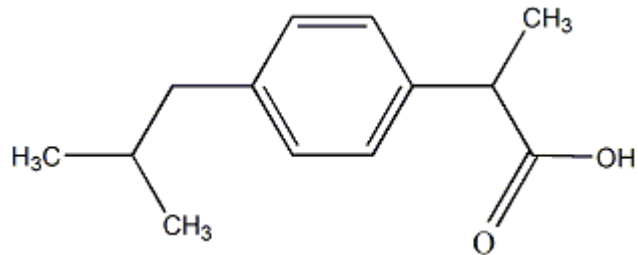
Name	Structure	m/z	Treatment
Parent Compound: Naproxen (I)		230	
1- ethyl-6-methoxynaphthalene (IV)		186	UV and UV/H ₂ O ₂
NXP 2- acetyl-6-methoxynaphthalene (VI)		200	UV/H ₂ O ₂

1-(6-methoxy-2-naphthyl)ethanol
(V)



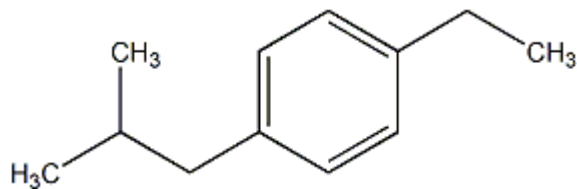
184 UV and UV/H₂O₂

Parent Compound: Ibuprofen
(VII)



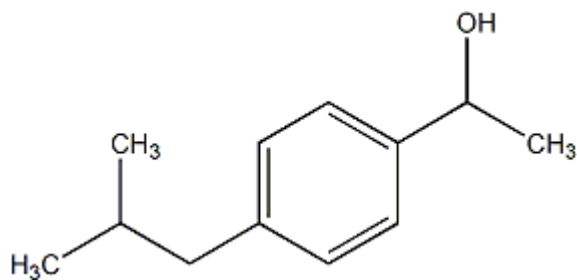
203

1-ethyl-4-(2-methylpropyl)-benzene
(XI)



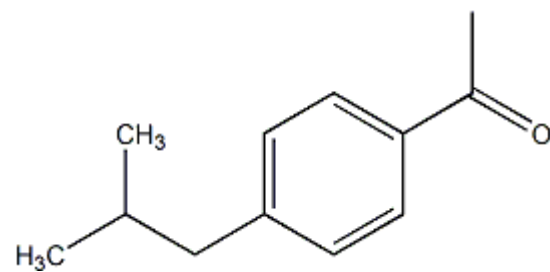
162 UV and UV/H₂O₂

IBP 1-(1-hydroxyethyl)-4-isobutyl-benzene
(X)



178 UV and UV/H₂O₂

4-(2-methylpropyl) acetophenone
(XII)

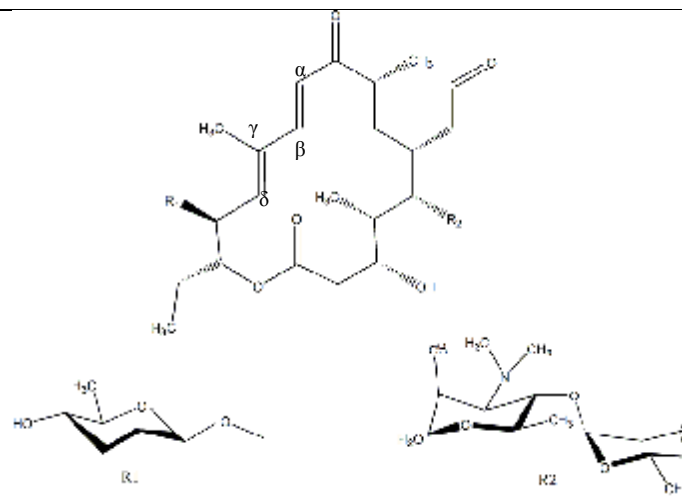


176

UV/H₂O₂

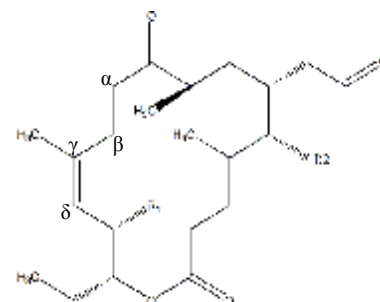
TYL

Parent Compound: TYLA

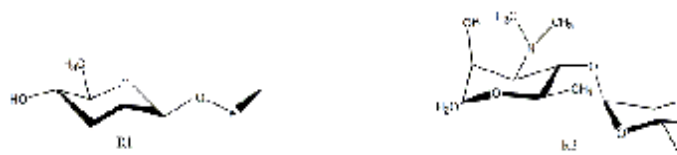


916

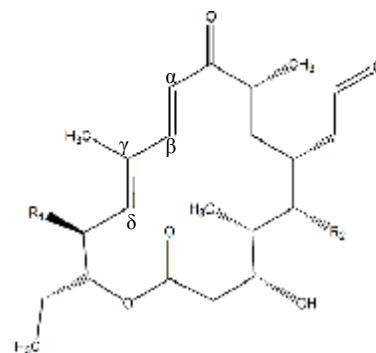
TYLA isomer



916 UV and UV/H₂O₂



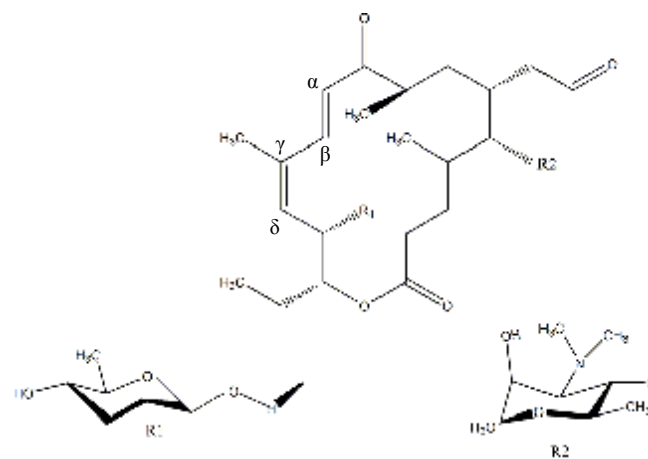
Parent Compound: TYLB



772



TYLB isomer

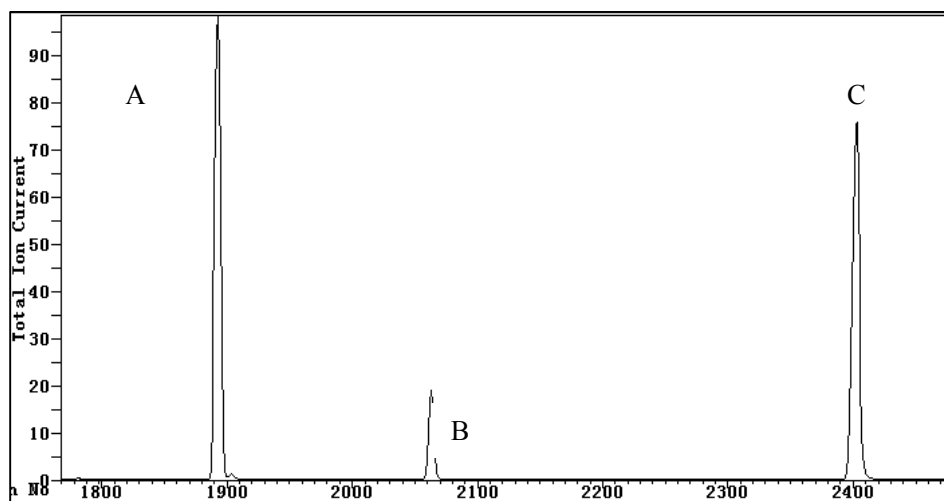


772 UV and UV/H₂O₂

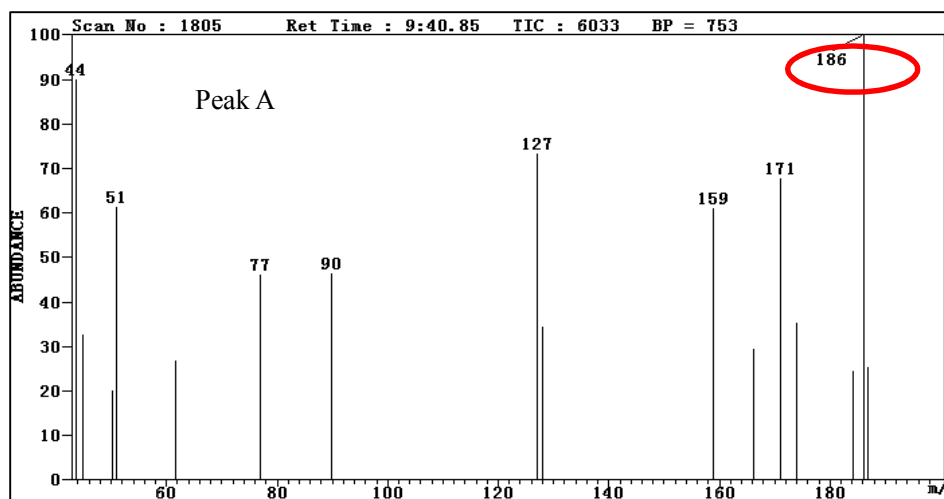
4.3.1 NXP degradation mechanism

The mass spectrum of photoproducts of NXP solution at pH = 7 after direct photolysis (UV) and indirect photolysis (UV/1 mM H₂O₂) are displayed in Figure 4.1 a), b) and c) and Figure 4.2 a), b) and c). It could be seen that all products had a lower retention times than the parent compounds, so the change of molecule polarity resulting from the transformation of -COOH could be responsible for it.

a)



b)



c)

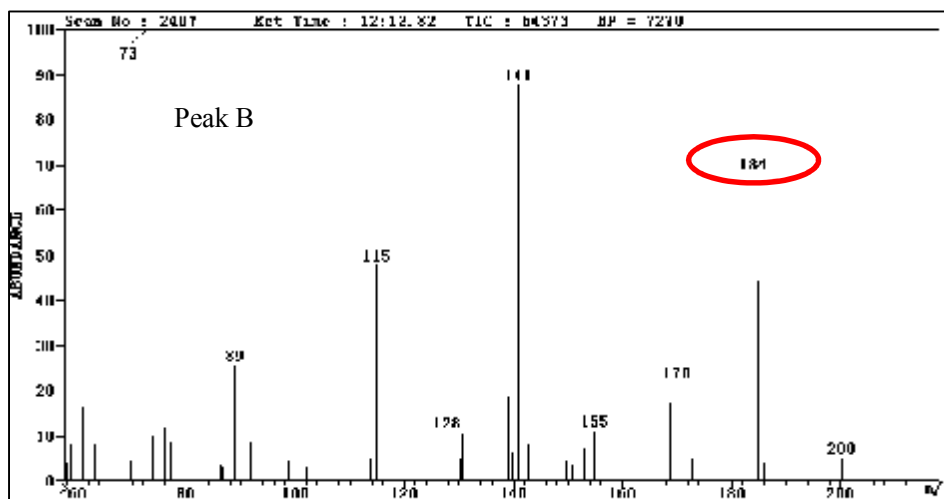
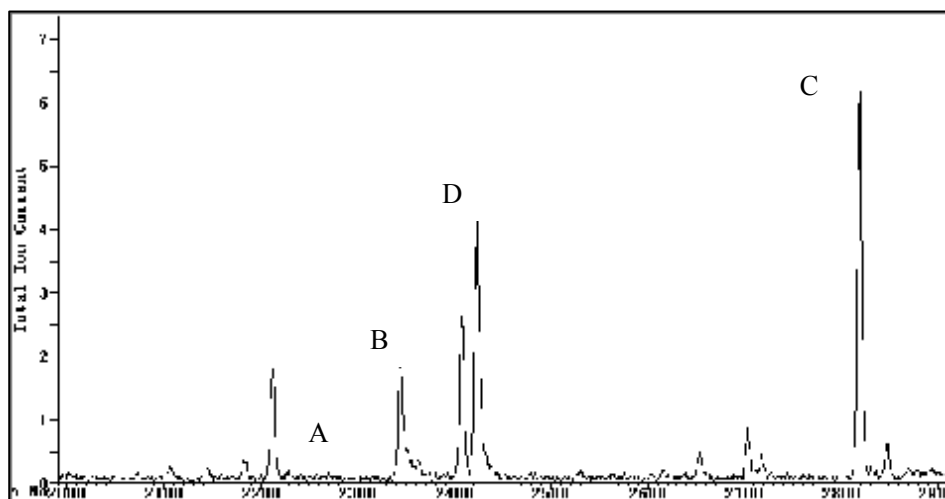


Figure 4.1: The spectrum of photoproducts of NXP after direct photolysis. a) TIC spectrum; b) spectrum of peak A; c) spectrum of peak B

In Figure 4.1 a), peak C is the parent compound of NXP (I), and peak A (product IV) and B (product V) are two products. For photolytic reaction, photodecarboxylation is the replacement of $-\text{COOH}$ with the corresponding hydrocarbon. In our case, decarboxylation could lead to a benzylic radical, followed by abstraction of H^\bullet or $\cdot\text{OH}$ oxidation to the alcohol or ketone, as illustrated in Figure 4.3 [4].

As shown in the Figure 4.3, under UV condition, 1-ethyl-6 methoxynaphthalene (IV) and 1-(6-methoxy-2-naphthyl) ethanol (V) are detected. The first step is that the carboxylate group was transferred to a benzylic radical (III) by photoionization [4]. Such photochemically activated electron transfer results in loss of CO_2 [5]. The second step is benzylic radical abstraction of H^\bullet or $\cdot\text{OH}$ from H_2O to form the products.

a)



b)

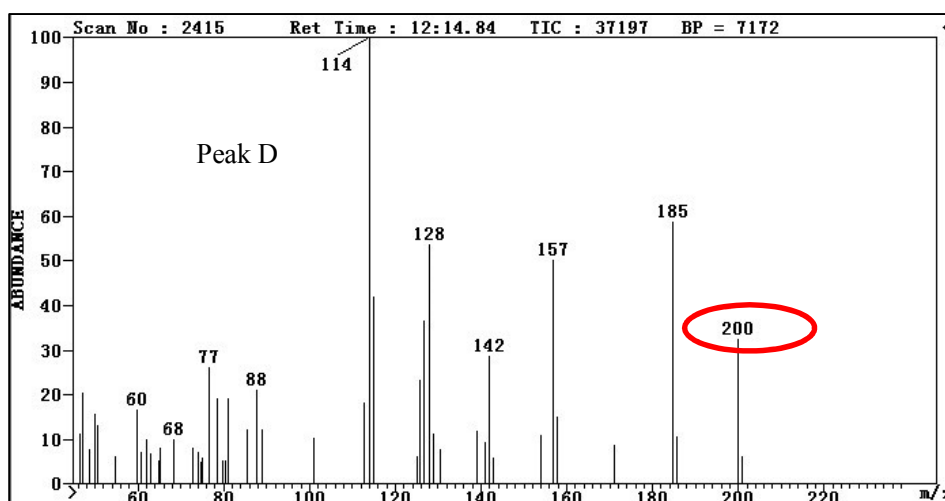


Figure 4.2: The spectrum of photoproducts of NXP after indirect photolysis. a) TIC spectrum; b) spectrum of product (VI)

Under UV/H₂O₂ condition, the product (IV) and (V) also are detected, and a new product (VI) is identified. As Figure 4.2 shows, the peak A, B and C are significantly smaller than those in Figure 4.2, indicating that the parent compound (I) decayed more with

the addition of H_2O_2 and product (IV) and (V) were further oxidized. The mechanism for the degradation of NXP was likely that the parent compound underwent the photoionization process where the carboxylate group was converted to a radical, then H^\bullet or $\cdot\text{OH}$ atom were added the radical to produce product (IV) and (V), the same as the pathway under the direct photolysis. Such products could be subsequently oxidized to by $\cdot\text{OH}$ 2-acetyl-6-methoxynaphthalene, product (VI). Moreover, the concentration of product (VI) was relatively low at the beginning of the photolysis, but the concentration was higher than product (IV) and (V) after 30 min photolysis.

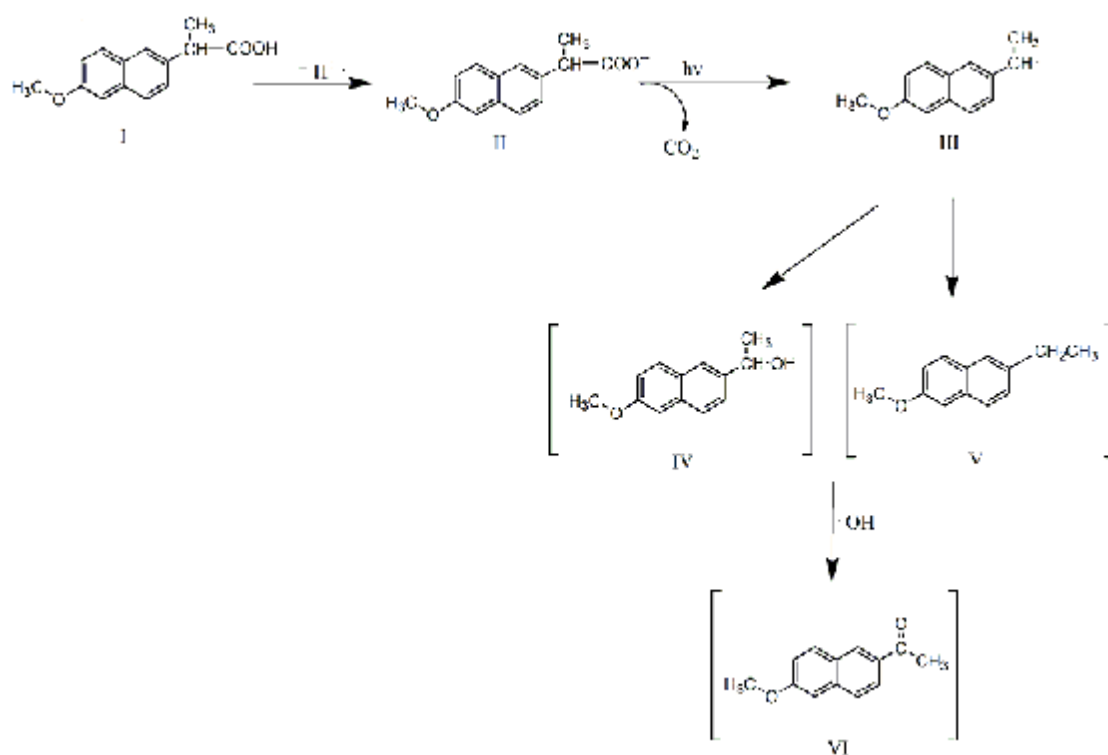
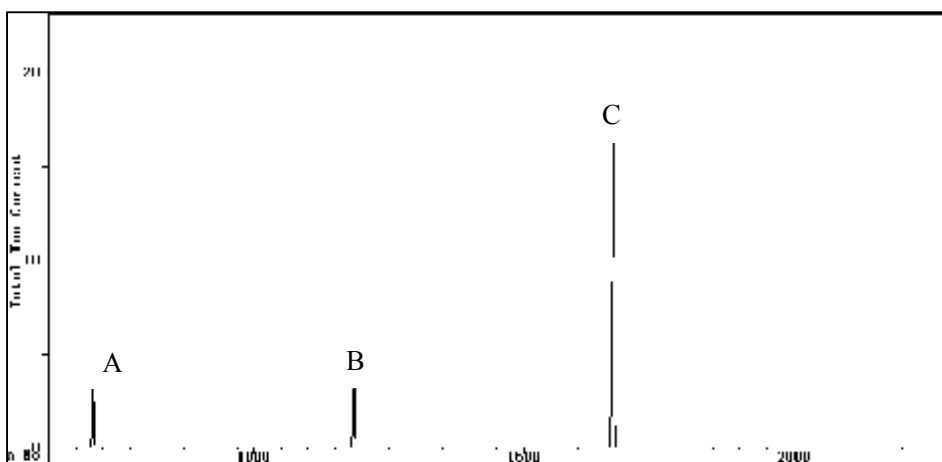


Figure 4.3: Possible pathways of NXP under UV and UV/ H_2O_2 conditions

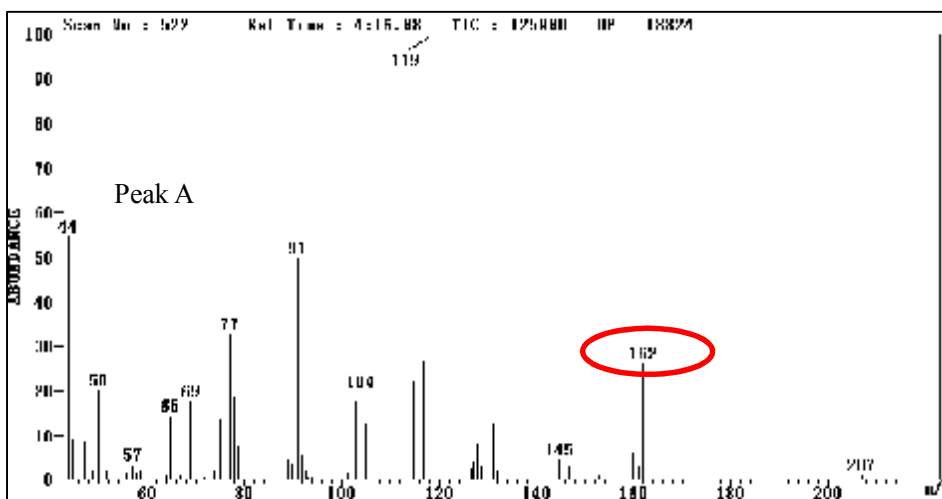
4.3.2 IBP degradation mechanism

Table 4.1 shows the IBP byproducts identified by GC/MS under the different experimental conditions. The mass spectrum is reported in Figure 4. 4.

a)



b)



c)

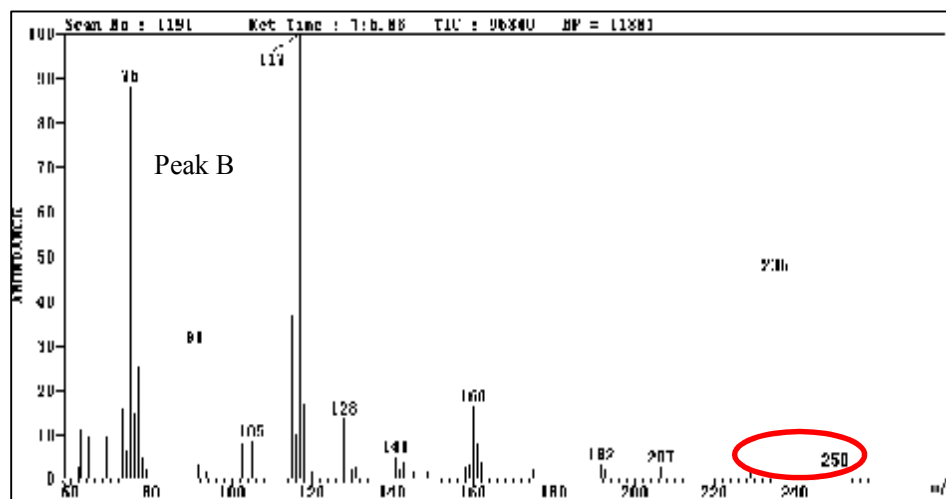
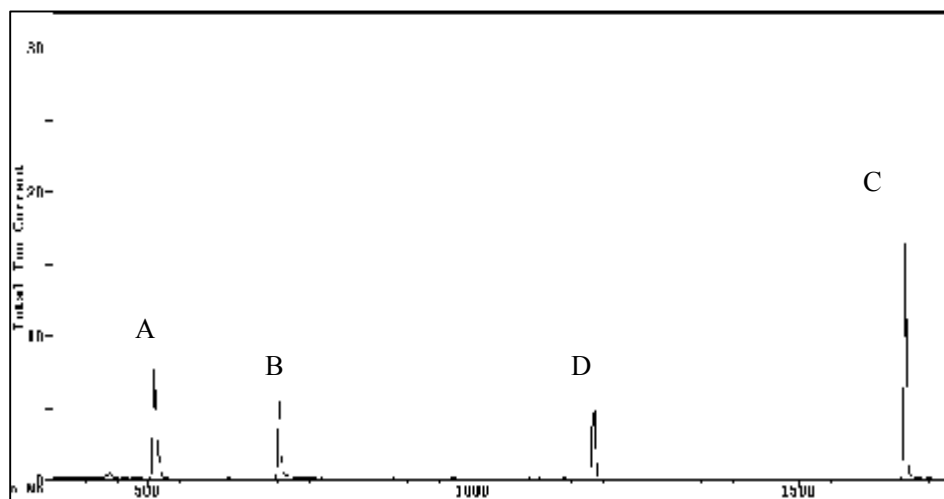


Figure 4.4: The spectrum of photoproducts of IBP after direct photolysis. a) TIC spectrum; b) spectrum of product (XI); c) spectrum of product (X)

In Figure 4.4 a), the peak C is the parent compound of IBP (VII). For peak B (product X), the samples were mixed with derivatizing reagent of the mass weight of 72g/mol, so the peak B represented the compound whose molar weight was $250-72=178$ g/mol.

The direct photolysis of IBP yielded 1-ethyl-4-(2-methylpropyl)-benzene (XI) as detected photodegradation products. This byproduct probably originated from the decarboxylation first, where there was a cleavage of the C-C bond to the carboxyl group, then followed by H^\bullet or $\cdot OH$ abstraction from H_2O . The photodecarboxylation process of PPCPs in aqueous solution has been widely demonstrated [6-8], and it is common step in photolytic reaction. Castell *et al.* [7] designed IBP experiments in methanol at $\lambda = 254$ nm, and observed the product (XI), (X) and (XII), indicating that the photodegradation behavior of IBP in organic solvent is similar to pathway in aqueous solution.

a)



b)

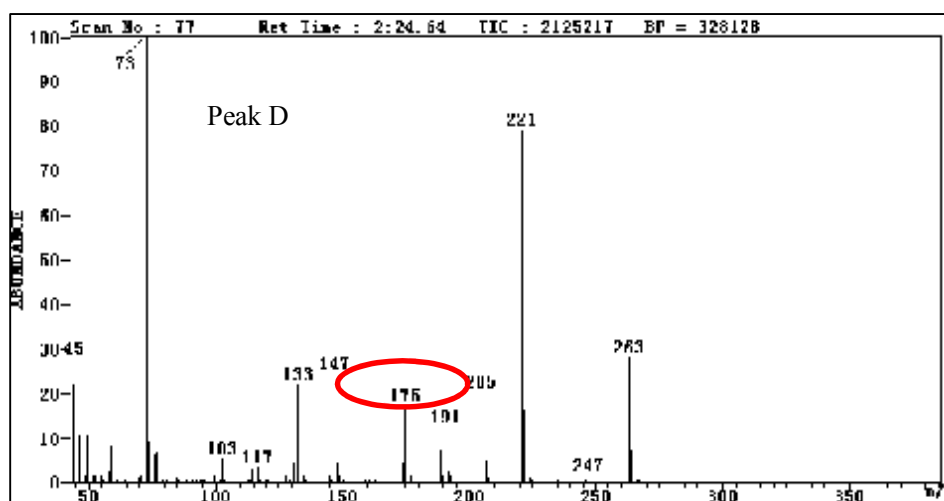


Figure 4.5: The spectrum of photoproducts of IBP after indirect photolysis. a) TIC spectrum; b) spectrum of product (XII)

1-(1-hydroxyethyl)-4-isobutyl-benzene (X) was found both under UV and UV/H₂O₂ condition. This could be explained by the attachment of OH from H₂O or ·OH from photolysis of H₂O₂ to the benzylic radical after the photodecarboxylation. The formation

of product 4-(2-methylpropyl) acetophenone (XII) probably involved the reaction of $\cdot\text{OH}$. The mass spectrum of products are shown in the Figure 4.5, and the possible degradation pathways are illustrated in the Figure 4.6.

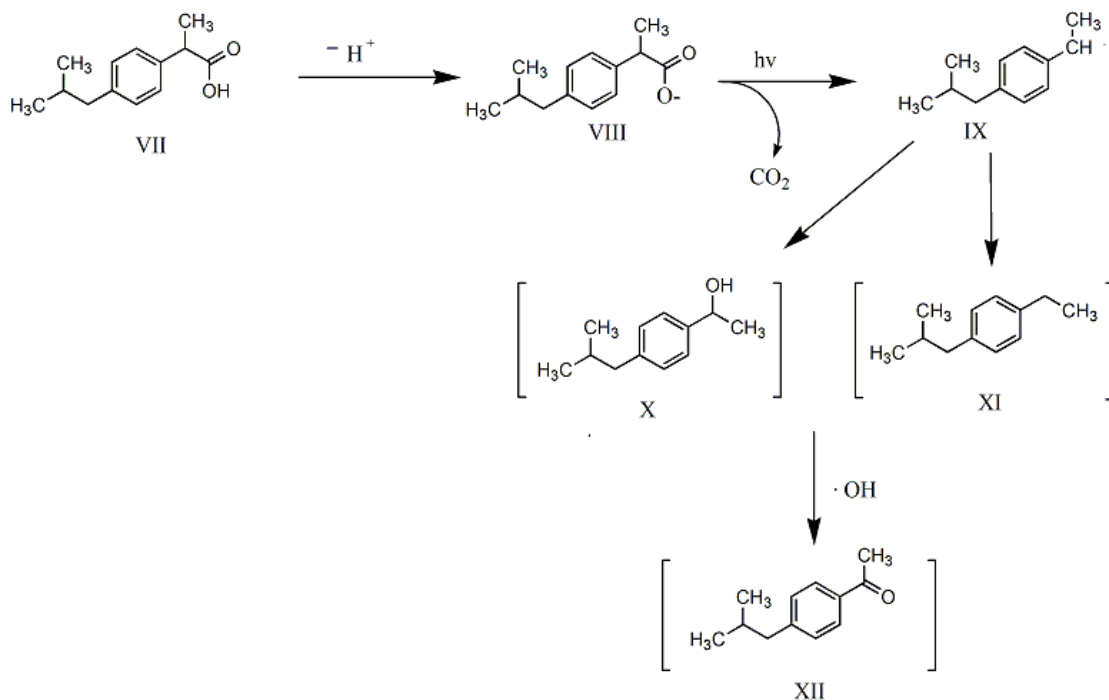


Figure 4.6: Possible pathways of IBP under UV and UV/H₂O₂ conditions

4.3.3 TYL degradation mechanism

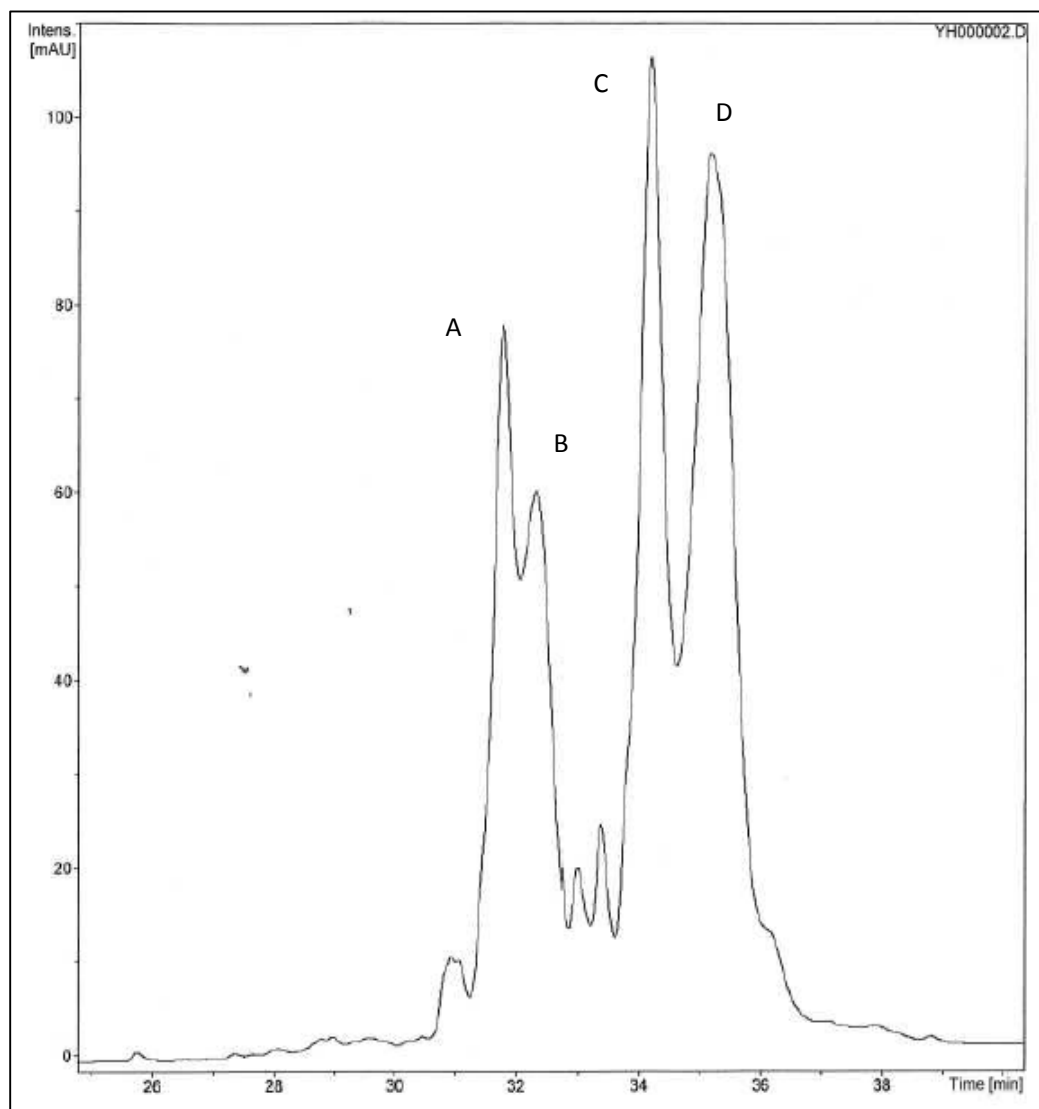
The chromatogram of the solution after direct photolysis of TYL is illustrated in Figure 4.7. There are four major peaks formed after 1 min UV degradation (peak A, B, C and D), corresponding to the TYLB, TYLB_{isomer}, TYLA and TYLA_{isomer}, respectively (Figure 4.7 a)). The structure of the parent compounds and photoisomers are listed in the Table 4.1. The photoisomerization mechanism is proposed to be the γ/δ rotation of double bond of the ketodiene chromophore on TYLA and TYLB, as was previously proposed by

other researchers [9-11]. Figure 4.8 shows the mass spectra data of TYL and its photoisomers. In the Figure 4.7 b), there are several new m/z peaks observed after 20 min UV treatment, and these relatively small peaks represent that TYL A and TYL B are degraded in to some lower molecular weight compounds.

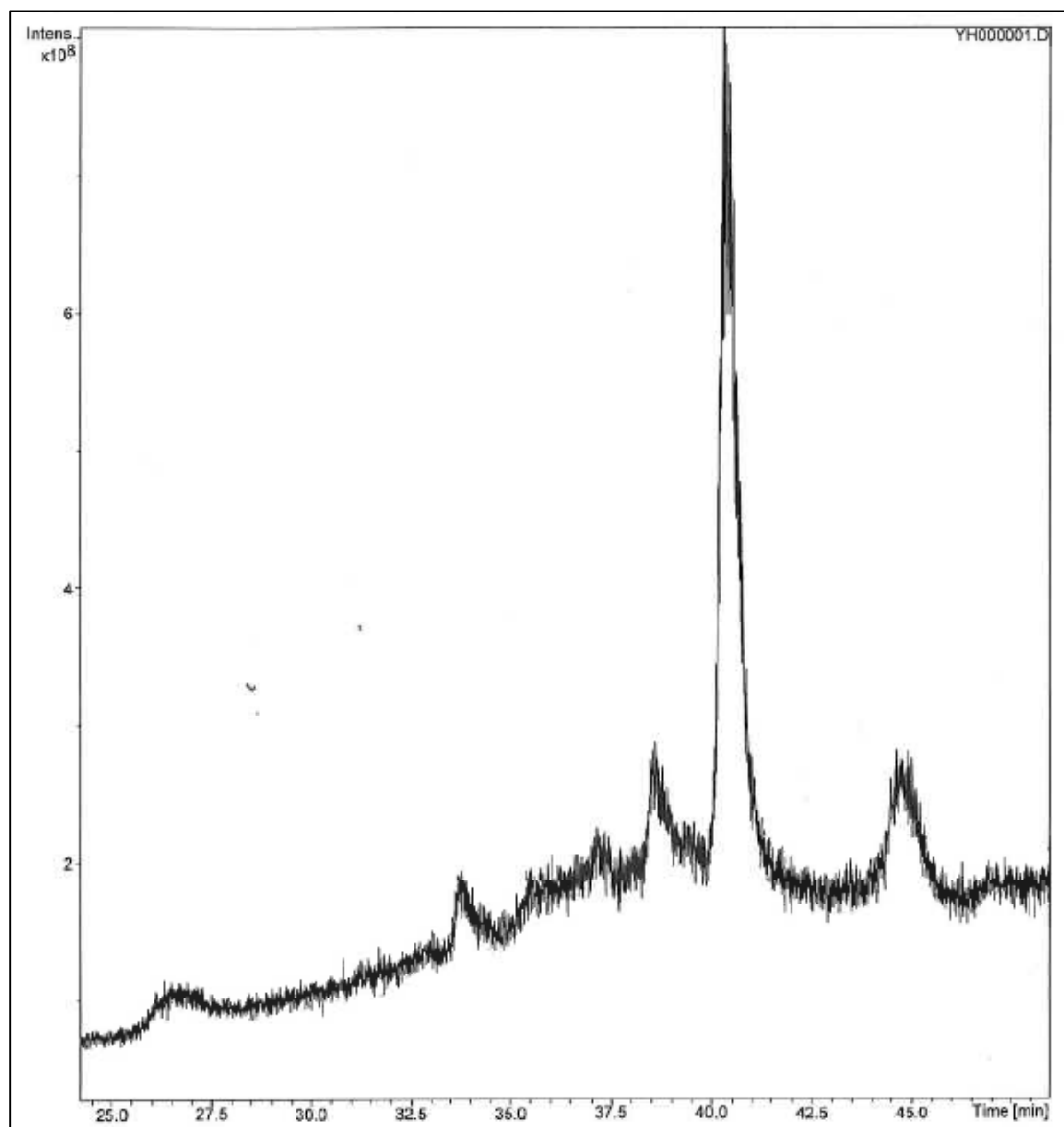
The comparison of Figure 4.7 a) and c) give information that 1 mM oxidant seems to have no significant effects on the phototransformation of TYL A and TYL B, because the chromatography of TYL is very close to that of TYL under direct photolysis. This is probably attributed to the rapidity of the photoisomerization reaction.

Werner *et al.*[10] investigated the phototransformation of TYLA in aqueous solution under sunlight, and just found photoisomer of TYLA, no new m/z peaks were observed. Possible reason for the difference between our results and theirs is the intensity of sunlight is less than the irradiation intensity we used in this study.

a)



b)



c)

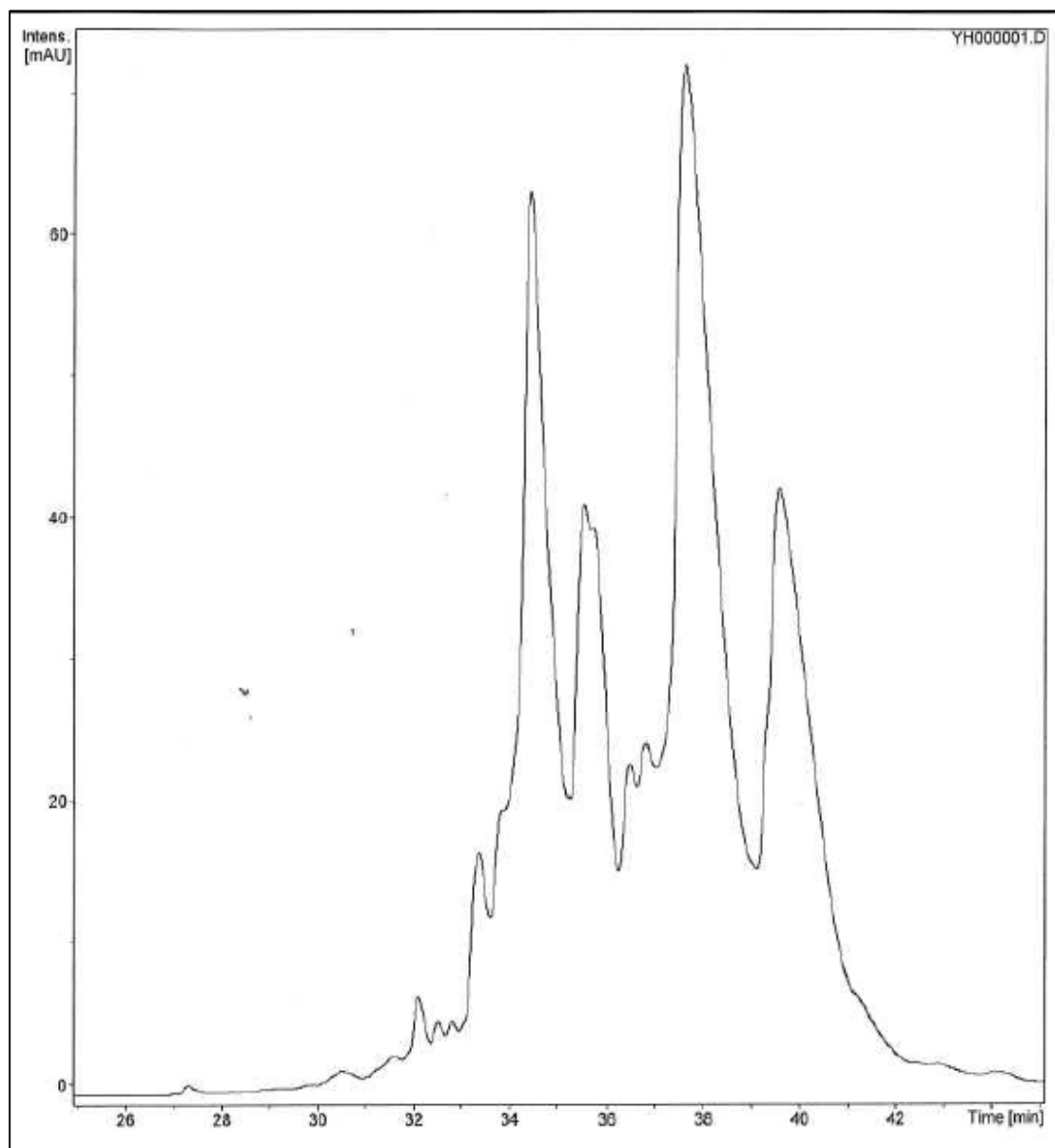
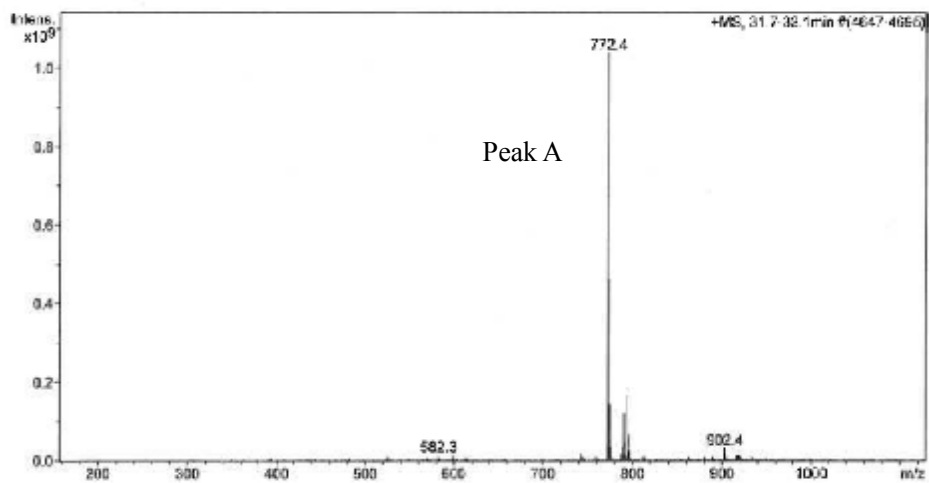
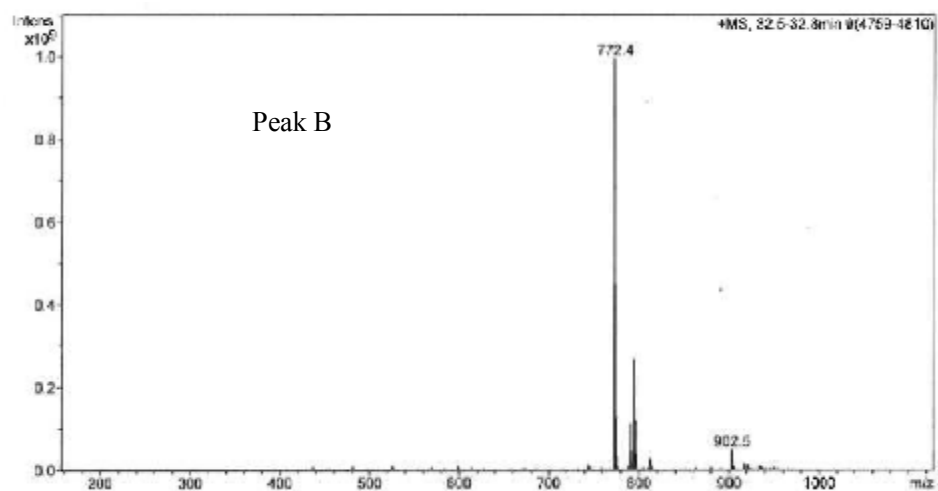


Figure 4.7: a) Chromatogram of TYL after 1min UV degradation; b) TIC chromatogram of TYL after 20 min UV treatment; c) Chromatogram of TYL after 1min UV /H₂O₂ degradation

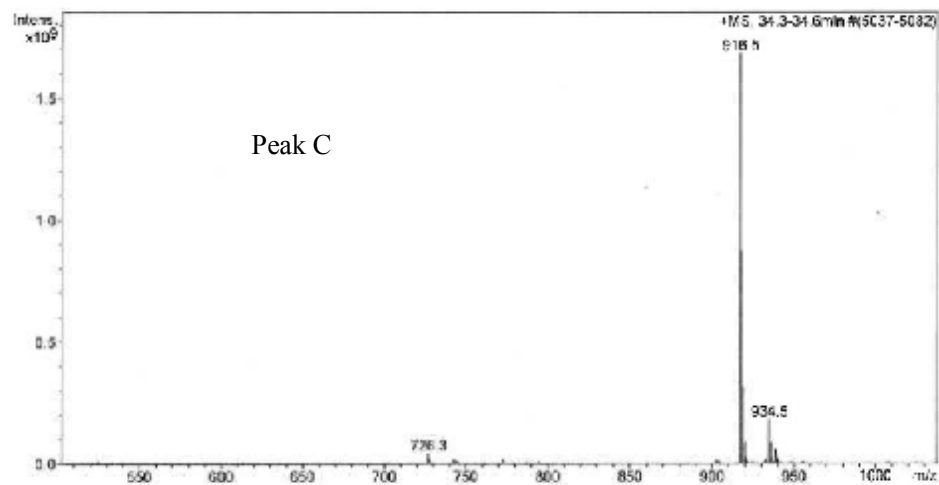
a)



b)



c)



d)

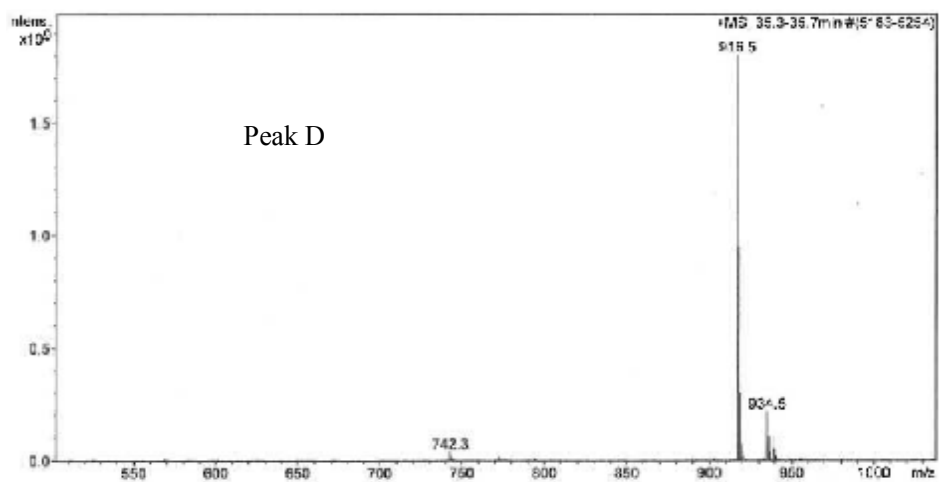


Figure 4.8: Mass spectra of parent compound and by products: a) TYLB; b) TYLB isomer; c) TYLA; d) TYLA isomer

List of References

1. Szabó, R.K., et al., Phototransformation of ibuprofen and ketoprofen in aqueous solutions. *Chemosphere*, 2011. **84**(11): p. 1658-1663.
2. Jacobs, L.E., et al., Fulvic acid mediated photolysis of ibuprofen in water. *Water Research*, 2011. **45**(15): p. 4449-4458.
3. Isidori, M., et al., Ecotoxicity of naproxen and its phototransformation products. *Science of The Total Environment*, 2005. **348**(1-3): p. 93-101.
4. Packer, J., et al., Photochemical fate of pharmaceuticals in the environment: Naproxen, diclofenac, clofibrac acid, and ibuprofen. *Aquatic Sciences*, 2003. **65**(4): p. 342-351.
5. Joschek, H.-I. and L.I. Grossweiner, Optical Generation of Hydrated Electrons from Aromatic Compounds. III. *Journal of the American Chemical Society*, 1966. **88**(14): p. 3261-3268.
6. Budac, D. and P. Wan, Photodecarboxylation: mechanism and synthetic utility. *Journal of Photochemistry and Photobiology A: Chemistry*, 1992. **67**(2): p. 135-166.
7. Castell, J.V., et al., Photolytic Degradation of Ibuprofen Toxicity of The Isolated Photoproducts on Fibroblasts and Erythrocytes. *Photochemistry and Photobiology*, 1987. **46**(6): p. 991-996.
8. Boscá, F., et al., Photochemical and Photobiological Properties of Ketoprofen Associated with The Benzophenone Chromophore. *Photochemistry and Photobiology*, 1994. **60**(2): p. 96-101.

9. Paesen, J., et al., Isolation of decomposition products of tylosin using liquid chromatography. *Journal of Chromatography A*, 1995. **699**(1-2): p. 99-106.
10. Werner, J.J., et al., Environmental Photochemistry of Tylosin: Efficient, Reversible Photoisomerization to a Less-Active Isomer, Followed by Photolysis. *Journal of Agricultural and Food Chemistry*, 2007. **55**(17): p. 7062-7068.
11. Hu, D. and J.R. Coats, Aerobic degradation and photolysis of tylosin in water and soil. *Environmental Toxicology and Chemistry*, 2007. **26**(5): p. 884-889.

CHAPTER 5. OVERALL CONCLUSIONS

The primary objective of this study was to investigate the efficiency of UV_{254nm} and UV_{254nm}/H₂O₂ to degrade Pharmaceuticals and personal care products (PPCPs).

Under UV_{254nm}/3mM H₂O₂ conditions, at a light intensity of $I = 7.2 \times 10^{-5}$ einstein sec⁻¹, naproxen (NXP) and ibuprofen (IBP) degraded rapidly (all kinetic rate constants obtained from experimental data listed in Table 2.2 and 3.1). For NXP, rate constants were $k = 0.0028$ sec⁻¹ (direct photolysis, UV_{254nm}), 0.018 sec⁻¹ (UV/3mM H₂O₂), 0.0029 sec⁻¹ (~320 μM UV_{254nm} NO₃⁻), 0.0023 sec⁻¹ (UV_{254nm} ~10 mg/L fulvic acid) and 0.0018 sec⁻¹ (UV_{254nm} ~10 mg/L humic acid). For IBP, rate constants were $k = 0.0023$ sec⁻¹ (direct photolysis, UV_{254nm}), 0.023 sec⁻¹ (UV/3mM H₂O₂), 0.0030 sec⁻¹ (~320 μM UV_{254nm} NO₃⁻), 0.0016 sec⁻¹ (UV_{254nm} ~10 mg/L fulvic acid) and 0.0013 sec⁻¹ (UV_{254nm} ~10 mg/L humic acid). For Tylosin (TYL), the rate constants of forward photoisomerization $k_f = 0.066$ sec⁻¹, backward photoisomerization $k_r = 0.016$ sec⁻¹, photodegradation $k_d = 0.00057$ sec⁻¹ for TYLA, and $k_f = 0.066$ sec⁻¹, $k_r = 0.016$ sec⁻¹, $k_d = 0.00057$ sec⁻¹ for TYLB. In addition, the quantum yield (ϕ) was 0.008 and 0.098 for NXP and IBP, respectively, measured in buffered solution at pH = 7 under light at 254 nm, and quantum yield values of forward photoisomerization of TYLA and TYLB were 0.21 and 0.35 at pH = 7 solution.

Photochemical reaction intermediates were identified. For NXP, three by-products

were detected, two specific to both direct and indirect photolysis and one specific to indirect photolysis. There were also three intermediates detected for IBP, one specific to indirect photolysis and two to both. The behavior of TYL was different from the performance of NXP and IBP. Only photoisomer was formed for TYLA and TYLB, respectively.

APPENDICES

Appendix A. Chemical Actinometry

In chemical actinometry, an accurate quantum yield (Φ) of a compound is used to determine the amount of incident radiation (I_λ). Therefore, a potassium ferrioxalate actinometer was used to measure photon flux in this research.

According to Kuhn [1], the change in concentration of the ferrous ion (Fe^{2+}) over time is equal to the product of its quantum yield and incident radiation at 254 nm:

$$\left(\frac{d[\text{Fe}^{2+}]}{dt}\right) = \Phi I \quad (1)$$

The reaction is zero-order, so the disappearance rate of Fe^{2+} is determined from the slope of a linear regression of the data set (concentration of ferrous iron versus time).

$$[\text{Fe}^{2+}] = kt \quad (2)$$

For potassium ferrioxalate actinometry, $\Phi = 1.25$ [2], the incident radiation I_λ is calculated on rearrangement:

$$I_\lambda = k/\Phi \quad (3)$$

Based on the principle described above, solution preparation and experimental procedures outlined here.

10-phenanthroline (> 99%), sulfuric acid (95-98%), sodium acetate (99%) and iron sulfate hydrate (99%) were obtained from Sigma-Aldrich, and potassium oxalate monohydrate (99%) was purchased from Mallinckrodt Inc..

Stock solutions preparation:

1. 1 N CH_3COONa : dissolved 41.02 g sodium acetate in a 500 mL flask and dilute to mark by DI water.
2. 1 N H_2SO_4 : diluted 27.62 mL sulfuric acid (95-98%) to 1 L by DI water.

3. Acetate buffer solution: added 300 mL and 1 N sodium acetate and 180 mL H_2SO_4 in a 500 mL volumetric flask and diluted to 500 mL by water.
4. 0.1 M FeSO_4 : mixed 2.78 g $\text{FeSO}_4 \cdot 7\text{H}_2\text{O}$ and 10 mL 1 N H_2SO_4 in a 100 mL volumetric flask and diluted to mark by DI water.
5. 0.4 mM ferrous iron: transferred 0.8 mL 0.1 M FeSO_4 and 20 mL 1N H_2SO_4 in a bottle and diluted to 200 mL by DI water.
6. 0.1 wt% 1,10-phenanthroline: dissolved 109.99 mg 1,10-phenanthroline monohydrate in 100 mL DI water and stored in the dark.
7. 30 mM $\text{K}_2\text{Fe}(\text{C}_2\text{O}_4)_3$: added 1.47 g $\text{K}_2\text{Fe}(\text{C}_2\text{O}_4)_3$ to 100 mL volumetric flask with 10 mL 1N H_2SO_4 , then diluted to mark.

Then, a standard curve of $[\text{Fe}^{2+}]$ was prepared:

1. 0, 1.25, 2.5, 3.75, 5, and 6.25 mL of 0.4 mM FeSO_4 were transferred to six 25 mL volumetric flasks and mixed with 1.25 mL 1 N H_2SO_4 and 6.25 mL acetate buffer solution.
2. To the volumetric flasks, 2.5 mL 0.1 wt% 1,10-phenanthroline monohydrate was transferred and stored for 30 min to let the complex of ferrous iron completely react with 1,10-phenanthroline.
3. Standard solutions range from 0-0.1 mM were analyzed on a UV-vis spectrophotometer at $\lambda = 510$ nm. The standard curve was constructed by correlating the absorbance at 510 nm of each standard solution to the corresponding concentration.

Actinometry experiments were conducted:

1. Quartz tubes containing 10 mL of 30 mM potassium ferrioxalate solution were irradiated with 8 lamps in the Rayonet 100 UV reactor.

2. Tubes were removed periodically. 0.1 mL sample was quickly taken from each tube and mixed with 0.05 mL acetate buffer solution and 2 mL 0.1 wt% 1,10-phenanthroline in a 50 mL volumetric flask, diluted to mark by DI water. The flasks were kept in dark for 30 min to allow ferrous iron and 1,10-phenanthroline to fully react.
3. The complex concentration was analyzed on UV-vis spectrometer at $\lambda=510$ nm and determined using standard curve prepared above.

Figure A illustrated the decay of $[\text{Fe}^{2+}]$, and the incident radiation I_λ was determined to be 3.2×10^{-5} einstein/min according to Eq. (3).

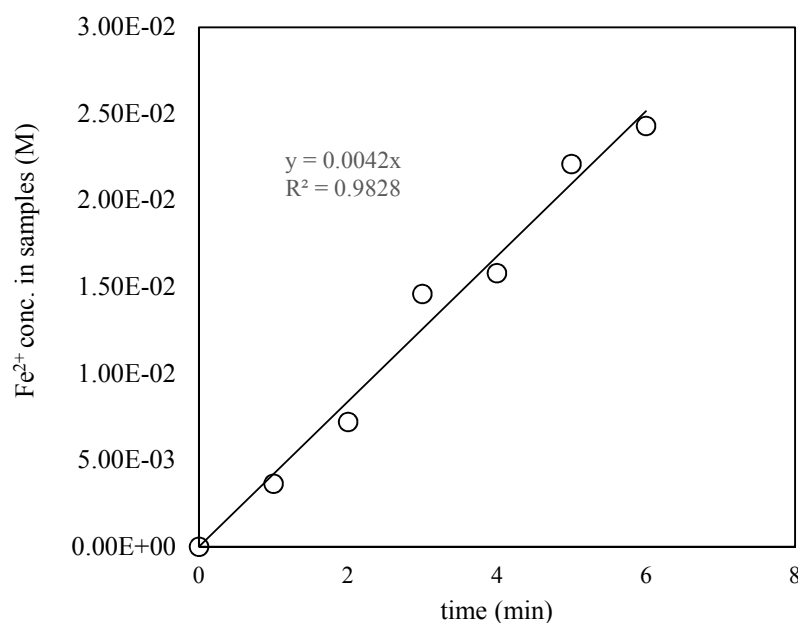


Figure A: Linear regression of data set determines the decay rate of the ferrous ion $[\text{Fe}^{2+}]$

$$(k=4 \times 10^{-5} \text{ M/min})$$

List of References

1. H. J. Kuhn, S.E.B.a.R.S., *Chemical actinometry*. Pure and Applied Chemistry, 1989.
61(2): p. 187-210.
2. *The Kinetics of Environmental Aquatic Photochemistry*. Analytical Chemistry, 1989.
61(3): p. 220A-220A.

Appendix B. Measurement of Residual Concentration of H₂O₂

An iodometric method described by Klassen *et al.* [1], was followed to measure the residual concentration of H₂O₂. The principle of the method is the color reaction of the H₂O₂ with potassium iodide (KI) in the presence of starch solution.

115.7, 231.5, 347.2, 463.0, and 578.7 μ L of 1.27 M H₂O₂ standard solution were added to a series of 25 ml amber volumetric flasks and mixed with 10 mL of 3.42 M NaCl and 1 ml of 0.5 mol/L HCl for 2 minutes. Then 1 mL of 0.03 M KI and 1mL 10 g/L starch solution were transferred to the flasks and diluted to mark. The resulting concentration of H₂O₂ ranged from 0.00000599 mM to 0.0000294 mM. The excess iodide in solution was oxidized to iodine by H₂O₂. The standard H₂O₂ solutions were analyzed at 585 nm wavelength where the maximum absorbance of iodine-starch blue compound was on a UV-vis spectrometer and standard curve was constructed by linearly correlating the absorbance at 585 nm of each solution to the corresponding concentration (shown in the Figure B).

Each PPCPs sample after photolysis was quickly transferred to a 25 mL amber volumetric flask containing the identical solution as the standard curve (minus the addition of H₂O₂). The residual concentration of H₂O₂ was determined on a UV-vis spectrophotometer at 585 nm using the standard curve.

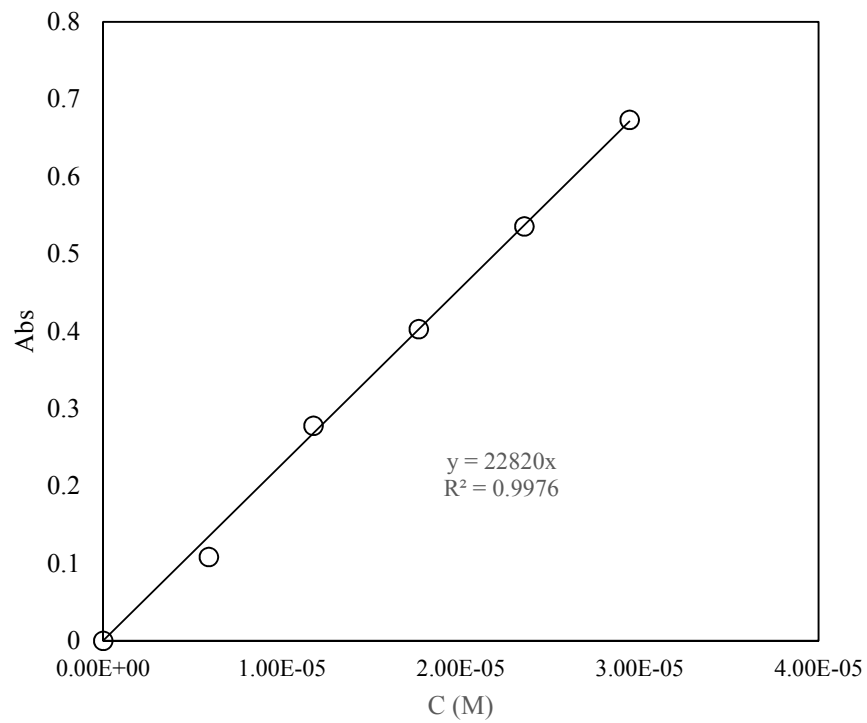


Figure B: H₂O₂ standard curve

List of References

1. Klassen, N.V., D. Marchington, and H.C.E. McGowan, *H₂O₂ Determination by the I³⁻ Method and by KMnO₄ Titration*. Analytical Chemistry, 1994. **66**(18): p. 2921-2925.

Appendix C. Ion Selective Electrode (ISE)

Carbon dioxide can be measured in units of moles per liter ranging from 0.0001 to 0.001 M. Samples should be measured as soon as possible after collection, waiting only a time for the sample to get the same temperature of the electrode (room temperature, $\sim 25\text{ }^{\circ}\text{C}$), so that the loss of carbon dioxide can be minimized. Moreover, samples should be stirred at a uniform and slow rate during the measurement.

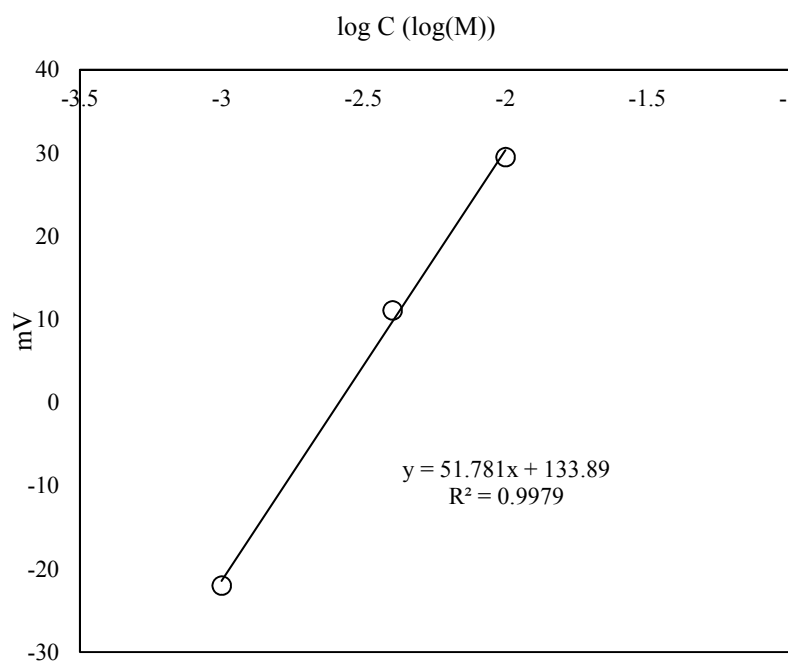


Figure C: ISE calibration curve at room temperature ($25\text{ }^{\circ}\text{C}$)